Increasing aortic endothelial cell aquaporin-1 expression upregulates endothelial hydraulic conductivity in monolayers and in whole vessels *ex vivo*.

by

CHIRAG B. RAVAL

A dissertation submitted to the Graduate Faculty in Biomedical Engineering in fulfillment of the requirements for the degree of Doctor of Philosophy, The City University of New York

2012

This manuscript has been read and accepted by the Graduate Faculty in Engineering in satisfaction of the dissertation requirement for the degree of Doctor of Philosophy.

_____	_____
Date	Professor David S. Rumschitzki
	Chair of Examining Committee
_____	_____
Date	Professor Mumtaz K. Kassir
	Executive Officer
	Professor Bingmei Fu
	Dr. Kung-Ming Jan, M.D., PhD.
	Professor Lane Gilchrist
	Professor Sheldon Weinbaum
	Professor John Tarbell
	Supervisory Committee

THE CITY UNIVERSITY OF NEW YORK

Abstract

INCREASING AORTIC ENDOTHELIAL CELL AQUAPORIN-1 EXPRESSION UPREGULATES ENDOTHELIAL HYDRAULIC CONDUCTIVITY IN MONOLAYERS AND IN WHOLE VESSELS *EX* VIVO

By

Chirag B. Raval

Adviser: Professor David Rumschitzki

The pressure inside large arteries is typically ~100 mmHg higher than outside of them. This difference, ΔP, drives a flow of plasma, mainly water and advected/swept-along solutes that would otherwise only transport by (much slower) diffusion (Huang, Rumschitzki et al. 1997), across the porous vessel wall. This water flow strongly influences interstitial residence times, a determinant of the solubility and stability of macro-molecules within the arterial wall. Recent studies in our group have asked whether this flow crosses the arterial endothelium solely through inter-endothelial cell (EC) junctions or whether a portion of the water traverses the ECs through the cells, e.g., via endocytosis or from the ubiquitous aquaporin (AQP) family or water channel membrane proteins (Preston and Agre 1991). Data from our group show that bovine (B) aortic (A) ECs express AQP-1 in cultured monolayers and that rat (R) AECs express AQP-1 in culture (Xue 2011) and in excised vessels (Nguyen 2008). In this thesis we ask whether upregulating AQP-1 expression also increases endothelial hydraulic conductivity (Lpe) in vessels and monolayers. If so, it might be a route towards washing LDL out of the subendothelial intima (SI) before it can bind significantly, a process that can begin the cascade to atherosclerotic lesions.

Belkacemi et al. showed a 4-fold protein expressional change of AQP-1 in trophoblast cells after treatment with arginine vasopressin (AVP) (Belkacemi, Marsiglia et al. 2008). Additionally, expression of vasopressin type-2 receptors (V2R) has been confirmed in human lung

microvascular endothelial cells (Kaufmann, Oksche et al. 2000) and in rat aortic strips (Mechaly, Laurent et al. 1999). We examined the effect of V2R stimulation on both Lpe and AQP-1 expression in BAEC monolayers for both short and long term treatments. Both short-term AVP and forskolin (F) treatment are known to increase intracellular cyclic adenosine monophosphate (cAMP) by virtue of membrane adenylyl cyclase (AC). Such increases cause membrane shuttling of internal AQP-2 to the cell membrane in the principal cells of the renal collecting duct. Long term AVP treatment also causes constitutive or synthetic upregulation of AQP-1 in these cells. Patil et al. (Patil, Han et al. 1997) and Yool et al. (Yool, Stamer et al. 1996) observed increases in single cell water permeability in response to osmotic challenge after short-term AVP and F treatment in oocytes, suggesting AQP-1 may incur membrane shuttling as well.

Our results show that cAMP stimulation with arginine vasopressin AVP or F induces AQP-1 shuttling in cultured BAEC monolayers and in whole rat aortas *ex vivo* that increases endothelial cell membrane AQP-1 concentration and, consistently, endothelial and the whole wall Lp. We found that 20 hr. AVP treatment increased Lpe 34±9% and AQP-1 expression 52% in BAEC monolayers as compared to untreated monolayers. Short term F treatment increased Lpe 172±49% but did not significantly change AQP-1 expression, which is consistent with the shuttling hypothesis. Satavaptan (S), an inverse V2R agonist, treatment decreased Lpe -46±7% and AQP-1 expression -44%. F/S treatment did not significantly change Lpe and decreased AQP-1 expression -29%. AVP/S treatment decreased Lpe -38±9% and caused no significant change in AQP-1 expression. To see whether a portion of the increase in Lp due to F treatment resulted from a change in junctional transport, we challenged monolayers with Dextran-70kDa, a tracer molecule that can cross the membrane paracellularly and not transcellularly. F treatment decreased Dextran-70kDa transport across BAEC monolayers under convective but not diffusive

conditions, indicating treatment had an effect on junctional tightness or length. This indicates that F treatment decreases paracellular solute transport and the increase in Lpe is likely due to an augmented transcellular AQP-1 route. These data indicate a reciprocal relationship between transcellular and paracellular flow in endothelial cells by F-triggered cAMP upregulation.

The next logical step investigates the effect of F treatment on whole rat aortas *ex vivo*. S. Joshi's theory for wall Lp, which includes the effects of subendothelial compression and IEL fenestral blockage, predicts that upregulation of Lpe should have a maximum effect on wall Lp in the 70-90 mmHg regime, and little effect by 120 mmHg transmural pressure. We excised rat aortas and measured Lp before and after treatment with F or with a blank solution. We observed a 35±5% % increase in Lp at 75 mmHg but no significant difference at 120 mmHg after F treatment. In contrast to our *in vitro* results, immunohistochemical analysis coupled to quantitative fluorescence of rat aortas revealed higher AQP-1 expression in the aortic endothelium of F treated versus untreated vessels. In addition, F treatment significantly caused a significant decrease in smooth muscle cell (SMC) AQP-1 expression in these whole rat aortas.

In contrast our *in vitro* studies showed no effect on AQP-1 expression in F-treated monocultures of SMCs. This suggests some communication between SMCs and ECs in the aorta upon activation of adenylyl cyclase with F so that a reciprocal relationship exists for AQP-1 in these adjacent cells of the arterial wall. A number of potential mechanisms could possibly explain how the EC influences SMC behavior. Paracrine signaling between the EC and SMC has been described in terms of eNOS produced NO transport from ECs to SMCs, EC natriuretic peptide (NP) release and transport to SMC NP receptors (NPR), and the SMC anti-mitogenic response to microRNA which post-transcriptionally control gene expression mediated by Krüppel-like transcription factor 2 (KLF-2). KLF-2 is a critical regulator of endothelial gene expression patterns

triggered by atheroprotective flow. The dynamics at play in the cardiovascular system between ECs and SMCs may also occur in other organs and potentially play an important role in the pathophysiology of other organ specific diseases and maladies involving dysfunction in paracrine communication between ECs and SMCs.

Acknowledgements

I would like to acknowledge my advisor, David Rumschitzki for whose guidance I will be forever grateful. I would also like to thank the Departments of Biomedical and Chemical Engineering at the Grove School of Engineering for providing the facilities to perform interdisciplinary research.

To my fellow research group members, both past and present, thank you for everything. A very special thanks goes to Shripad Joshi, whose great maturity has proved invaluable over the years. I acknowledge the Tarbell Research group, especially Limary Cancel for cell culture direction and resources. I would like to thank all my committee members for their input in research direction, especially Dr. Kung-Ming Jan and Dr. Steven Quarfordt for their physiological expertise.

Finally I would like to thank my mother Darshana and my father Bharavi for making me work hard and pushing me to reach my potential. To my sister Amee thank you for your support. To my grandmother Sudhaben Trivedi, thank you for the epic books and encouragement which aided me in finishing this quest.

IN MEMORIAM

Maganbhai & Taraben Raval

Hasmukhbhai Trivedi

Table of Contents

List of Tables

List of Figures

List of Acronyms

A	*area of monolayer*
ACE	*angiotensin-converting enzyme*
ADH	*anti-diuretic hormone*
AJs	*adherens junctions*
ANP	*atrial natriuretic peptide*
AQP	*aquaporin*
AVP	*arginine vasopressin*
AC	*actin cytoskeleton*
BAEC	*bovine aortic endothelial cell*
BNP	*brain natriuretic peptide*
BSA	*bovine serum albumin*
cAMP	*cyclic adenosine monophosphate*
CBP	*CREB-binding protein*
CNP	*C-type natriuretic peptide*
Cp	*luminal solute concentration*
CRE	*cyclic response element*
CREB	*cyclic response element-binding*
DAG	*diacylglycerol*
DDAVP	*desmopressin*
DMSO	*dimethyl sulfoxide*
EC	*endothelial cell*
EDRF	*endothelium derived relaxing factor*
ECM	*extracellular matrix*
eNOS	*endothelial nitric oxide synthase*
F	*forskolin*
FBS	*fetal bovine serum*
F-actin	*filamentous actin*
FSS	*fluid shear stress*
GPCR	*G-protein coupled receptors*
Gi	*guanine nucleotide regulatory protein*
HDL-C	*high density lipoprotein bound cholesterol*
HDL	*high density lipoprotein*
HRP	*horseradish peroxidase*
IEL	*internal elastic lamina*
IP3	*inositol triphosphate*
IVC	*inferior vena cava*
Jv	*water flux*
kp	*SI Darcy permeability*
Lp	*hydraulic conductivity*
Lpe	*endothelial hydraulic conductivity*
LDL	*low density lipoprotein*
miRNA	*micro RNA*

NP	*natriuretic peptide*
NPR	*natriuretic peptide receptor*
PA	*pulmonary artery*
PBS	*phosphate buffered saline*
Pe	*solute permeability*
PFA	*paraformaldehyde*
PI	*phosphatidyl inositol*
PLC	*phospholipase C*
PKA	*protein kinase A*
Q	*quiescent*
RAEC	*rat aortic endothelial cell*
RBC	*red blood cell*
SMC	*smooth muscle cell*
S	*satavaptan*
SES	*subendothelial space*
SEM	*scanning electron microscopy*
SI	*subendothelial intima*
siRNA	*small interfering RNA*
TEM	*transmission electron microscopy*
TI	*total intensity*
TJs	*tight junctions*
TV	*total volume*
Va	*fluid volume of the abluminal chamber*
V2R	*vasopressin type-2 receptor*
VCAM	*vascular cell adhesion molecules*
VEGF	*vascular endothelial growth factor*
VSMC	*vascular smooth muscle cell*
WCVs	*water channel containing vesicles*

Chapter 1. Introduction and Literature Review

Atherosclerosis

General

Atherosclerosis is a disease that develops in large arteries and valves (Ross 1986; Wilson 1991). The earliest events leading to atherosclerosis involve the transport of macromolecules such as low-density lipoprotein (LDL) cholesterol from the blood across the arterial endothelium into the inner layers of the vessel wall and their subsequent accumulation by attachment to subendothelial intimal (SI) extracellular matrix (EM). Blood-borne monocytes enter the arterial intima in regions with high subendothelial lipid concentration, maturing to become macrophages that attempt to scavenge the extracellular cholesterol (Vander 2001). When overwhelmed, they form foam cells. Lipid and necrotic cells accumulate to comprise the earliest atherosclerotic legions (Steinberg 1983; Simionescu 1986).

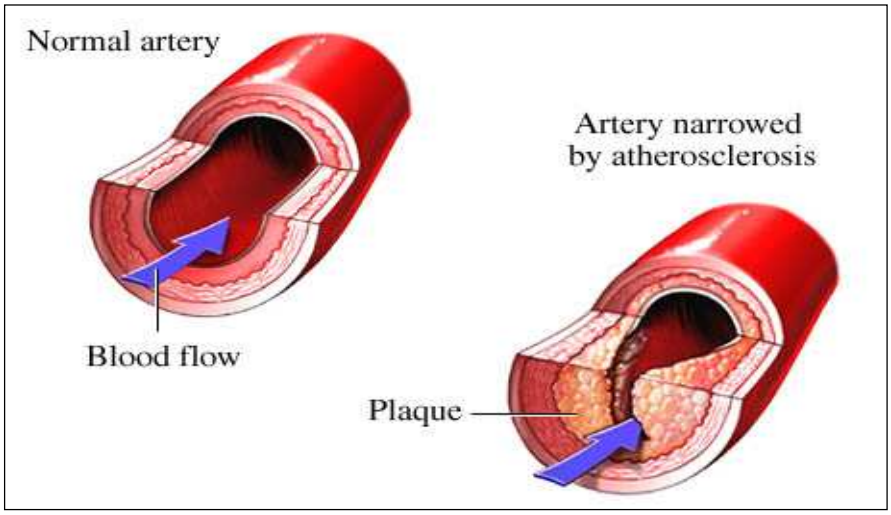

Figure 1: Obstruction of an artery due to atherosclerotic plaque formation (http://www.nucleusinc.com)

Figure 1 shows a schematic depicting obstruction of an artery due to atherosclerotic plaque formation and its contrast to a normal artery. An important route by which low-density lipo-

protein (LDL) cholesterol enters the vessel wall is by pressure driven transport from the blood into the arterial intima around rare isolated sites of tight junction disruptions. These sites cluster around branch sites in arteries, regions where blood flow is disturbed. The local blood fluid mechanics result in shear stress on the arterial wall that are lower in magnitude but have far higher gradients than in the straight portions of the artery and coupling to the cardiac cycle can generate spots along the wall where the wall shear stresses oscillate in direction. A number of other factors, such as high blood pressure, also correlates with an increased density of macromolecular leakage sites in rat aortic endothelium (Wu, Chi et al. 1990). As noted, the accumulation of low density lipoprotein (LDL) deposits can set off a cascade of processes that eventually leads to the thickening and hardening of the arterial wall, including the formation of fibrous plaques, and the occlusion of the arterial lumen resulting in a decrease in blood flow to distant tissues. Furthermore, a part of a lesion may break off and lodge downstream as a clot, completely blocking a smaller artery and causing ischemic damage to tissue downstream of the occlusion.

Wall Structure

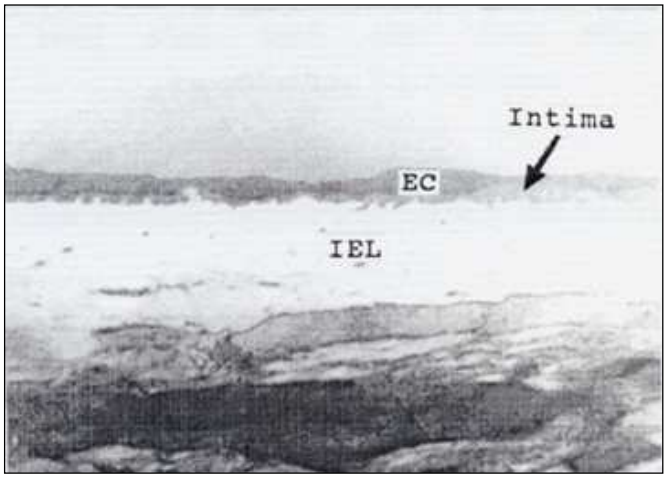

Figure 2: Electron micrograph of Aorta. Magnification x8, 000 (Huang et al. 1997)

Let us briefly review the structure of the aorta, illustrated in Figure 2 (Huang 1998). The aortic endothelium, a continuous, quiescent monolayer of endothelial cells (ECs), covers the lumen side of the arterial wall. ECs communicate with each other through cell-cell contact, creating junctions which control paracellular solute flow. The endothelial glycocalyx is a network of membrane-bound proteoglycans and glycoproteins, covering the luminal surface of the endothelium mediating mechanotransduction, homeostasis, and blood cell–vessel wall interactions (Reitsma, Slaaf et al. 2007). Under normal (laminar and steady) blood flow conditions, the quiescent endothelium functions as a semi permeable membrane separating tissue from blood, regulating molecular transport across the vessel wall to maintain homeostasis. Under chemical injury or abnormal (turbulent and non-steady) flow conditions, the endothelium becomes reactive and changes its phenotype and that of the adjacent SMCs to induce inflammation, proliferation, and migration. The SI, which, in healthy animals, is a thin (less than 1 μm thick in rats and rabbits) region comprised of collagen and proteoglycans, separates the endothelium from the internal elastic lamina (IEL).

The IEL in the aorta and in other large arteries is a ~1 μm thick, continuous, cylindrical elastin sheet with numerous fenestral holes. Adjacent to the IEL is the media, which contains smooth muscle cells (SMCs), proteoglycans, and repeated sheets of elastin, and is much thicker (~100-150μm in rat) than the previous layers' combined thickness (1-2μm in rat). Quiescent SMCs are in a non-proliferative state and have a contractile function to provide appropriate mechanical responses to blood flow by the vessel wall. Recent data indicate this quiescent phenotype is dependent on signaling from the endothelium, possibly via micro RNA (miRNA) in a paracrine manner (Hergenreider, Heydt et al. 2012). Conversely the endothelium response to chemical injury or abnormal flow induces SMCs to become reactive and transformed into a pro-

liferative and migratory state. The adventitia, a layer of loose connective tissue, adjoins the media. In large vessels it can contain its own micro-blood supply called the *vaso vasorum*. Small molecules continuously traverse all layers of the vessel during filtration and each layer has its characteristic transport properties. The early phase of atherosclerosis is characterized by the transport and accumulation of large macromolecules, most notably LDL cholesterol and other lipids, into the SI, where they can bind to extracellular matrix, or their transport into the subsequent inner layers of the blood vessel walls.

Lipoproteins

There is more than one type of lipoprotein cholesterol. LDL cholesterol is the vehicle by which cholesterol is transported from their source of origin to use in the peripheral tissue. It is termed the "bad" cholesterol because of its association with atherosclerotic lesions. High-density lipoprotein (HDL) returns cholesterol from peripheral tissue. Moderate concentrations of LDLs are needed by cells to produce membranes (Simionescu 1986). The body has two sources of cholesterol one diet-derived, absorbed from the intestines on chylomicrons which go to the liver and then transported to peripheral tissue on LDL primarily for incorporation in cell membranes. The other is synthetic cholesterol primarily from the liver (Brown and Goldstein 1984). An overabundance of cholesterol due to high blood LDL concentration secondary to low or defective tissue LDL receptors can eventually lead to plaque formation and atherosclerosis (Clayman 1989).

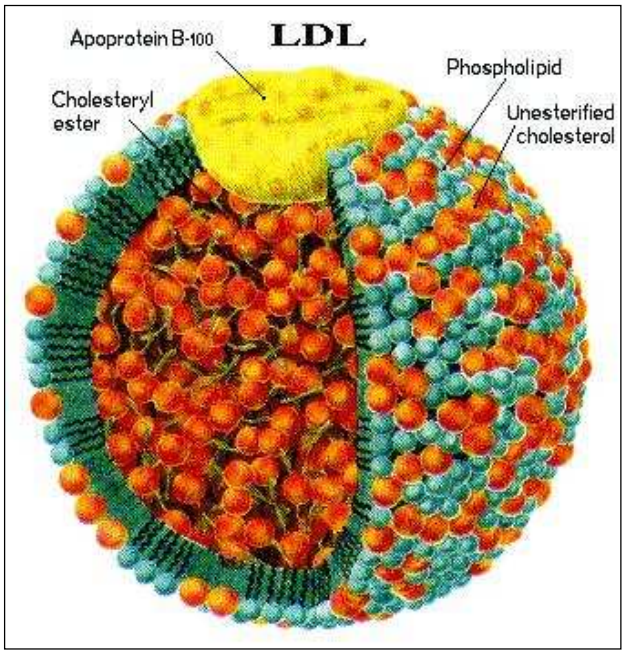

Figure 3: LDL molecule. (http://www.cholesterol-and-health.org.uk/hdl-ldl.html)

Figure 3 depicts a single LDL molecule, whose diameter ranges from 19 to 22 nm, with an average of ~22 nm. It is the smaller denser LDL particles that are considered the more dangerous ones associated with an increased risk of atherosclerosis. The larger buoyant LDL particles are the safer ones, causing less risk (Clayman 1989). An LDL particle is comprised of about 2000 cholesterol and cholesterol ester molecules (66% ester) with this hydrophobic ester surrounded by a phospholipid free cholesterol coat to produce water solubility. The LDL coat also includes an apoprotein B-100 molecule, which allows the LDL to be specifically recognized and bound with high affinity by specific receptors present on the surface of most body cells.

Lesion Formation

ECs have junctions that are tight enough to severely restrict the trans-endothelial migration of molecules with sizes as small as that of albumin (~8 nm diameter), which can be transported both through the cell via endocytosis as well as paracellular junctional network. This raises the question: how can a 22 nm LDL particle penetrate the endothelium's tight junctions? The

two most commonly accepted pathways for the transendothelial transport of macromolecules are through transcellular pathways by endocytosis in clathrin coated pits and transport across large paracellular channels. Transcellular transport of LDL may occur by transcytosis, which involves the shuttling of macromolecules back and forth within the cell. The relative contribution of transcytosis was questioned by Rosengren et al. (Rosengren, Carlsson et al. 2004) who showed that impairing this pathway by inducing hypothermia in peritoneal microvessels of rats *in vivo* did not result in any appreciable decrease in overall LDL transport. This group concluded that the paracellular route is the dominant pathway for LDL contribution; the observation of accelerated atherosclerosis in humans and experimental animals without these receptors precluding endocytosis supports this conclusion. More recently, Cancel et al. (Cancel, Fitting et al. 2007) measured the permeability of water, albumin and low-density-lipoprotein (LDL) to bovine aortic endothelial cell (BAEC) monolayers under both convective and diffusive conditions. By using a fixative to arrest vesicular motion, they were able to calculate the contribution of the vesicular endocytotic pathway to overall LDL transport. Cancel et al. report that transcytosis is not a major contributor for LDL transport, accounting for less than 10% of LDL permeability.

Transport of LDL through tight and leaky junctions

Weinbaum, Chien et al. (Weinbaum 1985; Lin, Jan et al. 1988; Lin, Jan et al. 1989; Chuang, Cheng et al. 1990; Lin 1990) established that large molecules such as LDL can cross the arterial endothelium via focal endothelial leaks, many associated with widened junctions around endothelial cells that are either dividing or dying or have stigmata. Stigmata is the traditional name for focal deposits of solid black metallic silver seen by light microscopy in blood vessels treated with silver nitrate solution (Majno, Underwood et al. 1985). It should be recognized that all these studies were performed on vessels with quiescent endothelium and smooth muscle, and thus possibly less prone to the atherosclerotic process. At the same time, Stemerman

(Stemerman 1986) showed that large molecules traverse the aortic endothelium at focal hot spots, rather than uniformly, for short tracer circulation times. Our group (Chuang 1990; Huang 1994) showed that this focal transport arose from transmural pressure-driven water advection of macromolecules through these rare, focal leaks into the SI. Once there, a spreading flow in the SI, generally parallel to the endothelium, spreads the tracer radially away from the leak, while transmural filtration through the far more abundant normal endothelium (Tedgui 1984) dilutes LDL already in the vessel's SI and further transports it into the media and beyond.

These results motivated our group's two-dimension, convection/diffusion model for tracer transport into the arterial wall (Yuan 1991; Huang 1994). The key ingredients of this model (Huang 1994) were the use of Frank & Fogelgman's (Frank and Fogelman 1989) ultra-rapid freezing-rotary shadow etchings that revealed the extremely loose SI matrix structure, with fluid and tracer void spaces far larger than in the media. An ultrastructure-based, *ab initio* theory for the SI's transport parameters translated this sparseness into transport parameter values that turned out to be one to two orders of magnitude higher than the media's values. Zeng's corrections (Zeng, Jan et al. 2011) to Huang's work applied subsequently measured parameter data to replace some previously guesstimated values and other calculated parameters. Although some corrected parameters differed significantly from the original guesstimates, the model with either set of values fit the experimental data well, although the latter values did introduce noticeable improvement. The model yielded a convection-dominated rapid tracer spread in the intima that accounted for the large observed tracer (horseradish peroxidase, HRP) spots (Huang 1994).

Atherosclerosis is characterized by the infiltration of these LDL molecules into the subendothelial space (SES). The first visual sign of lesion formation comes in the form of fatty

streaks. As noted, these fatty streaks are commonly found at sites of altered blood flow such as at branch points, bifurcations, and curves in the arterial tree (Wissler and Vesselinovitch 1983).

After LDL has localized in the SI, blood-borne monocytes adhere to the luminal surface of the endothelial layer, which is well recognized as one of the first events in plaque formation. In response to the subendothelial accumulation of lipids, the endothelial surface is believed to promote monocyte adhesion by expressing vascular cell adhesion molecules (VCAM). Once monocytes adhere to the endothelial surface, they transmigrate through the endothelial tight junctions (typical width of ~ 7 nm (Bell, Adamson et al. 1974)) into the subendothelial space where they mature to become macrophages and ingest lipids, primarily of the modified oxidized form (oxLDL), and can either escape into the blood stream with its load of ingested lipid or, when overwhelmed, eventually evolve into foam cells *in situ*. As foam cells begin to accumulate, smooth muscle cells (SMC) from the media slowly migrate past the internal elastic lamina (IEL) and proliferate in the SI. These SMCs synthesize and release primary components of extracellular matrix (ECM) that makes up the majority of the bulk in these fatty lesions (Ross 1993).

Consequently, the overall diluting transmural water transport, and not just the portion of the water transport that occurs through the rare focal leaky junctions that delivers LDL cholesterol from blood to the SES, appears to play a central role in controlling whether that LDL spends enough time there at high enough concentration to bind to SI ECM (Simionescu 1986; Mora 1987; Schwenke 1988; Frank and Fogelman 1989; Schwenke 1989). That is, overall transendothelial water flux and not just that through rare leaky EC, presumably can dilute SI LDL concentration and thereby affect the kinetics of liposome formation and growth. Potentially this

could slow lipid binding to SI ECM and wash unbound lipid from the SI before it binds to SI ECM.

Potential approaches to mitigate lipid infiltration/accumulation

Lifestyle changes, such as eating a healthy diet and exercising, are often the first line of defense in treating atherosclerosis. But sometimes, medication or surgical procedures may be recommended as well. Various drugs can slow — or sometimes even reverse — the effects of atherosclerosis. Cholesterol medications that aggressively lower blood concentrations of LDL cholesterol, the "bad" cholesterol, can slow stop or even reverse the buildup of fatty deposits in one's arteries. Boosting high-density lipoprotein (HDL) cholesterol, often called the "good" cholesterol, may help, too. It is hypothesized that HDL can remove cholesterol from atheromas within arteries and transport it back to the liver for excretion or re-utilization—which is the main reason why HDL-bound cholesterol is sometimes called "good cholesterol", or HDL-C. Drugs known as statins and fibrates constitute a range of cholesterol medications. Anti-platelet medications such as aspirin can reduce the likelihood that platelets will clump in narrowed arteries, form a blood clot and cause further blockage. Anticoagulants such as heparin or warfarin can help thin blood to prevent clots from forming. High blood pressure is a known risk factor for atherosclerosis, specifically by causing greater swelling and stretching of the arteries throughout the body. It is believed that this stretching can injure the endothelium and thereby increase its permeability to "bad" LDL cholesterol, which, as noted, leads to the increased attraction of white blood cells. Cholesterol and cells build up in the artery wall, eventually forming the plaque of atherosclerosis. Blood pressure medications— such as beta blockers, angiotensin-converting enzyme (ACE) inhibitors and calcium channel blockers — can control blood pressure and help slow the progression of atherosclerosis.

These commonly-used medications are typically prescribed after the formation of lesions, and often when there is an elevated risk of a crisis event, such as stroke or heart attack, occurring. Significant coronary atherosclerosis occurs in over 90% of our population after the age of approximately 30 years (Strong, Richards et al. 1969). Controlling modifiable, multiple cardiovascular risk factors early in life is especially important. The control of obesity in childhood through a prudent diet that is balanced in composition and through physical activity aims to achieve an energy balance and to maintain a desirable weight. Along with other healthy lifestyle choices, such early life choices are primary to the prevention of coronary artery disease later in life. Various studies confirm that atherosclerosis is a life-long process that starts at a very early age (Srinivasan, Frontini et al. 2003).

Sometimes more aggressive treatment in the form of invasive surgery is needed in the most serious cases of plaque formation. These surgical treatments include angioplasty, endarterectomy and bypass surgery. As with any surgery, there is a risk of complication and success is not guaranteed. Thus it is natural to consider exploring drug targets that would focus on treatment or prevention before atherosclerotic lesions have formed or progressed. The impression that all atherosclerosis is caused by LDL influx doesn't recognize that primary changes in the vessel wall (i.e. reactive endothelium, vascular inflammation, reactive SMC etc.) may be a major cause rather than lipoproteins.

Transport model

We now examine the details of transport in the arterial wall and the logistical mechanics of LDL infiltration as codified in our group's mathematical artery wall transport models. Our long-term goal is to eventually see where further progress on this mechanism can suggest possi-

ble therapeutic targets that could potentially drastically slow the progress of or arrest the development of lesions long before they become atherosclerotic.

Hydraulic Conductivity Parameter

One of the transport properties of greatest importance in the arterial wall is its hydraulic conductivity, Lp, the ratio of the transmural water flux to the hydrostatic transmural pressure difference ΔP (in the absence of an osmotic pressure difference). The advection caused by this water flux can transport macromolecules and molecular aggregates such as lipoproteins into the artery wall directly through focal leakage spots in the arterial endothelium. Numerous researchers (Yamartino 1974; Vargas 1979; Tedgui 1984; Baldwin 1992; Baldwin 1993; Shou 2005; Shou 2006) have employed various experimental methods to measure the Lp of aortas from various species as a function of transmural pressure *ex vivo*. The contribution of the endothelium to the wall's overall hydraulic conductivity was evaluated directly by Lp measurement of vessels with an intact endothelium layer and then comparing them with Lp measurements of either another or the same portion of the same vessel after denuding its endothelium layer. Whereas diffusion alone had traditionally been thought to be the sole mechanism that delivered nutrients and large and small molecules to the internal layers of the vessel wall, Lp measurements indicated that in reality the transmural pressure-driven water flux may be a very significant contributor to this delivery. This flow likely advects, or sweeps along, solutes across the endothelium into and across the wall. For large solutes such as LDL, it likely sweeps them into the vessel wall through leaky junctions. The overall transmural-pressure-driven flow, by diluting and cleansing the SI, very likely plays a central role in the fate of LDL that has already entered the subendothelial space.

Mathematical Model based on Experimental Lp Trends

Experimental Trends

See Appendix II for a detailed review of the historic methods that have been used to measure Lp on whole aortas *ex vivo*. Baldwin and Wilson's *ex vivo* Lp measurements with intact and denuded endothelium extended Tedgui and Lever's work, both on rabbit aortas, to allow multiple measurements, at different pressures and with and without endothelium, on the same vessel. Their results turned out to be uniformly double those obtained by Tedgui and Lever, but nevertheless showed similar trends: Both groups' results show a high value of Lp at low pressures that quickly decreases 30-40% to a plateau as the pressure increases. Endothelial denudation roughly doubles the high-pressure Lp value and leaves it pressure- insensitive. Tedgui and Lever's measurements, though at fewer pressures, clearly show these same trends. It is important to note that, whereas Baldwin & Wilson's data seem to also display the trends just noted, at their lowest transmural pressure of P=50mmHg, the error bars of the two measurements, one with intact and one with denuded endothelium, were so large that one cannot reliably infer a statistically significant change in Lp upon endothelial removal or upon raising the pressure to 75 mmHg.

Shou, of our group, repeated these Lp measurements on the much smaller rat model and found permeability trends, both with intact and denuded endothelium, that agree even quantitatively with Tedgui and Lever (Tedgui 1984) and qualitatively with Baldwin and Wilson (Baldwin 1993), suggesting that there is little species variation in Lp-trends in large arteries (Shou 2006), at least between these two species. An attempt to explain the observed Lp dependence on transmural pressure and on denudation led to the development of our group's mathematical model based on the experimental Lp-trends observed in whole vessels *ex vivo*.

Huang 1998 Mathematical Model

Huang et al. (Huang 1998) proposed a possible explanation for the apparent trend of an initial decrease in Lp with increasing transmural pressure by attributing it to subendothelial intimal compaction upon pressure loading. They predicted that, at lower pressures, the sparse SI layer is not fully compressed, which then allows for easy, efficient transmural fluid flow at low transmural pressure. Increased pressure initially compresses the intima until it achieves a maximal compression determined by its collagen fibers' stiffness. The fiber density in the intima increases due to this compaction, leading to a decrease in SI Darcy permeability, Kp, and thus in the effective Lp for the intima plus endothelium. More importantly, however, for Lp, intima compaction also causes the endothelial cells to block some IEL fenestrae, thus critically inhibiting flow through the IEL and causing a substantial decrease in the measured wall Lp. Moreover, endothelial denudation removes the possibility of fenestral blockage, and the resulting Lp should be found to be pressure-independent, as observed by both groups cited. Huang et al. filtration theory based on this hypothesis of vessel wall compressibility provides a quantitative explanation for these observed Lp-trends.

Aquaporin-1 (AQP-1)

History

A host of mobile biologically relevant molecules exist, but none so ubiquitous as water. Over 2/3 of the human body mass is water (Kozono, Yasui et al. 2002). Scientists since the mid-19th century (Bruecke 1843) postulated the existence of water channel molecules. In the late 1950s Solomon and Sidel showed that red blood cells (RBC) had such channels that selectively excluded ions and other solutes (Sidel and Solomon 1957). These channels seemed to allow high throughputs of water (~$3x10^9$ molecules/sec) (Murata, Mitsuoka et al. 2000) in response to osmotic gradients via passive transport with little or no ATP expenditure. In 1988, Agre et al. iso-

lated and characterized a 28KD membrane protein, CHIP29, now called aquaporin-1 (AQP-1), from red blood cells and from renal tubules (Denker, Smith et al. 1988). After sequencing the protein (Preston and Agre 1991; Smith and Agre 1991), his group proved it was indeed the ubiquitous water channel protein (Preston, Carroll et al. 1992). Eleven AQPs (AQP-1–10) have been discovered so far in humans and 35 in plants (Javot and Maurel 2002). In humans, AQP-1 and AQP-2 are abundant in the kidney, where 150-200 liters of water per day are resorbed from the primary glomerular filtrate.

Various AQPs have so far been found in the hypothalamus, heart, liver, brain, the lung's bronchial epithelium, the salivary and lactrinal glands, the lens and corneal epithelium, the testes, pancreas, liver, through the gastrointestinal tract, in epithelial cells and in its lymphatic ECs, and in sperm and leukocytes (Nielsen, Smith et al. 1993; Jung, Bhat et al. 1994; Connolly, Shanahan et al. 1998; Koyama, Yamamoto et al. 1999; Agre, King et al. 2002). AQP deficiencies or mutations underlie clinical maladies such as certain cataracts, congestive heart failure and certain kidney diseases, among others (Agre, King et al. 2002; King and Yasui 2002; Schrier and Cadnapaphornchai 2003).

ECs express AQP-1

Our group is currently focused on showing the presence of and on understanding the potential role of AQP in water transport across the arterial endothelium. By interpreting variations in the reflection coefficient vs permeability for the same solute between different capillaries, an earlier study in frog mesentery indirectly estimated the contribution of a specific channel exclusive to water only to be no greater than 10% of the total hydraulic conductivity of those capillaries (sometimes called filtration coefficient) (Curry, Michel et al. 1976). This estimate, again, based on capillary data, was based on the values of slopes of plots of data with wide scatter and

low correlation coefficients. My colleagues Toussaint showed that rat aortic ECs express AQP-1 in whole rat aortas and Nguyen showed that bovine aortic ECs express AQP-1 in cultured monolayers. Toussaint found that whole rat aortas upregulate the numbers of AQPs that they express in response to a chronic increase in ΔP (Toussaint 2009). Chemically blocking AQP-1 or knocking down AQP-1 expression significantly reduces BAEC and RAEC monolayer hydraulic conductivity Lp (Nguyen 2008; Russell 2009; Xue 2011). Chemically blocking EC AQP-1s with low concentrations of $HgCl_2$ (Nguyen 2008) also reduces Lp of excised whole vessels by more than 1/3 at ΔP=60mmHg (Shou 2005; Nguyen 2008). Although the experiment is far more complex, a nearly identical drop in Lp at 60 mmHg results from EC AQP-1 knockdown in whole rat aortas *ex vivo* (Xue 2011). The results of both of these experiments suggest a significant AQP-mediated transcellular flow. Interestingly, both of these experiments showed far smaller Lp drops upon chemical blocking or knockdown of AQP-1 at the higher pressures of 100 and 140 mmHg, suggesting the explanation must be more nuanced. Considering that total wall resistance, the inverse of Lp, is the sum of the resistances of tissue layers in series, i.e., of the endothelium plus SI and of the IEL plus the media, and presuming that endothelial denudation does not appreciably change medial flow resistance (e.g., by significant hydration changes), Lp for the endothelium plus intima goes down ~56% upon chemically blocking with $HgCl_2$ and ~60% after downregulation of AQP-1 via siRNA at 60 mmHg transmural pressure (Nguyen 2008; Xue 2011).

Transport Hypothesis: Role of AQP-1 in ECs

It is hard to imagine that AQPs account for such a large fraction of the transendothelial water flow. In order to explain these large drops in Lp, recall that Lp(ΔP) measurements (Tedgui, Merval et al. 1992; Baldwin 1993) on intact vessels found Lp high at low ΔP (60-70 mmHg), quickly dropping ~40% by ΔP~100 mmHg and remaining ΔP-insensitive beyond to ~180

mmHg. Endothelial denudation made Lp fairly ΔP-insensitive at ~double the intact vessel's high ΔP value.

In addition, Huang reported that the arterial SI had a much higher void space (Huang 1994) than the media (~95% vs. ~40)(Tedgui 1987). They postulated that the dense media is incompressible, but that the very sparse SI would easily compress with increasing ΔP. This compression would increase fiber density and flow resistance in the SI. Under maximum subendothelial intimal compression, when the intima's collagen matrix supports the load, the ECs might block some of the fenestrae in the IEL through which water apparently enters the media, which quantitatively accounts for the sharp decrease in wall Lp with increasing ΔP. Our group has suggested (Joshi et al., pending) that blocking or knocking down EC AQPs increases the endothelium's hydraulic resistance and thereby lowers the ΔP at which intimal compaction, and thus fenestral blockage, occurs. Thus only a fraction of the drastic drop in Lp that we observed at 60 mmHg would then be due directly to a drop in endothelial Lpe, and the balance to the consequent SI compaction and fenestral blockage. The result is a shift in the ΔPs over which the SI goes from uncompressed to fully compressed to lower ΔPs with EC AQP-1 blockage or knockdown. The theory in fact quantitatively explains the different drops in Lp with EC AQP-1 chemical blocking or knockdown, as well as the effect of denudation reported above.

If AQPs indeed play such roles, the understanding of the details of their contribution and potential regulation would provide valuable insight into early mechanical events that influence prelesion events in the arterial wall. The regulation of AQP-1 expression in the aortic endothelium with chronic transmural pressure might also provide clues as to one of the reasons for the well-known but poorly understood link between hypertension and atherosclerosis. In the short term, we employ the experimental Lp techniques cited above and detailed in Appendix II, to-

gether with methods for directly manipulating the expression of AQPs in aortic endothelial cells, to ferret out AQP's contribution to transport in the vessel wall and to see how changes in AQP expression modify its contribution. We have already seen that decreasing AQP-1 decreases Lp; so inversely we would like to ascertain the effect of upregulating AQP-1 expression on Lp (and Lpe). We predict, qualitatively, that the dynamic range of intima compaction, i.e., the pressures over which the SI goes from uncompressed to fully compressed, would shift to higher ΔPs in response to upregulating AQP-1 in whole vessels. We shall first make such predictions quantitative, using my colleague, S. Joshi's, model. We have already seen that decreasing AQP-1 decreases Lp; so inversely we would like to ascertain the effect of upregulating AQP-1 expression on Lp (and Lpe). Naturally, before embarking on whole vessel work, we shall show that our techniques can successfully upregulate BAEC AQP-1 expression and/or reorganize its distribution towards the extracellular membrane in monolayers and examine the corresponding effect on monolayer Lp.

The motivation for my work is that if water flow affects SI LDL concentration and thereby its binding kinetics to the SI ECM, maybe increasing this water flow can beneficially affect these processes. If decreasing the membrane concentration of active EC AQP-1 can lower the ΔP at which SI compresses and thereby lowers Lp, then maybe increasing EC AQP-1 expression can decompress the SI at physiological pressures, which would increase Lp and slow lipid entrapment to SI ECM. In this thesis we focus on accomplishing such an increase in EC AQP-1 expression and on investigating whether this upregulation results in a substantial increase in Lp at physiological pressures.

Specifically, we predict, qualitatively, that the increasing EC AQP-1 expression and/or association with the EC's extracellular membrane increases endothelial monolayer Lp. Once this

has been established, we predict that, in a whole aorta *ex vivo*, the dynamic range of intima compaction, i.e., the pressures over which the SI goes from uncompressed to fully compressed, would shift to higher pressures, possibly encompassing physiological pressures, if one could successfully upregulate endothelial AQP-1 expression in whole vessels.

Chemical Agents to increase AQP-1 expression

Schewenger et al. has shown that activation of protein kinase C by1-oleoyl-2-acetyl-sn-glycerol induced a marked increase of AQP-1-dependent water permeability (Zhang, Zitron et al. 2007). This regulation was abolished in mutated AQP-1 channels lacking both consensus protein kinase C sites Thr^{157} and Thr^{239}. Additionally, LaRusso et al. have proven that secretin induces the apical insertion of AQP-1 water channels in rat cholangiocytes. Secretin increased bile flow (78%, $P < 0.01$) as well as the amount of AQP-1 in the apical cholangiocyte plasma membrane (127%, $P<0.05$)(Marinelli, Tietz et al. 1999). In contrast, the amount of AQP-1 in the basolateral cholangiocyte membrane and the specific activity of an apical cholangiocyte marker enzyme (i.e., γ-glutamyltranspeptidase) were unaffected by secretin (Marinelli, Tietz et al. 1999). Finally, Agre et al. reported that corticosteroids or dimethyl sulfoxide exposure induced AQP protein expression in mouse erythroleukemia (MEL) cells (Moon, King et al. 1997). The MEL cell line is a reproducible erythroid model system for studying the transcriptional regulation of the AQP-1 gene while determining the consequences on AQP-1 protein biosynthesis (Moon, King et al. 1997). Cell lines allow living cells to proliferate outside the organ, and allow for isolated study given fresh media and space.

Belkacemi et al. obtained a 5-fold expression change with arginine vasopressin (AVP), also known as the anti-diuretic hormone (ADH) in trophoblasts, which are cells forming the outer layer of a blastocyst. Unlike endothelial cells, blastocysts provide nutrients to the embryo and

develop into a large part of the placenta and require a substrate, such as a monolayer of cells, to attach *in vitro*.

AVP is stored in the posterior pituitary and is released into the blood stream; however, some AVP is also released directly into the brain, where it plays an important role in social behavior and bonding. Belkacemi et al. used experimental and culture conditions comparable to those used in our group, but on trophoblasts, rather than on BAECs or RAECs.

In 2008 Belkacemi et al. reported a 5-fold upregulation of AQP-1 expression in trophoblast cells after treatment with AVP and cAMP agonists (Belkacemi, Beall et al. 2008). For some time it was believed that kidney AQP-2 was the only AQP that was regulated by AVP (Fushimi, Uchida et al. 1993; Nielsen, Chou et al. 1995). Patil et al. (2007) found AQP-1 may also be regulated by AVP in Xenopus oocytes (Patil, Han et al. 1997). Since AQP-1 is a candidate to regulate placental fluid exchange, Belkacemi et al. sought to investigate the effect of AVP and cAMP agonists on AQP-1 gene expression in first trimester-derived extravillous cytotrophoblasts (HTR-8/Svneo) and two highly proliferative carcinoma trophoblast-like cell lines.

Cells were grown to confluence and detached from flasks using trypsin-EDTA mixture and seeded and cultured in serum-free and hormone-deprived RPMI for another 12 hours before treatment with 0.1 or 10nM (final concentrations) of AVP in RPMI 1640 medium supplemented with 1% FBS. Cells were than treated for 20 hours after starvation in serum free medium, with controls in 1% FBS supplemented media alone and treatments formulated as aforementioned (Belkacemi, Beall et al. 2008).

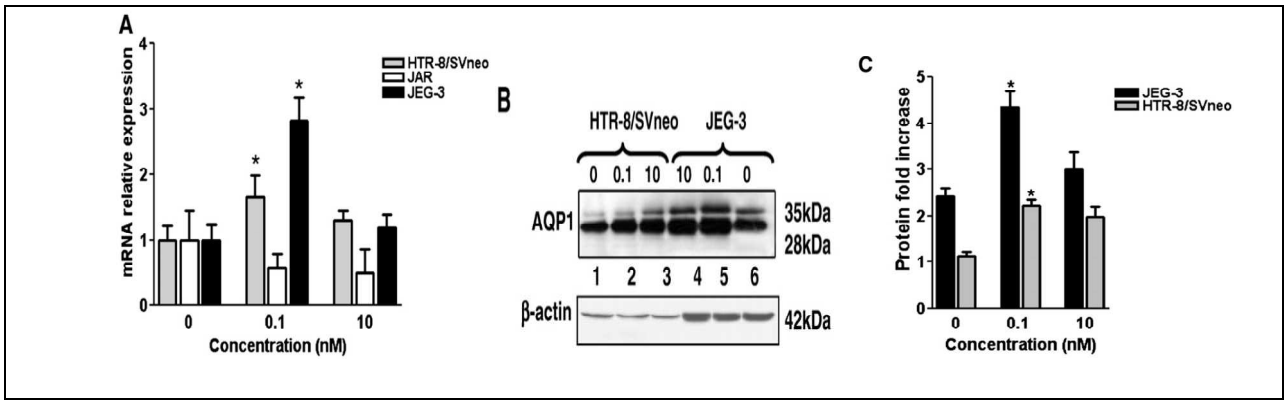

Figure 4: Effect of AVP on AQP-1 gene expression in trophoblasts-like cells (Belkacemi 2008). (A) Dose dependent effect of AVP on AQP-1 mRNA expression. (B) Representative Western blot of AQP-1 protein expression in HTR-8/SVneo (Lanes 1–3) and JEG-3 cells (Lanes 4-6)

AVP (0.1 nM) significantly increased the expression of AQP-1 mRNA and AQP-1 protein expression at 10 h in first trimester derived extravillous HTR-8/SVneo and trophoblast-like choriocarcinoma JEG-3 cells (Belkacemi, Beall et al. 2008), see Figure 4. These results suggest agents that stimulate intracellular cAMP and may provide a possible route to upregulate AQP-1 production/expression in other cells such as ECs.

Forskolin (F) is produced by the Indian Coleus plant and is commonly used to raise levels of cAMP in cell physiology for the last 30 years. F resensitizes cell receptors by activating the enzyme adenylyl cyclase and increasing the intracellular levels of cAMP.

We sought to see if the observed effects of AVP and cAMP agonists on AQP-1 expression in the cell lines used in Belkacemi et al. carried over to BAEC monolayers and to the endothelium of the intact arterial wall.

Vasopressin Type-2 Receptors (V2R) in ECs

AVP is a constituent of whole blood in mammals, including rats and humans, and is primarily released in response to osmotic conditions and secondary to decreases in blood volume to affect water homeostasis in the renal collecting duct. AVP transported through the lumen can

potentially interact directly with receptors in the endothelium of the vessel wall. Expression of vasopressin type-2 receptors (V2R) has been confirmed in human lung microvascular endothelial cells (Kaufmann, Oksche et al. 2000) and in rat aortic strips (Mechaly, Laurent et al. 1999). These observations hold out the possibility that AVP may bind to V2Rs on ECs leading to V2R coupling to Gs, a membrane-associated heterotrimeric G-protein, to stimulate adenylyl cyclase activity, similar to V2R activity reported in the principal cells in the renal collecting duct (Nielsen, Chou et al. 1995).

The consequence of short-term V2R stimulation is activation of membrane adenyl cyclase with an increase in cellular cAMP content and in protein kinase A (PKA) activity. If consistent with renal action of V2R, this would trigger an increased rate of insertion of intracellular water channel containing or AQP vesicles (WCVs) into the EC membrane and a decreased rate of endocytosis of WCVs from the EC membrane. The distribution of WCVs between the cytosolic compartment and the EC membrane compartment would thus shift in favor of the EC membrane component (Nielsen, Kwon et al. 1999) during short term stimulation of V2R or transmembrane cAMP stimulation, as seen in Figure 5 below (Katsura, Verbavatz et al. 1995).

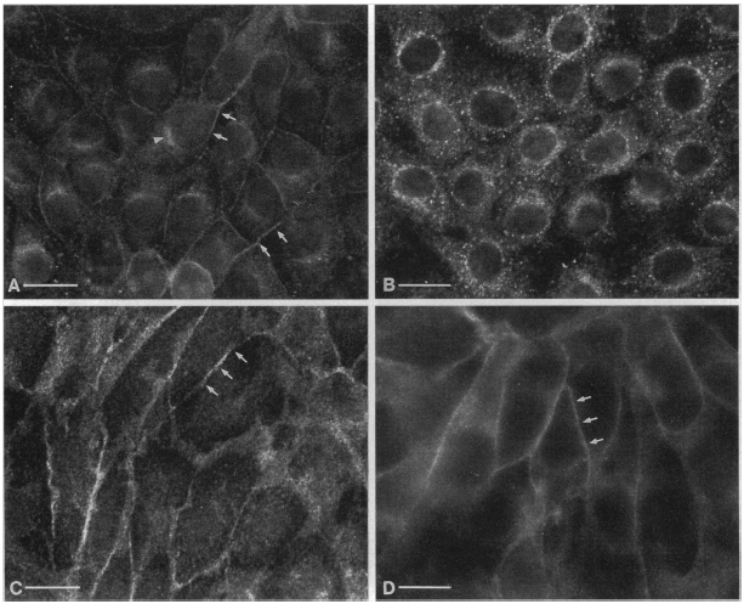

Figure 5: Immunofluorescence localization of AQP-1 in transfected LLC-PK1 cells (A). The protein is located on the plasma membrane (arrows) as well as on an intracellular perinuclear structure, probably the Golgi apparatus (arrowhead). In AQP-2-transfected cells (B), the c-Myc antibody stains many cytoplasmic vesicles, but the plasma membrane of most cells is unstained under basal conditions. AQP-2 shows plasma membrane localization (arrows) after AVP (C) or F (D) treatment. (Bar = 20 microns) (Katsura 1995)

PKA also mediates longer-term regulation by enhancing transcription of the AQP gene, thereby promoting AQP synthesis by translocating to the cell nucleus where it activates a cAMP response element-binding (CREB) protein. The activated CREB protein then binds to a cAMP response element (CRE) region of DNA, and is then bound to by a CREB-binding protein (CBP), which coactivates it, allowing it to switch certain genes on or off.

The V2R belongs to the seven transmembrane G protein-adenylyl cyclase system, and thus has the characteristics of G protein coupled receptors (GPCR), one of which is that an inverse agonist can stimulate a physiological effect opposite to that by its normal ligand. Satavaptan is a potent and selective V2R inverse agonist that binds to V2R. Rather than increasing camp, it increases intracellular cGMP (Serradeil-Le Gal, Lacour et al. 1996). This leads to short term

shuttling of membrane-bound AQP from the cell membrane to vesicles inside the cell. Long-term stimulation of V2R by satavaptan leads to a constitutive decreases in AQP expression.

We predict that because WCVs contain preformed functional water channels (AQP-1 and/or AQP-2), their net shift into EC membranes in response to short term V2R stimulation would increase the water permeability of the EC membrane. Membrane shuttling via vasopressin-regulated short-term stimulation of V2R has been limited to AQP-2, but several studies have suggested the possibility of AQP-1 shuttling by V2R stimulation (Yool, Stamer et al. 1996; Patil, Han et al. 1997). We shall test this possibility.

The Endothelium

Endothelium Barrier Function

As seen in primary epithelial cells from the collecting duct of the nephron, movement of vesicles to the membrane is facilitated by the local depolymerization of F-actin (Riethmuller, Oberleithner et al. 2008). A similar mechanism may be at play in ECs. ECs have several functions. AVP-stimulated epithelial cells can be expected to exhibit decreased rigidity, as studies have shown through atomic force microscopy force mapping (Riethmuller, Oberleithner et al. 2008). *In vivo*, *t*he physical forces exerted by blood flow and pressure are directly applied to the vascular ECs that line the luminal surface of blood vessels (Ali and Schumacker 2002). ECs must be both mechanically robust and compliant to endure these forces (Malek and Izumo 1996). The endothelium also serves to initiate vasoconstriction and vasodilation in response to chemical or physical changes in blood flow by releasing several factors, including NO.

The endothelium acts as a semi-permeable barrier that is responsible for keeping blood separated from the underlying tissue (Prasain and Stevens 2009). Endothelium cell-cell and cell-matrix contacts establish the semipermeable barrier that regulates passage of proteins, fluid, and

leukocytes between the blood and interstitium (Patterson and Lum 2001). Cell-cell and cell-matrix tethering depends on the nature of adherence within the EC itself (Prasain and Stevens 2009), and the actin cytoskeleton (AC) is responsible for this essential function. Actin tethering to adhesion complexes and to intracellular organelles is required to sustain a functional EC barrier (Birukov, Csortos et al. 2001; Lee and Gotlieb 2003; Lee and Gotlieb 2003) and is mediated by environmental cues that instigate the AC to orchestrate the cell shape accordingly (Prasain and Stevens 2009).

Actinmyosin Relaxation Facilitates the Translocation of Vesicles to the Plasma Membrane

Intracellular vesicles dock and fuse to the plasma membrane in living cells (Riethmuller, Oberleithner et al. 2008). The binding of the AVP to V2R on renal principal cells stimulates cAMP synthesis via activation of adenylate cyclase. The subsequent activation of PKA leads to phosphorylation of AQP-2 at serine256, and this phosphorylation event is required to increase the water permeability and water reabsorption of renal principal cells (Noda, Horikawa et al. 2008). Noda et al. showed that when AQP-2 in intracellular vesicles becomes phosphorylated at 256, it binds to tropomyosin 5b, which in turn depletes free tropomyosin from the vicinity of the AQP-2 vesicle, thereby fostering local filamentous actin (F-actin) depolymerization (Noda, Horikawa et al. 2008). This has the effect of cutting a hole in the cortical actin network around the vesicles, liberating AQP-2 vesicles from their F-actin cage to reach the plasma membrane, as illustrated in Figure 6 (Riethmuller, Oberleithner et al. 2008). As noted above, AVP stimulation also decreases epithelial cell stiffness, as measured by Young's modulus measured by atomic force microscopy force mapping (Riethmuller, Oberleithner et al. 2008).

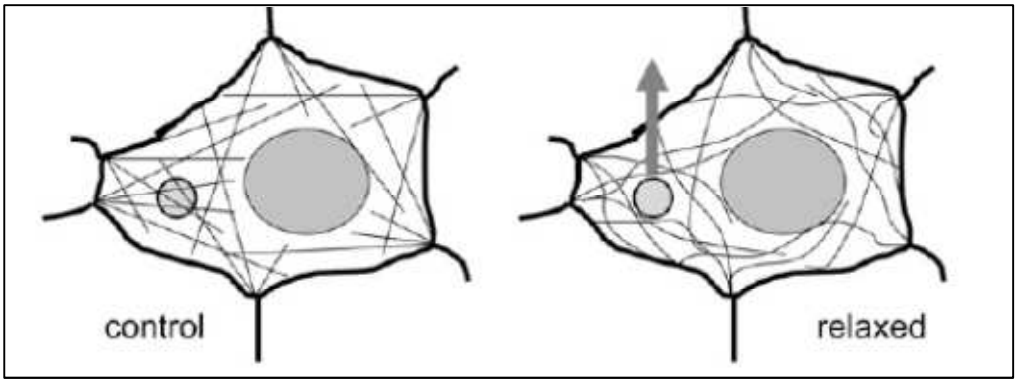

Figure 6: Sketch of the mechanical model depicting (left) a vesicle (small circle) spun into the web of actin filaments, and (right) relaxation of actomyosin interaction mediates the movement of vesicles due to relaxed steric hindrance. (Riethmuller, Oberleithner et al. 2008)

Approximately 5-15% of the total protein in ECs is actin. The AC undergoes polymerization and depolymerization based upon cellular demand and physico-chemical environmental cues. Actin polymerization is required for the formation of F-actin, which is a fundamental structural unit for actin-based cytoskeletal structures. F-actin assembles into three cytoskeletal structures: the membrane skeleton, the cortical actin rim and stress fibers. The membrane skeleton determines membrane architecture, and facilitates membrane distensibility (De Matteis and Morrow 2000). Just beneath the membrane skeleton resides the cortical actin rim, which facilitates the assembly of endothelial cell-cell and cell-matrix adhesions (Millard, Sharp et al. 2004). The cortical F-actin rim is subject to disruption by cAMP induced translocation of AQP to the cell membrane at a time that intercellular permeability is decreased possibly because a tighter F-actin belt contiguous to the adherens junctions (Thi, Tarbell et al. 2004; Boucher, Laprise et al. 2005). Stress fibers are actomyosin bundles that dramatically influence the rate and size of inter-endothelial cell gaps that form as cells retract (Birukov, Csortos et al. 2001) and usually occur in response to physical force (very high shear, trauma etc.) or chemical stimuli (thrombin, histamines, TNF-α etc.). The membrane skeleton and the cortical actin rim are close to the cell membrane, while stress fibers extend throughout the cell's cytoplasm.

cAMP Regulation of the Endothelial Barrier

cAMP has been implicated in the regulation of the endothelial barrier (Sayner 2011). Five hours after a step increase in pressure across the monolayer, which induces a sharp rise in Lp, Tarbell et al. directly applied dibutyryl cAMP, a stable cAMP analog, onto the cell monolayer. This aplication causes Lp to drop precipitously for 30 minutes, where it appears to begin to (at least) level off (Tarbell, Demaio et al. 1999). However, it is known that cAMP stimulation can cause opposing effects in ECs, and the direction of this effect might be dependent on the duration of treatment as well as the fluidic environment. In fact, several findings suggested that two different agonists could both generate a cAMP signal yet impart very different physiological responses. This fact gave rise to the idea that cAMP signals may be spatially segregated into isolated subcellular compartments within a single cell (where different ACs reside) (Hayes, Brunton et al. 1979; Jurevicius and Fischmeister 1996; Willoughby and Cooper 2007). Within the endothelium's plasma membrane, cAMP protects the endothelial barrier, whereas cytosolic cAMP disrupts that barrier (Sayner 2011).

Endothelial Cell-Cell Junctions

The interaction between cell adhesion proteins and the AC plays a key role in regulating endothelium barrier function (Prasain and Stevens 2009). The cortical actin rim tends to reorganize into stress fibers. This process promotes gap formation in response to physico-chemical signals such as cAMP that induce cell border retraction (Pannekoek, van Dijk et al. 2011). Cell-cell contact is provided by several specialized adhesion complexes, the major ones being tight junctions (TJs) and adherens junctions (AJs) which have a different relationship in endothelial cells than the classic geometry of epithelial cells.

Epac1, a cAMP responsive guanine nucleotide exchange factor for the Rap family of small G-proteins, and its effector Rap1 are important mediators of the cAMP-induced tightening of endothelial junctions and consequential increased barrier function(Gloerich, Ponsioen et al. 2010). Recent findings have suggested activation of Rap1 by cAMP/Epac1 induces junctional actin to further tighten EC cell–cell contacts (Gloerich, Ponsioen et al. 2010). Thus, the potential for paracellular transport is directly influenced by the TJs and AJs that connect adjacent cells in the endothelium (Bazzoni and Dejana 2004).

Vascular endothelial-cadherin (VE-cadherin) is a cell–cell adhesion molecule involved in endothelial barrier functions and also plays a central role in proper AJ assembly (Prasain and Stevens 2009). cAMP has been implicated in potentiating VE-cadherin-mediated endothelial cell-cell junctions via ligand binding to GPCRs, such as AVP binding to V2Rs (Noda, Zhang et al. 2010). If ECs indeed have V2Rs and if cAMP has this effect in ECs this would result in enhancing endothelium barrier function reducing paracellular permeability at the same time that cell membrane water transport is enhanced.

Endothelium Control of Vascular Tone

Since EC mechanical properties influence the cellular production of nitric oxide (NO), these properties also dictate the endothelium-dependent control of vasomotor action in the vessel wall: rigid ECs create limited NO, while more compliant cells increase their NO production (Fels, Callies et al. 2010). It has been suggested that changes in the electrical field from altering endothelial plasma membrane potential could affect the polymerization status of the submembranous actin network, which is known to be an important contributor to the mechanical stiffness of a cell (Callies, Fels et al. 2011). ECs respond to blood flow by a membrane potential depolarization due to the activation of Cl^- selective ion channels (Barakat, Leaver et al. 1999; Qiu, Hu

et al. 2003; Barakat, Lieu et al. 2006). Depolarization may soften the ECs to enhance NO transport to the SMCs for vasorelaxation in response to increased blood flow (Callies, Fels et al. 2011). Though it has not yet been shown whether flow changes alter the stiffness of ECs, recent evidence by Callies et al. suggest depolarization caused by flow may soften the EC cortex and account for an increased NO production (Callies, Fels et al. 2011).

Vasopressin type 1a receptors (V1aR) in SMCs are responsible for mediating AVP's effect on vascular tone, i.e., as a vasoconstrictor. The endothelium plays a key role in mediating the effect of AVP on SMCs through V2Rs and hybrid vasopressin type V1a receptor/V2R (V1aR/V2R) (Mechaly, Laurent et al. 1999). In rat aortic strips with intact endothelium, the V2R agonist desmopressin (DDAVP) results in the relaxation of aortic strips precontracted with norepinephrine, while no relaxation was observed in denuded aortic strips (Yamada, Nakayama et al. 1993). Yamada et al. also demonstrated that DDAVP relaxation effect was blocked by a specific inhibitor of NO synthesis, indicating that DDAVP stimulation of vasopressin receptors on the endothelium is at least partially mediated by NO production in the endothelium (Yamada, Nakayama et al. 1993). In addition, V1aRs in rat aorta respond to vasoconstrictors, such as AVP and angiotensin-II, by evoking a response that is transferred to the endothelium and evokes depolarization of EC membrane potential (Marchenko and Sage 1994). This two-way communication within the vessel wall may allow the endothelium to regulate the contraction of VSMC to influence the endothelium, and thus regulate endothelial permeability (Marchenko and Sage 1994).

Natriuretic Peptide Receptor (NPR) system in SMCs and ECs: Communication between cell types

Increases in EC cAMP levels trigger a cascade of cellular responses in adjacent SMCs *in vivo*. These responses originate from the natriuretic peptide receptor (NPR) system. The vascu-

lar smooth muscle is one of the major target tissues of natriuretic peptides (NPs) that induce relaxation and growth inhibition of vascular SMCs (VSMC) (Kishimoto, Yoshimasa et al. 1994). Atrial natriuretic peptide (ANP), brain natriuretic peptide (BNP), and C-type natriuretic peptide (CNP) are the polypeptide hormones that constitute NPs. Mammals, including humans, produce all NPs in their hearts (Levin, Gardner et al. 1998). The vascular endothelium also produces CNP. NPs interact with both the guanylyl cyclase-activated NPRs, NPR-A and NPR-B as well as the non-guanylyl cyclase activating NPR, termed NPR-C (Anand-Srivastava 2005). NPR-A and NPR-B are membrane guanylyl cyclase receptors, while NPR-C is present as monomers and dimers and is coupled to adenylyl cyclase inhibition through inhibitory guanine nucleotide regulatory protein (Gi) (Anand-Srivastava, Srivastava et al. 1987). Figure 7 below illustrates the cascade response of NPs binding to NPRs.

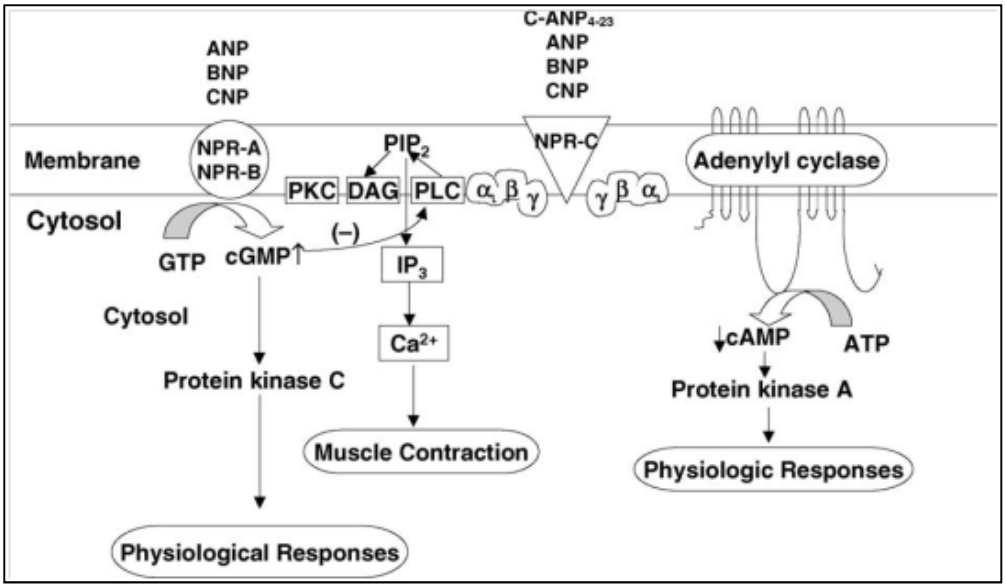

Figure 7: NPR and associated signal transduction mechanisms activated by different NPs. cGMP formation is stimulated by activation of NPR-A and NPR-B by ANP, BNP, and CNP. ANP, BNP, and CNP interact with NPR-C and inhibit adenylyl cyclase activity and suppress cAMP concentrations. *(Anand-Srivastava 2005)*

Stimulation of NPR-A and NPR-B by their respective agonists augments intracellular levels of cyclic guanosine monophosphate (cGMP), whereas NPR-C does not have guanlyl cyclase activity. Stimulation of cGMP inhibits phospholipase C (PLC) activity and results in decreased production of diacylglycerol (DAG) and inositol triphosphate (IP3) as seen in figure 7. NPR-C is coupled to adenylyl cyclase through Gi protein. NPR-C stimulation by any of the NPs results in suppression of cAMP concentrations (Anand-Srivastava 2005). However, NPR-C is also coupled to endothelial nitric oxide synthase (eNOS)-dependent signal transduction, in which NO activates a soluble form of guanylate cyclase and in turn leads to production of cGMP (Murthy, Teng et al. 1998), as seen in Figure 8 below.

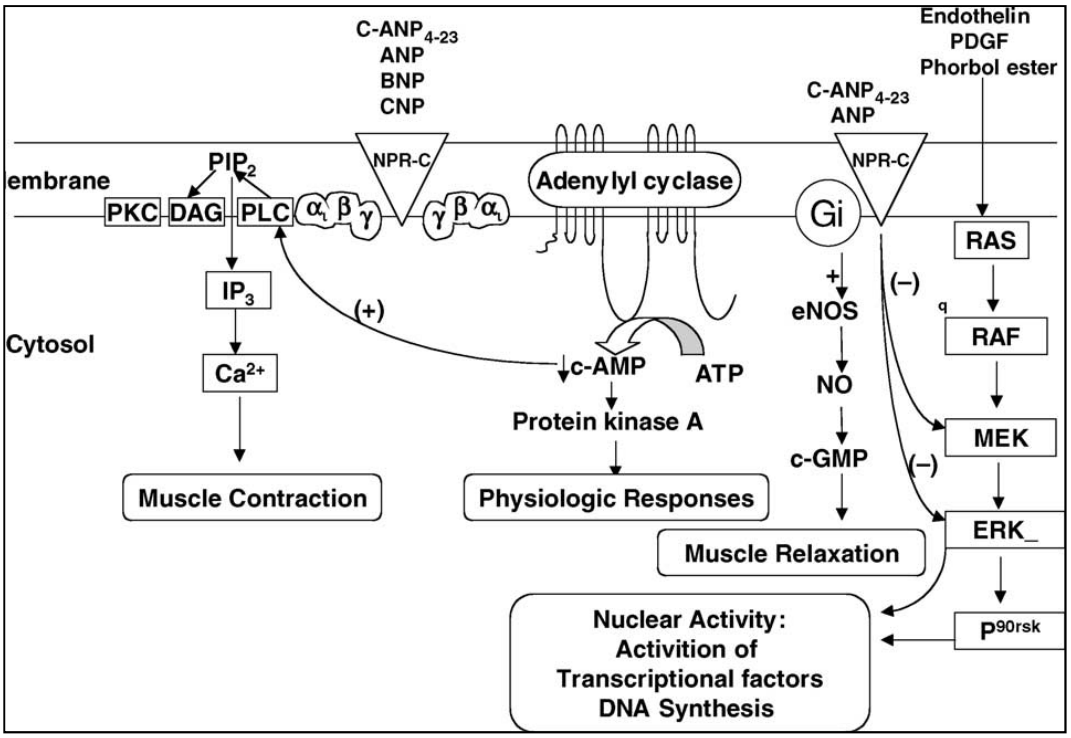

Figure 8: NPR-C and associated signal transduction mechanisms activated by different NPs. *(Anand-Srivastava 2005)*

Activation of the intracellular cAMP-signaling pathway by either F or the cAMP-mimetic dibutyryl cAMP (dbcAMP), a synthetic cAMP analog, significantly increased transcript levels of

NPR-C in primary cultures of human aortic smooth muscle cells (Sellitti and Doi 1999) after 3 hours, but opposite behavior has been observed by Kishimoto et al. (Kishimoto, Yoshimasa et al. 1994) on rat aortic smooth muscle cultures after 24 hours. In contrast cAMP-stimulatory agonists attenuated phosphatidyl inositol (PI) turnover in vascular SMCs in rabbit renal arteries by ANP, suggesting that NPR-C receptor-mediated inhibition of adenylyl cyclase and the resultant decreased levels of cAMP may be responsible for NPR-C-mediated stimulation of PI turnover (Anand-Srivastava 2005).

Studies have also suggested that the antimitogenic effect of atrial peptides is mediated through interaction with the NPR-C receptor and may be independent of changes in cellular cyclic nucleotide levels (Cahill and Hassid 1991). A recent demonstration of a 15-fold increase in CNP transcript in rat thyroid cells in response to dbcAMP (Sellitti, Puggina et al. 2004) invites speculation as to whether endothelial CNP may be up-regulated by cAMP in a similar manner, and thus compensate for an increased clearance by NPR-C. NPR-C-binding to ANP inhibits mitogenesis and proliferation of rat aortic smooth muscle cells (Cahill and Hassid 1991; Anand-Srivastava 2005). AQPs facilitate cell migration by a mechanism that might involve water transport in lamellipodia of migrating cells (Verkman 2005). Antimitogenic cellular responses may lead to reductions in AQP-1 expression in affected cells. It may be possible that cAMP modulation could have alternative effects when both the endothelium and media smooth muscle are present together in contrast to when they are tested as isolated *in vitro* systems.

Above we have reviewed the critical works that have acted as guides and references to the surgical, experimental, and chemical considerations that I have utilized in both the *in vitro* and *ex vivo* studies that I shall present in the subsequent chapters of my thesis. The well-established *ex vivo* (Tedgui 1984; Baldwin 1993; Shou 2006) and *in vitro* models provide a

strong foundation for my further investigation of transport properties in vessels. In these studies we shall investigate the effect of V2R stimulation on Lpe and on AQP-1 expression in BAEC monolayers and in whole rat aortas *ex vivo* for both short and long term treatments. We shall then consider its potential relevance to overall water and macromolecular transport in the artery wall.

Fluid-shear-stress-induced translocation of AQP

Jang et al. have reported that fluid-shear-stress induces the translocation of AQP-2 and actin cytoskeleton (AC) reorganization in renal tubular epithelial cells (Jang, Cho et al. 2011). Exposure to luminal fluid shear stress (FSS) at 1 dyn cm^{-2} induced depolymerization of F-actin in the culture system after 3 hr. This effect peaked at 5 hr. exposure. After 2 h of removing luminal FSS, the actin re-polymerized. Jang et al. also examined the effect of AVP stimulation on these cells both with and without luminal FSS. See Figure 9 below. Vesicle trafficking to epithelial cell membranes appears to be most pronounced under conditions with hormonal (AVP) and luminal FSS (1 dyn cm^{-2}) Figure 9-D. We see the AQP-2 depleted cytoplasmic regions are in stark contrast to the membrane of the cells where FITC-labeled AQP-2 is abundant.

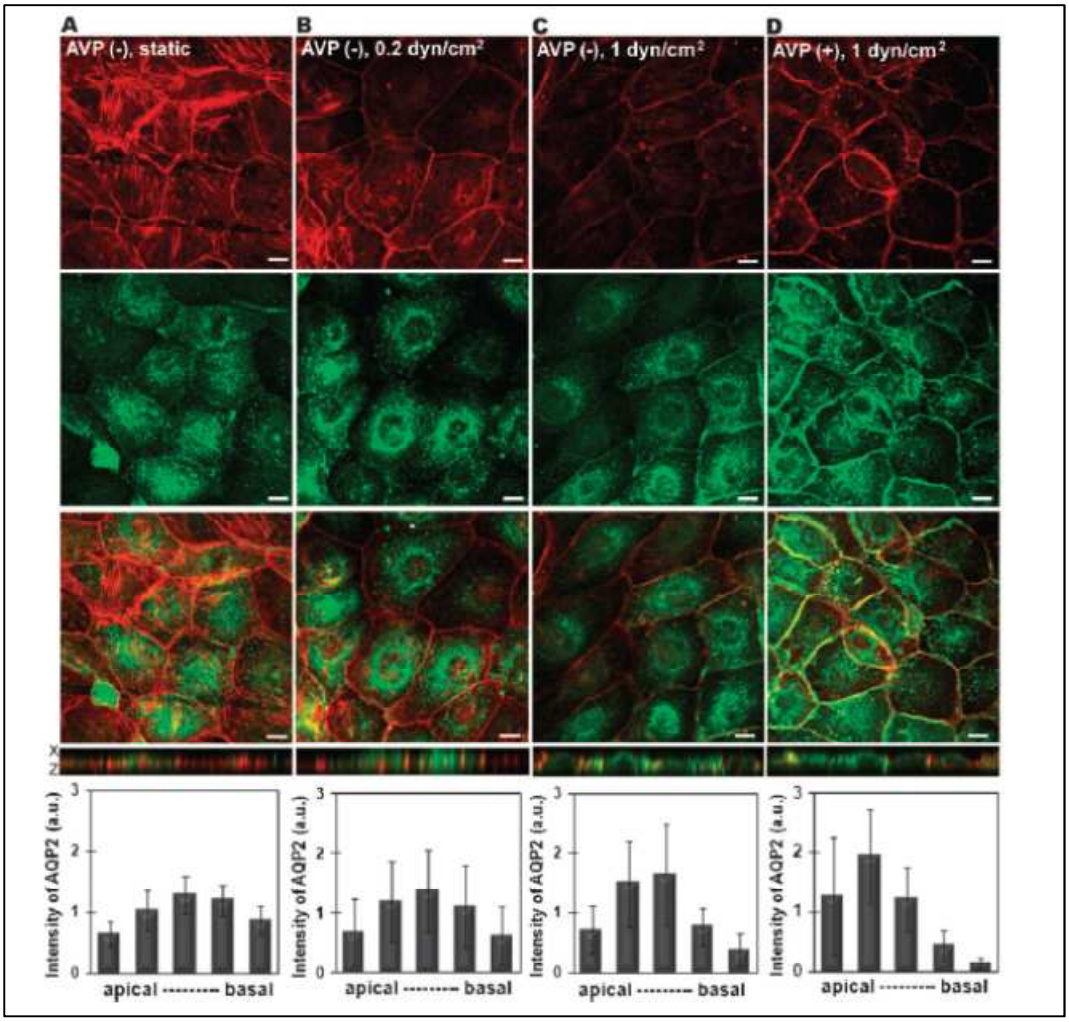

Figure 9: Effects of luminal fluid shear stress (FSS) on F-actin and AQP-2. Confocal micrographs of IMCD cells with TRITC-labeled F-actin (top) and FITC-labeled AQP-2 (below top). Merged channels with x–z reconstructions are shown (2 rows below top). Quantitative analysis of AQP-2 intensity is shown at bottom. Ten regions of interest (each 100 μm^2) at five different sections are randomly selected and compared by using ImageJ™ (bottom). In column A the effects of no hormone or FSS is seen with AQP-2 and F-actin distributed within the cytoplasm of the cell. In B the effects of 0.2 dyn cm^{-2} FSS to the luminal side for 5 h in the absence of AVP, AQP-2 labeling was still largely dispersed in the cytoplasm but initiation of F-actin depolymerization is apparent. Full depolymerization of actin was observed with 1 dyn cm^{-2} and no hormonal stimulation. Greatest AQP-2 localization to cell membrane was observed with 1 dyn cm^{-2} FSS and AVP stimulation on basolateral surface of cell.

Suh et al. also examined the effect of an osmotic gradient on the AQP-2 distribution and on F-actin organization, as illustrated below in Figure 10. An osmotic gradient seems to stimulate F-actin reorganization to the cell membrane.

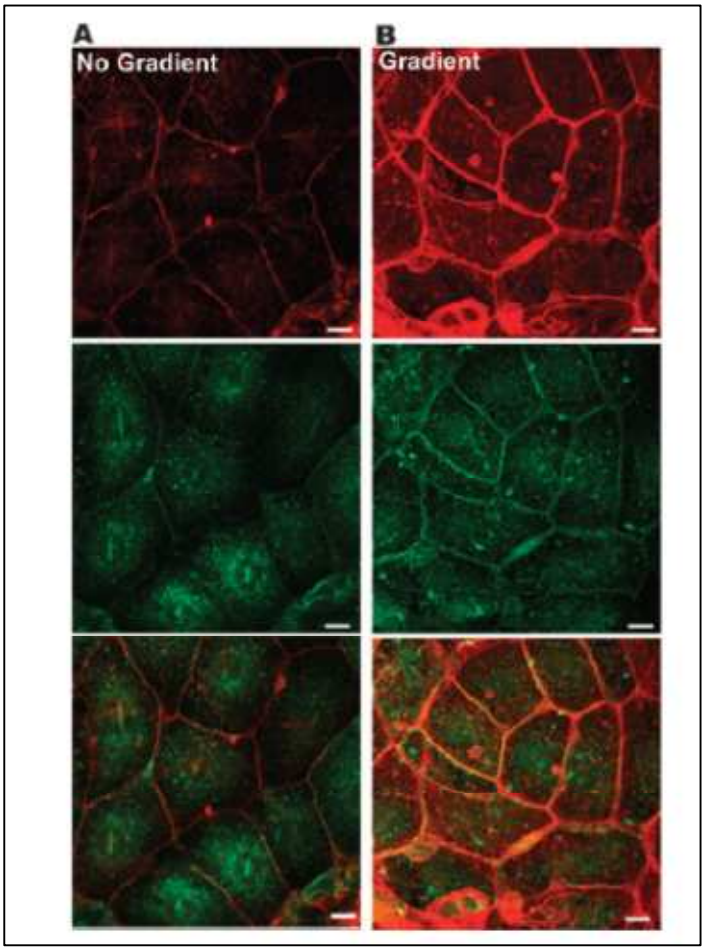

Figure 10: Effect of a transepithelial osmotic gradient on F-actin and AQP-2. Confocal micrographs of IMCD cells with TRITC-labeled F-actin (top) and FITC-labeled AQP-2 (below top). Merged channels with x–z reconstructions are shown (bottom). In this study, all experimental groups were exposed to 1 dyn cm^{-2}FSS. Gradient condition was 300 mOsm per kg H_2O on the luminal side and 600 mOsm per kg H_2O on the basolateral side. With no gradient (A), AQP-2 distribution is localized in the cytoplasm. Full F-actin depolymerization is observed under both conditions (A&B). With an osmotic challenge increased AQP-2 trafficking to the plasma membrane was observed (B). (Scale bar = 10 μm).

Chapter 2. Using chemical agents that upregulate intracellular cAMP to both enhance aortic endothelial cell aquaporin-1 expression and function, i.e., it upregulates endothelial hydraulic conductivity, in cultured monolayers.

Introduction

The pressure inside large arteries is typically ~100 mmHg higher than outside of them. This difference, ΔP, drives a flow of plasma, mainly water and advected/swept-along solutes that would otherwise only transport by (much slower) diffusion (Huang, Rumschitzki et al. 1997), across the porous vessel wall. It is natural to ask whether this flow crosses the arterial endothelium solely through inter-endothelial cell (EC) junctions or whether a portion of the water traverses the ECs via membrane proteins from the ubiquitous aquaporin (AQP) family (Preston and Agre 1991). Data from our group show that bovine (B) aortic endothelial cells (AEC) or BAECs express AQP-1 in cultured monolayers (Nguyen 2008) and that rat (R) AECs express AQP-1 in culture (Xue 2011) and in excised vessels (Toussaint 2009). Chemically blocking AQP-1 or knocking down AQP-1 expression significantly reduces endothelial hydraulic conductivity (Lpe) in both monolayers and in whole rat aortas *ex vivo* (Nguyen 2008; Xue 2011). Upregulating AQP-1 expression on Lpe in vessels and monolayers might be a route towards washing unbound LDL out of the subendothelial intima (SI) before it can bind significantly to SI extracellular matrix (ECM), a process that can lead to preatherosclerotic lesions. Belkacemi et al. obtained a 5-fold expression change in aquaporin-1 (AQP-1) expression after 24 hr. treatment with AVP in trophoblasts, which are cells that form the outer layer of a blastocyst. Unlike endothelial cells, blastocysts provide nutrients to the embryo and develop into a large part of the placenta, and need a monolayer of cells to adhere to in culture.

AVP is stored in the posterior pituitary and is released into the blood-stream; however, some AVP is also released directly into the brain. Belkacemi et al. used experimental and cul-

ture conditions comparable to those used in our group, but on trophoblasts, rather than on BAECs or RAECs. Another agent, forskolin (F) is commonly used to raise levels of cAMP in cell physiology. F resensitizes cell receptors by activating the enzyme adenylyl cyclase and increasing the intracellular levels of cAMP (Yool, Stamer et al. 1996).

Both short term (< 2 hours) AVP (0.1nM) and F (10μM) treatment are known to increase intracellular cAMP and to induce membrane shuttling of internal AQP-2 to the cell membrane in the principal cells of the renal collecting duct. This response is facilitated by vasopressin type 2 receptors (V2R). Long term (>8 hours) AVP and F treatment also causes constitutive upregulation of AQP-2 in these cells.

By measuring changes in cell volume after exposure to hypotonic saline Patil et al. (Patil, Han et al. 1997) and Yool et al. (Yool, Stamer et al. 1996) observed increases in cell membrane permeability after short-term AVP and F treatment in oocytes transfected with AQP-1, suggesting AQP-1 may incur membrane shuttling as well. Expression of V2R has been confirmed in human lung microvascular endothelial cells (Kaufmann, Oksche et al. 2000) and in the endothelium of rat aortic strips (Mechaly, Laurent et al. 1999). These observations suggest that AVP may bind to V2Rs on ECs leading to V2R coupling to Gs, a membrane-associated heterotrimeric G-protein, to stimulate adenylyl cyclase activity, similar to V2R activity reported in the principal cells in the renal collecting duct (Nielsen, Chou et al. 1995).

One consequence of short-term (<2 hours) V2R stimulation is an increase in cellular cAMP content and protein kinase A (PKA) activity which would, if consistent with renal action of V2R, trigger an increased rate of insertion of intracellular AQP containing vesicles into the EC membrane and a decreased rate of endocytosis of AQP from the EC membrane. The distri-

bution of AQP between the cytosolic compartment and the EC membrane compartment would thus shift in favor of the EC membrane component (Nielsen, Kwon et al. 1999) during short term stimulation of V2R or transmembrane cAMP stimulation (via F).

cAMP has been implicated in the regulation of the endothelium barrier (Sayner 2011). The interpretation of cAMP signaling specificity began at the tissue level. However, several findings that reported that two different agonists generate a cAMP signal yet each imparted a different physiological response. This fact gave rise to the idea that cAMP signals may be spatially segregated into isolated subcellular compartments within a single cell (Hayes, Brunton et al. 1979; Jurevicius and Fischmeister 1996; Willoughby and Cooper 2007). Within the endothelium, plasma membrane cAMP protects the endothelial barrier whereas cytosol cAMP disrupts the barrier (Sayner 2011).

V2R belongs to the seven transmembrane G protein-adenylyl cyclase system, and thus has the characteristic of G protein coupled receptors (GPCR) that stimulation by an inverse agonist can induce a physiological effect opposite to that caused by an agonist. Satavaptan (S) is a potent and selective V2R inverse agonist that binds to V2R, which increases intercellular cGMP (Serradeil-Le Gal, Lacour et al. 1996). This leads to the short term shuttling of membrane bound AQP-1 and/or AQP-2 from the cell membrane to vesicles inside of the cell. Long term stimulation of V2R by satavaptan also leads to constitutive decreases in AQP expression (Serradeil-Le Gal, Lacour et al. 1996).

The goal of the present study is to utilize AVP, F, and S to determine the contribution of AQP-1 to Lp in BAEC monolayers. We also seek to investigate the effect of the aforementioned agents in altering AQP-1 expression in BAEC monolayers and to evaluate the corresponding effects on monolayer Lp. Treatments that significantly alter monolayer Lp will then be included in

solute drag analysis under both convective and diffusive conditions to delineate if the said treatment has affected paracellular transport. This will allow us to see if observed changes in monolayer Lp derive from changes to one or both of paracellular and transcellular transport.

Materials and Methods

Reagents

The following chemicals were obtained from Sigma Chemical (St. Louis, MO): bovine serum albumin (BSA: 30% solution, fraction V), minimum essential media (MEM), penicillin-streptomycin solution, L-glutamine, trypsin-EDTA solution, paraformaldehyde (PFA), phosphate buffered saline (PBS), fluorophore 70-kDa TRITC-dextran, fluorophore TRITC-albumin, dimethyl sulfoxide (DMSO), arginine vasopressin (AVP), Triton X-100, forskolin (F), and fibernectin. SR121463A (Satavaptan (S)) was generously supplied by Sanofi Recherche (Toulouse, France). Fetal bovine serum (FBS) was purchased from Hyclone Laboratoies (Logan, UT).

Treatments

AVP was diluted in sterile double distilled water to a final concentration of 0.1nM and 10nM. Treatment time was 20 hours. F and S stock solutions were diluted in 0.1 wt% DMSO. The same final concentrations of DMSO were included in all respective controls. Treatment time for F and F/S was 2 hours. Treatment time for AVP, S and AVP/S was 20 hours.

Cell lines and culture conditions

Bovine aortic endothelial cells (BAECs) were purchased from VEC Technologies, Inc. (Rensselaer, NY) and grown in 10% fetal bovine serum (FBS) in Eagles Minimum Essential Media, penicillin 100U/ml, streptomycin 2.5 μg/ml, and L-glutamine. Cells were maintained at 5% CO_2 and 37ºC in an incubator for 3-4 days until confluent. Cells were plated onto fibronectin coated Transwell 12-well filters (Corning 3460) at a density of 0.625 x 10^5 cells/cm^2. Immu-

nocytochemistry was performed at confluence or 1-day post confluence. Transport experiments were performed 1-day post confluence.

Measurement of Water and Solute Flux

The experimental set-up, the same as used by the Tarbell group (Cancel, Fitting et al. 2007) is housed in a Plexiglas box kept at 37˚C. BAECs grown on a Transwell filter (surface area = 1.1cm^2, 12mm in diameter, 0.4μm pore size) are situated in an aluminum support ring and an O-ring to create a tight seal. This complex is then inserted into the black ethylene tetraphthalate (PET) chamber, thus dividing it into a luminal (top) and an abluminal (bottom) compartment. The luminal chamber is continuously supplied with 5% CO_2. The bottom chamber is connected via Tygon tubing to a borosilicate glass tube followed, via more Tygon tubing, by a fluid reservoir. This reservoir can be lowered to apply a 10cm hydraulic pressure across the monolayer. Water flux (Jv) was measured based on the automatic tracking of the position of the front meniscus of a bubble in the tube over time by a spectrophotometer mounted on a ball-screw with a feedback controller and whose output fed into a digital computer. The bubble velocity, along with the geometrical dimensions from within the glass tube is used to compute Lp.

The same chamber was also custom-fabricated to detect fluorescence intensity in the abluminal compartment so that solute and water flux can be measured simultaneously. Light is excited at 534.4nm by a uniphase helium-argon laser excitation machine (Manteca, CA) and transmitted through optic fibers to each chamber. A photomultiplier detects the emission signals generated by the dissolved fluorophores from excitation light at 543.5 nm via a separate optic-fiber oriented 90˚ to the excitation fiber. Data were collected by FluorMeasure program. At the beginning of the experiment 70-kDa dextran was added to the luminal chamber above the monolayer. After a 60-minute equilibration period under diffusive conditions, the differential 10-cm

hydrostatic pressure was applied across the monolayer and fluorescence data was collected for one additional hour to indicate the passage of solutes by convection. After this phase, the pressure gradient was eliminated and data was collected for another hour under diffusive conditions, completing the experiment.

Calibration curves were acquired on the same device. Fluorescence measurements were taken on solutions of various known tracer concentrations inserted into the lower chamber. The resulting plot of fluorescence intensity vs. concentration allowed for the conversion of fluorescence intensity to fluorophore concentration.

Experimental solute permeability, Pe, in units of area/time, was obtained from the following equation, which is based on the rate of change, $\Delta C_a/\Delta t$, in the abluminal solute concentration with respect to time:

$$P_e = [(\Delta C_a / \Delta t) \times V_a] / (C_p \times A)$$

Here Va is the fluid volume of the abluminal chamber, A is the area of the monolayer and Cp is the luminal concentration of the solute. This equation incorporates the facts that changes in both Va and Cp were negligible during an experiment, and Ca << Cp (Cancel, Fitting et al. 2007). The protocol described above was then followed to determine solute permeability.

Immunocytochemistry on BAEC Monolayers

BAECs were grown on round cover slips coated with fibernectin until confluence followed by treatment with AVP, F, S, AVP/S, F/S, or 0.1% DMSO. BAECs were fixed in 3.7% PFA for 10 minutes, washed three times in PBS, permeabilized 0.1% Triton X-100 in PBS for 10 minutes, and then blocked with 1% BSA for 30 minutes. The blocking solution was removed by aspiration, and the monolayers were exposed to rabbit anti-rat AQP-1 antiserum (Alpha Diagnos-

tics Intl, San Antonio, TX) diluted in 15% goat serum and 0.2% BSA in PBS. The primary antibody was diluted 1:500. The incubation was done in a humid chamber at room temperature for 60 minutes. The cell layers were subsequently washed three times with PBS. They were then incubated with Alexa-488 conjugated goat anti-rabbit IgG (Invitrogen, Carlsbad, CA) at a dilution of 1:200 (in PBS plus 1% goat serum) for 30 minutes, rinsed with PBS, and then mounted to a microscope slide. The samples were stored in a humid chamber in the dark before imaging with a Leica TCS SP2 AOBS confocal microscope using a 488nm Argon laser.

Image Acquisition

Samples were analyzed by performing quantitative confocal microscopy. Laser intensity was calibrated at the beginning and during image acquisition to allow for quantitative comparison between different samples. This ensured that each sample endured identical laser power and exposure. All other external conditions such as room temperature, humidity and stray lights were strictly monitored. The calibration of the microscope was done using a Coherent Ultima LabMaster Power and Energy Dual-Channel Meter attached to a LM-2 silicon HD visible optical detector wand. A sample was placed on the microscope stage and the embedded tissue was brought into focus using the 40x PL APO N.A. 1.25 oil immersion objective. The sample was then removed and replaced by the optical detector in the exact position over the objective. The 488nm Argon laser was then initiated and the detector was shifted around in order to find its "sweet spot," that is where the fullest intensity of the laser is felt. Both for different set of samples obtained after immunocytochemistry on different days and even for different samples from the same sample set, we adjusted the laser settings on the confocal microscope both before and periodically during the measurement procedure to obtain the same calibrated values on the laser meter for confocal scanning.

Image Processing

Figure 11 details the technique used to quantity confocal image stacks. Slides were imaged on a Leica TCS SP2 AOBS confocal microscope using a 488nm Argon laser (Figure 11, top left). All slides were exposed to the same laser duration and intensity. Regions of interests (ROIs) were auto-thresholded (Figure 11, bottom left) using NIH Image-J, which chooses a threshold based on the integrated intensity histogram and gradient data of a confocal image (z-)stack to obtain cell outlines (Figure 11, top right). Total area and total fluorescence intensity of cell outlines were computed in Image-J by applying outlines to original image (Figure 11, bottom right) and integrating either one or the fluorescence intensity over the outlined region. Integration of these images dz across the z-stack gives the total (volume) intensity (TI) and the total cell volume (TV). Comparing TI/TV for different samples gives relative values of their aquaporin-1 expression, expressed as total AQP-1/total cell volume.

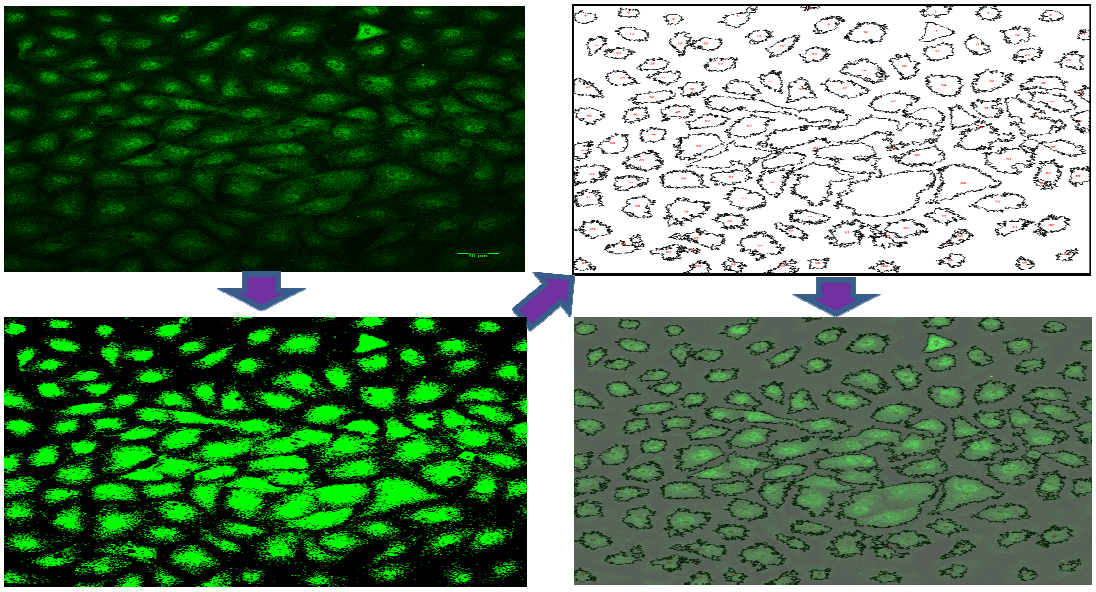

Figure 11: Immunocytochemistry routine to obtain cell monolayer outlines, total intensity (TI), and total volume (TV).

Results and Discussion

Quantification of Immunofluorescence

Figure 12 below summarizes the effect of various treatments on AQP-1 distribution in BAECs based on confocal microscopy analysis. See caption in Figure 12. The intensity of the green fluorescence indicates the level of expression of AQP-1, presumably in direct proportion to green intensity. These figures show that the control cells display bright green coloring, with particularly strong intensity near the cell centers or nuclei where the cells are at their thickest. S treatment yielded far dimmer images, indicating a downregulation of AQP-1, but with particular dimming in the cytoplasm, including the nuclear region. This likely indicates a cessation or near cessation of AQP1 production in response to S. In contrast, treatment with AVP alone yielded the opposite effect: images that were brighter overall and, in particular, in the nuclear area than control. Although F treatment yielded images in which the brightness appeared more intense near the cell perimeter and less intense near the cell center, the nuclei themselves looked darker than the cytoplasmic region. This trend is consistent with a reorganization of internal AQP-1 stores towards the cell membrane in response to F treatment, as seen in epithelial cells with AQP-2 (Jang, Cho et al. 2011). In contrast, the AVP images, especially the close-up of a single cell, are clearly brighter than control and, at the same time, still exhibit intense fluorescence in the nuclear region and similar intensity in the membrane region. We are currently reanalyzing these images to characterize AQP-1 expression in EC membrane versus EC cytosol. These trends are indicative of both insertion of internal AQP-1 into the cell membrane and the subsequent constitutive upregulation of AQP-1 in the nuclear region.

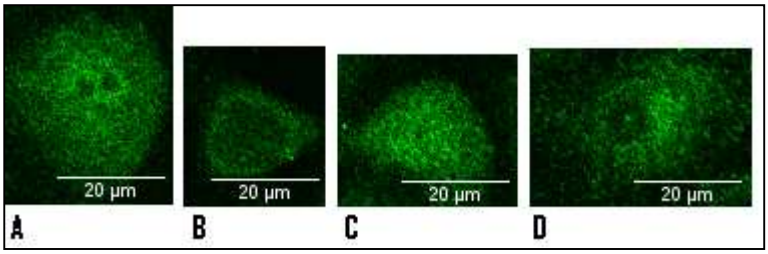

Figure 12: Summary of BAEC Immunocytochemistry results. From left to right, (A) untreated BAEC expressing AQP-1 in green distributed throughout cell, (B) S treated BAEC expressing AQP-1 distribution localized in membrane relative to AQP-1 deficient cytosolic region (C) AVP treated BAEC expressing greater AQP-1 labeling in nucleus and cytoplasm, and (D) F treated BAEC depicting AQP-1 labeling localized in membrane relative to AQP-1 deficient cytosol.

Figure 13 and Figure 14 show the results of the quantitative analysis of these images expressed in the form TI/TV, which represents the total green fluorescence per unit EC volume, which we presume to be proportional to the AQP-1 concentration per unit EC volume, expressed in arbitrary units. Control samples were treated with 0.1%wt DMSO to allow us to distinguish the effect of treatment with our agents of interest from background in altering TI/TV. TI/TV for untreated samples was 0.54 integrated intensity per cubic microns. Note that TI/TV levels below ~0.19 integrated intensity per cubic micron are essentially noise. This was determined from quantifying a series of controls which demonstrated nonspecific binding of the primary antibody, secondary antibody, isotype control, or AQP-2 antibody. Each of these controls yielded TI/TV < 0.19 integrated intensity per cubic micron.

AVP treatment raises TI/TV by 52% in BAEC monolayers as compared to untreated monolayers, again consistent with constitutive upregulation. Short term F treatment did not significantly change TI/TV relative to control, again consistent with a pure translocation of AQP-1 from internal stores to the cell membrane and no constitutive up or down regulation. 20 hour S treatment decreased TI/TV -44%, which is consistent with it being an inverse V2R agonist, and

not simply a V2R antagonist. However, Figure 12 does not indicate a reverse translocation of AQP1 from the membrane to the cytoplasm upon treatment with S. The mixed treatment results are a bit more subtle. Combined two-hour F/S treatment decreased TI/TV -29%. Apparently S is still able to downregulate AQP-1 expression, while F favors membrane insertion over cytoplasmic vesicles. The lower downregulation of TI/TV could indicate that F may partially mitigate the inverse agonist effect of S. 20 hr. AVP/S treatment caused no significant change in TI/TV; apparently the opposing effects of these agents nearly cancel, although AVP binding to V2R on EC is blocked in the presence of S. AQP-1 labeling intensity seemed fairly uniform in ECs treated with AVP/S treatment. As we shall see below, AVP/S treatment yielded similar decreases in Lp, suggesting complete blockage by S. See Figure 13 and Figure 14 below.

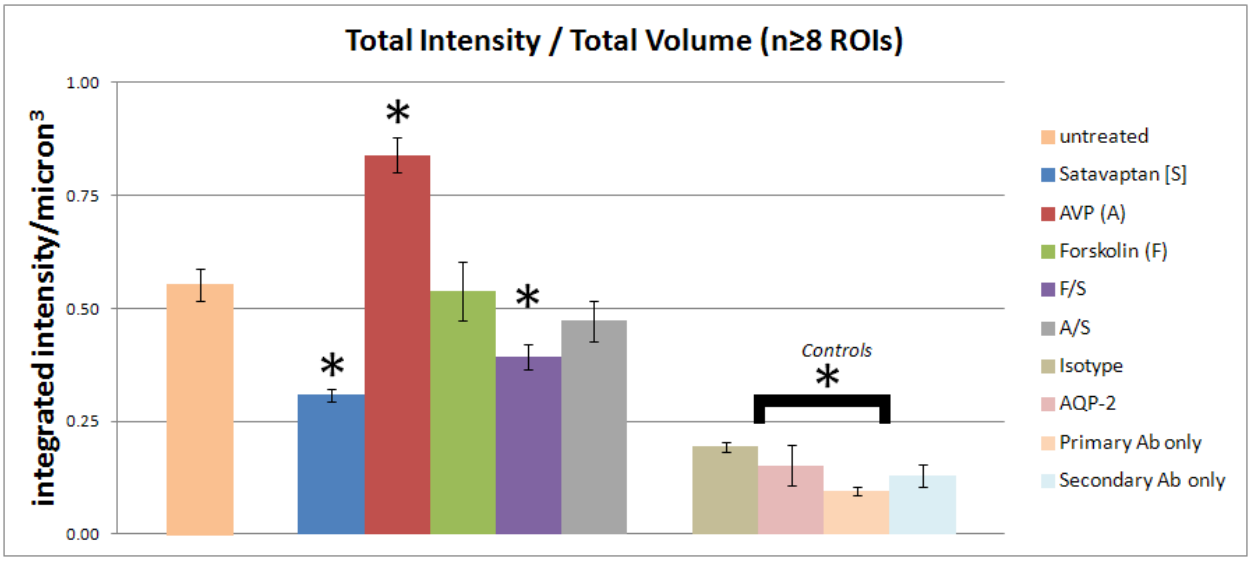

Figure 13: Immunocytochemistry analysis of AQP in BAEC monolayers. A series of controls, seen above, provided threshold for nonspecific binding of the primary antibody, secondary antibody, isotype control, or AQP-2 antibody. Each of these controls yielded TI/TV < 0.19 integrated intensity per cubic micron, which we interpret as noise. We note important trends in the next figure. (*indicates significant statistical difference against untreated sample (unpaired, $p<0.05$))

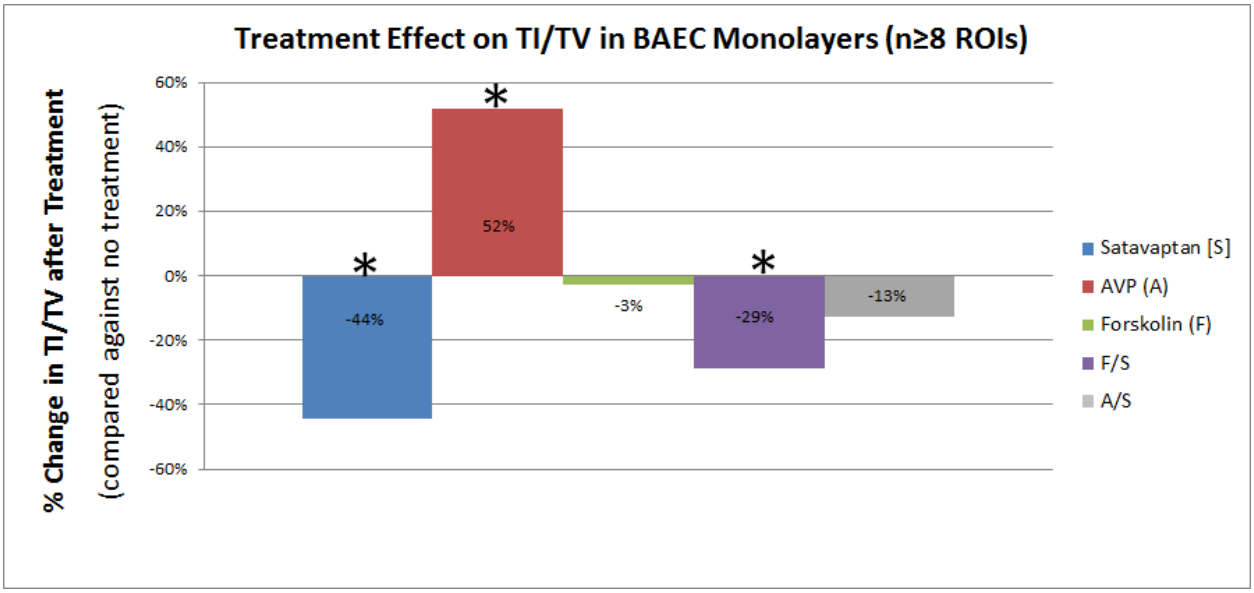

Figure 14: Treatment Effect on TI/TV in BAEC Monolayers. A/ S treatment significantly altered TI/TV compared to untreated monolayers. F and A/S did not significantly alter TI/TV versus untreated monolayers. F/S treatment reduced TI/TV compared against untreated monolayers. These results are consistent with F action to redistribute AQP-1 from cytosol to cell membrane, while A and S induce constitutive changes in AQP-1 expression. F/S did result in a constitutive change in AQP-1 expression based on TI/TV while A/S did not. (*indicate significant statistical difference against untreated sample (unpaired, $p<0.05$))

Water Flux Experiment

As described in the methods section, our functional, i.e., Lp, experiments complement our immunocytochemistry. The latter tell us how much AQP-1 is present and the former tell us the effective functionality of transcellular transport added to junctional transport. We shall then appeal to our tracer experiments to see whether measured functional differences are due solely to changes in the transcellular route, which we may then try to associate with changes in AQP-1 levels, or at least partially from changes in the junctional route.

Figure 15 shows that 20 hr. AVP treatment/ stimulation of V2R increases monolayer Lpe by 34±9%, which is consistent with constitutive AQP-1 upregulation by AVP, as observed in TI/TV analysis. After 20 hours, constitutive increases in AQP-1 expression appear to increase the presence of intracellular vesicles containing AQP-1, presumably as a means to store excess

protein for later migration to cell membrane in response to cellular demand and/or environmental queues. V2R may also be migrating from the membrane into intracellular vesicles in analogous fashion to epithelial cells after V2R stimulation to allow the cell to sense further increase in AVP (Bouley, Hawthorn et al. 2006).

Short term F treatment increased Lpe by an astonishing 172±49 %, presumably by a strong short term membrane shuttling of internal AQP-1 to the cell membrane, see comment in fig.19. Though two hr. F treatment did not significantly change AQP-1 numbers as expressed by TI/TV (consistent with F inducing only a shuttling effect and not a constitutive upregulatory effect at these treatment time), it drastically changed Lp. Since AVP acts on V2R to increase intracellular cAMP in renal epithelial cells, which then leads to constitutive upregulation of AQP1 and to AQP1 shuttling from internal stores to the cell membrane (Jang, Cho et al. 2011), perhaps F, acting through a non-V2R route, to also increases cytosolic cAMP in order to achieve translocation (Sayner 2011). Such AQP-1 insertion into the cell membrane is most likely responsible for this large increase in permeability. In contrast, 20 hr. treatment with S decreased Lpe -46±7 %, which is in accord with its observed effect of decreasing TI/TV, likely by increasing cGMP (Serradeil-Le Gal, Lacour et al. 1996). Higher cGMP is known to favor intracellular vesicle formation over AQP-1 residence in the cell membrane (Mechaly, Laurent et al. 1999; Jang, Cho et al. 2011). F/S treatment did not significantly change Lpe, agreeing with its lack of effect on TI/TV, and its slight apparent rearrangement towards the cell membrane does not appear to be enough to significantly affect Lp. AVP/S treatment decreased Lpe -38±9 %, which is consistent with AVP/S treatment effect on decreasing TI/TV, both by amounts less than with AVP alone. This supports S acting as an inverse agonist and not simply as an antagonist.

Recall that Figure 15 illustrates showed that short term F treatment has a greater then 4-fold greater increase in Lp compared to effect of long term AVP treatment, consistent with short term shuttling of intracellular vesicles containing AQP-1 to the cell membrane. The binding of the AVP to V2Rs on renal principal cells stimulates cAMP synthesis via activation of adenylate cyclase. The subsequent activation of PKA leads to phosphorylation of AQP-2 at serine256, and this phosphorylation event is required to increase the water permeability and water reabsorption of renal principal cells (Noda, Horikawa et al. 2008). Noda et al. showed that when AQP-2 in intracellular vesicles becomes phosphorylated at SER256, it binds to tropomyosin 5b, which in turn depletes free tropomyosin from the vicinity of the AQP-2 vesicle, thereby fostering local F-actin depolymerization (Noda, Horikawa et al. 2008). This has the effect of cutting a hole in the cortical actin network around the vesicles, liberating AQP-2 vesicles from their F-actin cage to reach the plasma membrane. Our results suggest that F treatment, through its transmembrane effect of increasing intracellular cAMP, has a similar effect on AQP-1 stored in intracellular vesicle in endothelial cells. This subsequent actin cytoskeleton reorganization, via recruitment of intracellular AQP-1 containing vesicles to the cell membrane, may account for the increase Lp in BAEC monolayers.

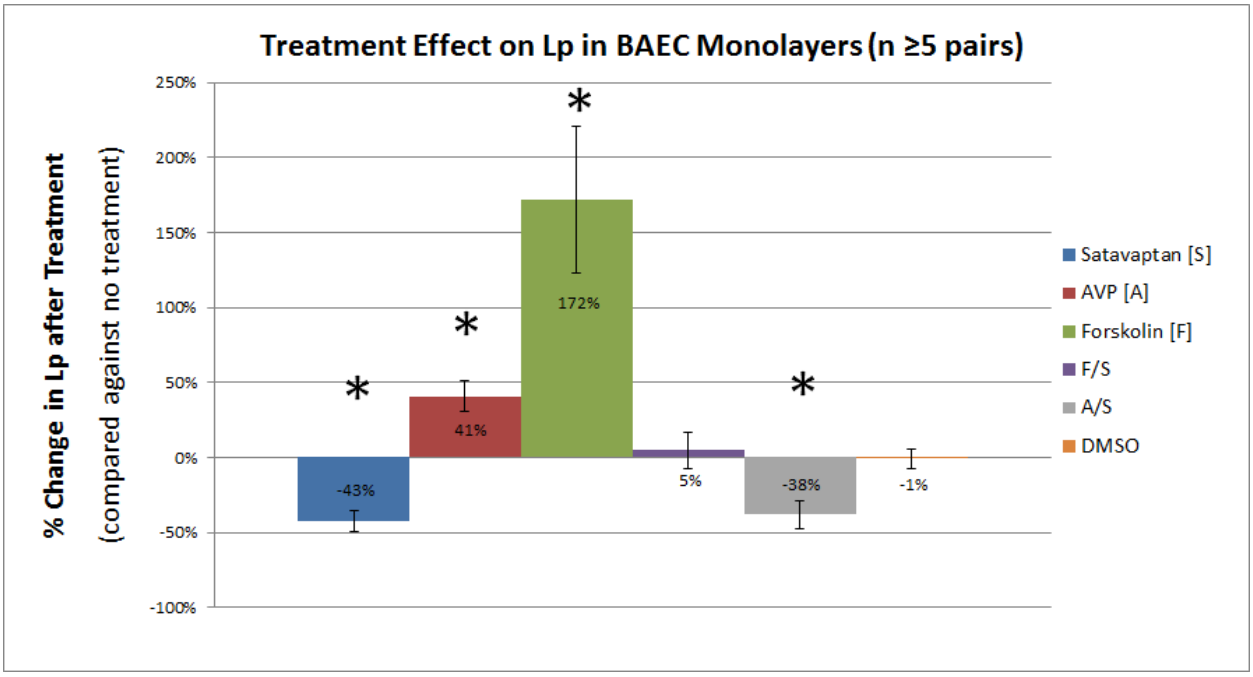

Figure 15: Treatment Effect on Lpe in BAEC Monolayers. F had a drastic effect on increasing Lp, presumably by increasing cytosolic cAMP and increasing permeability (Sayner 2011). AVP treatment modestly increases Lp with similar effectiveness as S treatment effect of decreasing Lp. A/S treatment decreases Lp in similar fashion to S treatment alone, confirming S acts as a blocker and inverse agonist to stop AVP effect. F/S did not significantly change Lp, suggesting competing effects of F and S on monolayer Lp. (*indicate significant statistical difference against untreated sample (paired, $p<0.05$))

Tracer Experiment

Our present Lp studies show that F treatment increases Lp by 171.1±49% (n=6 pairs) in BAEC monolayers, presumably by increasing intracellular cAMP, which subsequently translocates AQP-1 from intracellular vesicles to the cell membrane. However, F treatment may also affect the intercellular junctions, and some or all of this observed change in Lp may be due to junctional effects. In order to differentiate between changes in transport via the paracellular and the transcellular routes, we perform a study of monolayer permeability to 70-kDa dextran, a tracer that only traverses the paracellular route. In particular, this study will provide insight into what portion of the observed Lp increase is due directly to AQP-1 (transcellular pathway). Paracellular transport of 70-kDa dextran occurs by advection, where solutes are carried by the flow of bulk fluid (usually water), driven by a transmural pressure gradient; and by diffusion, the random

Brownian motion movement of solutes driven by a chemical potential gradient, which is closely related to the tracer's concentration (actually, thermodynamic activity) gradient. We have utilized a large tracer molecule (70-kDa dextran) because its transport is not dominated by advection, but rather has both diffusive and advective contributions. We know this by examining its Peclet number, which is the ratio of mass transport by convection along the channel to mass transport by diffusion across the channel, given by the equation below:

$$N_{Pe} = \frac{J_v}{A}\frac{(1-\sigma)}{P_e} \qquad (1)$$

where Jv/A is the volumetric flux, σ is the reflection coefficient of solute, and Pe is the diffusive permeability. The Peclet number for dextran-70kDa is order 1 in BAECs since both convection and diffusion contribute to transport (DeMaio, Tarbell et al. 2004). Figure 16 shows that F treatment reduces monolayer permeability Pe, by ~37% under advective conditions, but induces no significant difference in Pe under purely diffusive conditions. One of the structural end points of stimulated cAMP levels is an increase in the mean number of tight-junction strands between endothelial cells (Adamson, Liu et al. 1998). Whereas the change in Pe with F treatment under advective conditions is curious, it is important to stress that F's effect on tracer Pe is opposite to the change in Lp.

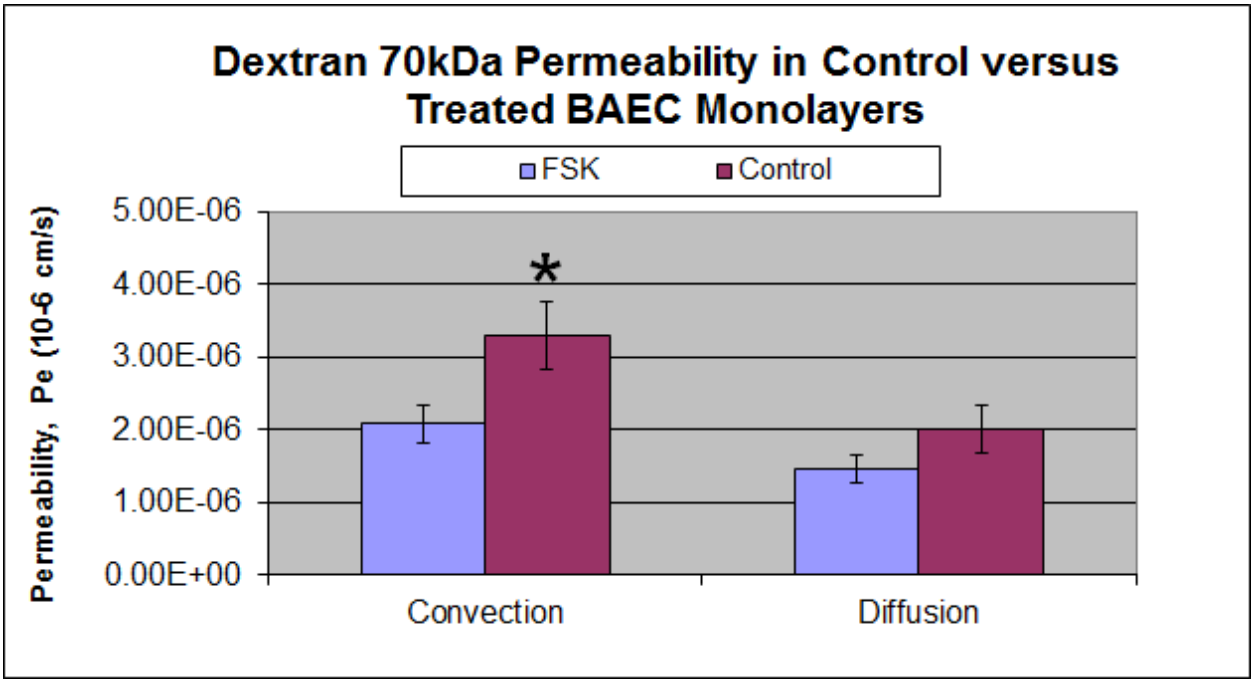

Figure 16: Forskolin's effect on Solute Transport under diffusive and advective conditions. Though F treatment increased overall Lp through BAEC monolayers, it had the opposite effect on convective solute permeability by reducing 70-kDa dextran Pe 37% under convective conditions, while causing no significant change to Pe under diffusive conditions. (*indicate significant statistical difference against untreated sample (ANOVA, $p<0.05$))

Summary

In the present study we have demonstrated that two agents that had previously been shown to cause a transfer of AQP-1 from intracellular stores to the cell membrane and, in longer treatments, constitutive upregulation of AQP-2 in renal epithelial cells (Jang, Cho et al. 2011) also so induce analogous effects with AQP-1 in BAEC monolayers. We have shown that long term (20 hr.) AVP treatment, which works via the V2R pathway that is present in kidney cells and has recently been identified in aortic endothelial cells as well, increases AQP-1 expression, demonstrated as a change in TI/TV, and Lp in BAEC monolayers. The increase in Lp is consistent with the constitutive upregulation of AQP-1. Short term (2 hr.) F treatment does not change TI/TV but seems to cause its localization to shift from the cytosol to the cell membrane. These

changes in AQP-1 distribution and expression are consistent with a cytosolic increase of cAMP. S, an inverse agonist of the V2 receptor, reduces TI/TV, which is consistent with it being an inverse V2R agonist, and not simply a V2R antagonist, but our results do not indicate that it causes reverse translocation of AQP-1.

In addition to inducing changes in AQP-1 distribution and expression, these treatments simultaneously and consistently cause changes in monolayer Lp. Both AVP and F increase monolayer Lp, the latter increase being far larger in magnitude while S decreases it. These results are consistent with the interpretation that cell membrane AQP-1 facilitates transcellular water transport (Nguyen 2008). In order to test this interpretation, we performed tracer experiments using 70kD dextran. Since the Peclet number for 70 kDa dextran is order one, both advective and diffusive transport are relevant. We found that F treatment did not change monolayer tracer permeability under diffusive conditions but reduced it slightly under convective conditions. This may be the result of F treatment altering the morphology of the EC junctions to lower solvent flow and/or to increase solute filtration. These results indicate that F treatment appears to slightly inhibit paracellular advective transport, and so the observed increase in Lp with F treatment apparently increases transcellular transport sufficiently to more than overcome any decrease in paracellular water flow that may be responsible for the observed decrease in paracellular tracer transport.

Thus we have clearly demonstrated that short-term treatment with F increases Lpe and cell membrane AQP-1; long-term AVP treatment increases both Lpe and cellular AQP-1 expression in BAEC monolayers. This holds out the possibility of the manipulation of transendothelial water flow in whole vessels by substantially upregulating the arterial endothelial cell AQP-1 expression and/or distribution in the those cells. Our earlier work indicated that, although the SI is

decompressed at low transmural pressures, it is fully compressed, leading to low overall wall Lp, at the mean physiological pressure of 100 mmHg. Therefore, chemical manipulation of endothelial AQP-1 expression and distribution may conceivably increase arterial endothelial Lpe sufficiently so as to decompress the arterial SI at physiological pressures, thereby resulting in a substantially increased overall wall Lp and therefore an increased overall transmural water flux. Such an increased flux might sufficiently dilute the concentration of the LDL that has entered the SI across localized endothelial macromolecular leaks so as to significantly slow the rate of LDL binding to SI extracellular matrix. This might have a beneficial impact in atherogenesis. The next step of our study is to investigate the short-term effects of F on Lpe as a function of transmural pressure in whole rat aortas *ex vivo*.

Chapter 3. An agent that increases endothelium cell membrane cAMP increases membrane bound aortic endothelial cell aquaporin-1 expression and simultaneously upregulates endothelial hydraulic conductivity in whole vessels *ex vivo*.

Introduction

A significant route for the transport of low-density lipoprotein (LDL) cholesterol, a large (~23nm) molecular aggregate that is too large to traverse normal interendothelial junctions, from the blood across the arterial endothelium and into the subendothelial intima (SI) region is through the widened junctions that surround roughly 1/200-5000 (in rat aorta) arterial endothelial cells (Chien 1988). Some of these cells have widened junctions because they are either dividing, dying or have stigmata. Our group has shown that this transport is advection dominated. That is, the pressure inside large arteries is typically ~100 mmHg higher than outside of them. This difference, ΔP, drives a flow of plasma, mainly water and small solutes, across the vessel wall. The flow through these rare widened junctions advects/sweeps-along larger solutes, such as LDL, that would otherwise only transport by (much slower) diffusion (Huang, Rumschitzki et al. 1997), across the porous vessel wall.

LDL that has entered the SI, where it can bind to SI extracellular matrix (ECM) and trigger processes that lead to preatherosclerotic lesion formation. The flow across the normal endothelium, which accounts for by far the major portion of the transendothelial plasma flow, has the potential to dilute the SI concentration of LDL and thereby slow own its kinetics of binding to SI ECM. In other words, it can potentially sweep unbound LDL from the SI before it has the chance to bind to SI ECM. It is natural to ask whether this flow crosses the arterial endothelium solely through the normal (not-widened) inter-endothelial cell (EC) junctions or whether a portion of the water traverses the ECs via membrane proteins from the ubiquitous aquaporin (AQP) family (Preston and Agre 1991). Data from our group show that BAECs express AQP-1 in cultured

monolayers (Nguyen 2008) and that RAECs express AQP-1 in cultured monolayers (Xue 2011) and in excised whole vessels (Nguyen 2008). Chemically blocking AQP-1 or knocking down AQP-1 expression significantly reduces endothelial hydraulic conductivity Lpe, the ratio of the transendothelial flux to pressure difference, in monolayers and in whole vessels (Nguyen 2008; Russell 2009; Xue 2011). Upregulating AQP-1 expression on Lpe in vessels and monolayers might be a route towards increasing the washing LDL out of the subendothelial intima (SI) before it can bind significantly, which, as noted, is a process that can lead to preatherosclerotic lesions. Our results in Chapter 2 show that cAMP stimulation with arginine vasopressin (AVP) or forskolin (F) induces AQP-1 shuttling in cultured BAEC monolayers that increases endothelial cell membrane AQP-1 concentration and, consistently, Lpe. In this chapter we examine if analogous treatments have similar effects in whole vessels *ex vivo*. In contrast to F treatment, in addition to increasing cAMP, AVP treatment triggers constrictive responses in SMCs via V1a receptors at the micromolar concentration range of dosage. To avoid such indirect treatment effects on SMCs, we focus on F as a potential agent to effect an increase in intracellular EC camp, and consequently in Lpe, in whole vessels.

Huang reported that the arterial SI had a much higher void space (Huang 1994) than the media (~95% vs. ~40) (Tedgui 1987). They postulated that the dense arterial media is incompressible, but that the very sparse SI would easily compress with increasing transmural pressure, ΔP. This compression would increase fiber density and flow resistance in the SI. Under maximum subendothelial intimal compression, when the intima's collagen matrix supports the pressure load, the ECs might block some of the fenestrae in the IEL through which water apparently enters the media. A theory incorporating these effects with compression quantitatively accounts for the observed sharp decrease in wall Lp with ΔP at low pressures, and the pressure-

independence of wall Lp at higher ΔP. Thus only a fraction of the drastic drop in Lp that we observed from 60 to 100 mmHg is due directly to a drop in endothelial Lpe, and the balance to the consequent SI compaction and fenestral blockage.

Our group has developed a filtration theory that suggests (Joshi et al., pending) that increasing in EC AQP-1 increases the endothelium's hydraulic conductivity (i.e., decreases its flow resistance). This would shift a larger portion of the transmural pressure from the endothelium to the media. Thus one would need a higher overall ΔP across the wall under increased endothelial Lpe in order to achieve the critical force/area (i.e., ΔP) on the endothelium in order to induce full SI compression, and thus fenestral blockage that drastically lowers wall Lp. See Figure 17. Thus an increase in endothelial Lpe brought on by shifting AQP-1 to the cell membrane and/or constitutively upregulating AQP-1 in aortic ECs, might be sufficient to move the critical ΔP above the normal time-average physiological ΔP. As such, at physiological conditions, the aortic SI would be decompressed, causing overall wall Lp to rise and increasing transmural water flow and the flushing of free LDL from the arterial SI.

Figure 17, from Joshi et al.'s theory, makes this prediction precise. The red curve is Lp vs. ΔP for the normal untreated aortic wall. Notice that, at low pressures up to ~60 mmHg, increasing ΔP, despite compressing the SI, does not cause fenestral blockage, and therefore does not significantly affect Lp. However, at 60 mmHg, such blockage and consequent Lp lowering begin and SI compression reaches its maximum value at ~100 mmHg. This curve agrees well with Lp vs. ΔP data on both rabbits and rats (Tedgui 1984; Shou 2006; Nguyen 2008; Xue 2011). The theory then predicts what specific percentage increases in endothelial AQP-1 expressions would do to Lpe (not shown) and consequently on whole wall Lp. At low ΔP, these curves have slightly higher Lp than the untreated vessel because increased AQP expression in the EC wall

increases Lpe and thus whole wall Lp. More critically, as we described qualitatively, the critical ΔP for full SI compression moves to the right with increasing AQP-1 expression. Beyond this maximum compression, Lp remains unchanged, since no further blockage can be affected. In order to test these predictions, one needs to choose a regime in which to measure Lp of whole vessels *ex vivo*, first without treatment and then with F treatment, on the same vessels.

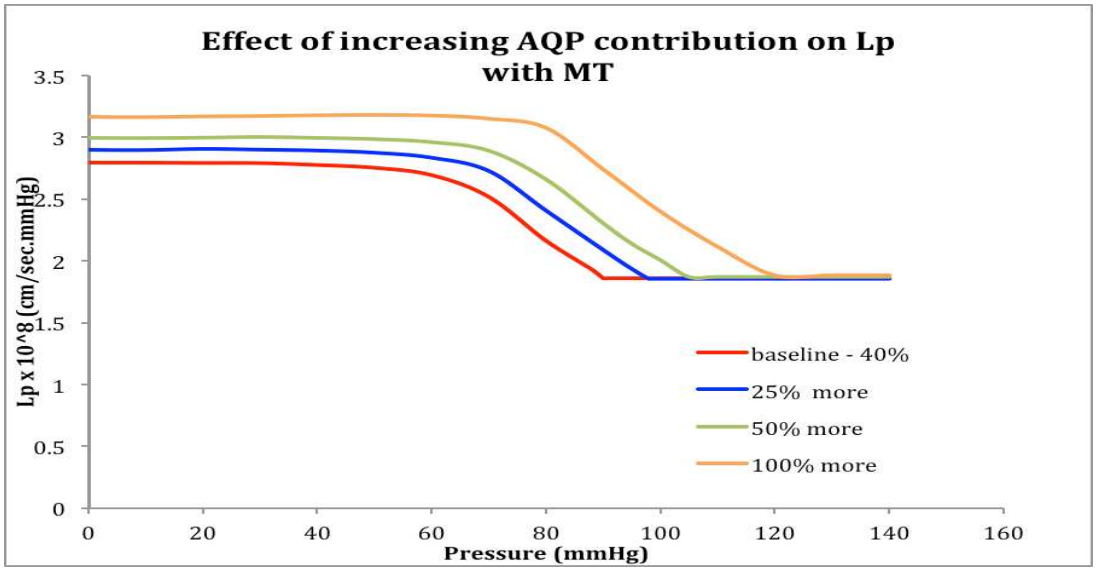

Figure 17: Effect of increasing AQP contribution on Lp with mass transfer (MT).

The figure suggests the dynamic range where one would observe large differences in both SI compaction and consequently in wall Lp from baseline conditions to F treatment is from roughly 60mmHg to 90mmHg. Moreover one would expect F treatment to effect only small changes in Lp is constant at pressure less than 60mmHg (these differences may not exceed the error of measurement) and little or no change in Lp with F treatment at ΔP greater then ~120mmHg. Thus we shall focus on Lp measurements, first before and then after F treatment, on vessels at 75mmHg and at 120mmHg. We predict a large increase in Lp at 75 and essentially no change in Lp at 120 mmHg. In this chapter we shall carry out these measurements and compare with this theory.

Methods

Hydraulic Conductivity Experimental Setup

In the Figure 18, Reservoir 1 controls the pressure of fluids in A&B, while Reservoir 2 controls the pressure of fluids in C&D. These large reservoirs provide a stable and sustained pressure for intubation of an excised vessel. A three-way connector is connected adjacent to the vessel to allow the insertion of a bubble and subsequent velocity tracking by the spectrophotometer tracking system within a glass tube. Using a forcep, one clamps off tubing at the proximal end of the excised vessel to quickly and reliably initiate the experiment. The valve connected to reservoir 2 is opened and one pumps reservoir 2 to the desired pressure. As fluid permeates through the vessel wall, the spectrophotometer continuously tracks the position of the bubble's leading meniscus and records for 30 minutes of steady bubble velocity. Vessel dimensions are obtained by measuring outside diameter at three points along length of aortic tissue digital calipers (accurate to ±0.1 mm (Shou 2006)). The solution used to perfuse the vessel contains 4% (w/v) bovine serum albumin (BSA), phosphate buffered saline (PBS), 10^{-3}M $NaNO_3$, and 0.03% trypan blue dye. The dye is used to identify leaks and nonviable cells The dye is used to identify leaks and nonviable cells (Tedgui 1984; Baldwin 1992). Vessels with blue dye seen seeping out were quickly retied; those that could not be fixed were discarded. Approximately 70% of the vessels excised did not exhibit any overt signs of cellular damage and were successfully used for Lp-measurements.

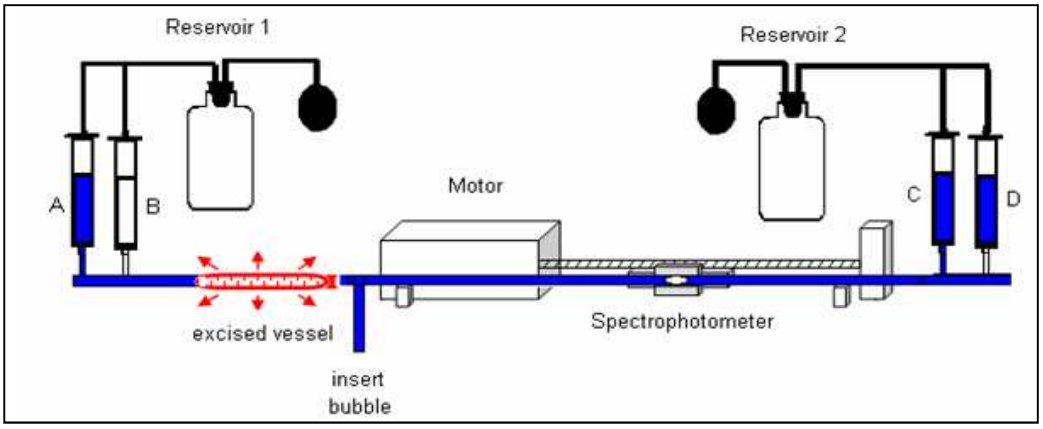

Figure 18: Experimental setup for hydraulic conductivity (Lp) measurement of an isolated vessel. A sphygmomanometer controls pressure in a large reservoir, from (Nguyen 2008). As Nguyen states, "Reservoirs 1 and 2 are connected to solution reservoirs (A, B, C, D). Reservoirs A and C contain trypan blue in PBS. Reservoir B contains HgCl2 in PBS solution and Reservoir D collects solution that is flushed through the vessel from Reservoir B when HgCl2 is introduced to the vessel. The transmural flux Jv is monitored with a bubble tracking system."

Surgical Procedure and Water Flux Measurement

For detailed description, please refer to Methods section of (Nguyen 2008) . Briefly, male Sprague Dawley rats (300-400 grams) were anesthetized (1% pentobartital sodium) intravenously (15mg/100g rat) and then connected to a respirator to provide mechanical ventilation by performing a tracheotomy. This was followed by an incision from the sternum up towards the heart exposing the chest cavity. We then carefully displaced the lungs and carefully remove the fat and connective tissue surrounding the aortic arch to isolate the vessel and allow us to ligate the aortic intercostal arteries down to descending limb. Suffusate solution (4% BSA in PBS) is applied to prevent the vessel from drying out. By utilizing two separate pressure reservoirs, we are able to cannulate both the distal and proximal end of the vessel under pressure to avoid collapse. The bathing solution is maintained at 37 C and aerated with an aquarium pump. We condition the vessel three times by lowering and raising the pressure difference between the pressure reservoirs to avoid any hysteresis effects. After conditioning we inject a bubble into our photospectometer system and measure flux.

We measured the flow rate through the vessel wall first at 75 mmHg by monitoring the movement of the air bubble after the vessel has reached steady state. The outer dimensions of the vessel were measured at three different positions at the end of each reading. This protocol was repeated at 120 mmHg. Reservoir D was then closed and C (initially empty) and B (containing F or 0.1wt% DMSO) were opened. Using an up- vs. downstream pressure difference of ~5 mmHg, we drive solution from reservoir B through the vessel into reservoir C for 2 hours. Then, we flush the vessel for 10 minutes via reservoir A. The proximal end was reclamped and Lp measurements were repeated at the same pressures. In blocking experiments, Reservoir D was then closed and C and B (containing 5 μM $HgCl_2$) was opened. Lastly, the vessel was unligated proximal end and denuded by working a glass rod with a 2.5 mm diameter Epon polymer tip back and forth inside the vessel and removing it with a twist. The vessel was then recannulated, flushed of cellular debris from the distal end, checked for leaks, and measurements were repeated as before at both pressures of interest.

Immunohistochemistry (performed by J. Toussaint)

For details please refer to Methods section of (Toussaint 2009). Briefly, analysis was performed on rat aortas by intubating (PE-50) the left femoral vein and the carotid artery to connect them with pressurized syringes containing pentobarbital, excess heparin (5000 USP unit/ml), PBS (with and without forskolin (F in 0.1% DMSO)), or Accustain Bouin's fixative followed by a tracheotomy to mechanically ventilate the animal. We then perfuse the animal with heparin followed by an overdose of sodium pentobarbital through the femoral vein to stop the heart and then PBS through the carotid artery until the efflux through the femoral vein was clear. Treatment with either F or 0.1%wt DMSO was then flushed for 2 hours. The perfusate

was switched to the Bouin's solution at the same pressure with the femoral arteries serving as exit points.

We then remove the aorta and remove the connective tissue and section the vessel into smaller segments which were then sliced into samples (thickness 10 μm) with a cryostat and finally mounted on microscope slides. These slides were then incubated in 0.5 % Pontamine Sky Blue 6BX (Alfa Aesar, Haverhill, MA) for five minutes followed by a five minute washing in PBS. For immunohistochemical study, the slides were then incubated in blocking solution (3% goat serum, 0.3%Triton-X, 20mM sodium phosphate, 0.9mM sodium chloride, 0.05% saponin) for 30 minutes followed by three washings in PBS. They were subsequently exposed to rabbit anti-rat AQP-1 antiserum (category AQP-11-A, Alpha Diagnostic International, San Antonio, TX (Denicola, Souza et al.)) diluted in PBS plus 3% goat serum, 0.2% bovine serum albumin (Sigma) in PBS for 18 –24 hours.

Afterwards, the slides were washed in PBS three times and incubated with Alexa 488 conjugated goat anti-rabbit IgG (Molecular Probes, Carlsbad, CA) at a dilution of 1:50 in PBS for 90 minutes at room temperature. Samples were washed in PBS three times and mounted with Vectashield mounting media for fluorescence (Vector Laboratories, Burlingame, CA). Coverslips were securely applied to the samples using clear nail polish. The samples were then kept in the dark to prevent damage to the Alexa 488 tag and subsequently viewed and captured using a Leica TCS SP2 AOBS confocal microscope described below.

Treatments

Forskolin (10μM), which increases the production of cAMP by adenylyl cyclase in ECs and, which we have shown in chapter 2, increases AQP-1 membrane expression and Lpe in aortic endothelial cell monlayers *in vitro*, was dissolved in dimethyl sulfoxide (DMSO) and further

diluted in distilled water and treated for 2 hours unless otherwise stated. Final solvent concentrations were <0.1% (vol/vol). The control treatment consisted of the same final concentrations of DMSO, but with no F. $HgCl_2$ (5μM), a blocker of water channels, was dissolved in double distilled water and was flushed through the vessel for 15 minutes.

Immunocytochemistry

SMCs were grown on round coverslips until confluence followed by F or blank (0.1wt% DMSO) treatment. SMCs were then fixed in 3.7% PFA for 10 minutes, washed three times in PBS, permeabilized with 0.1% Triton X-100 in PBS for 10 minutes, and then blocked with 1% BSA for 30 minutes. The blocking solution was removed by aspiration, and the monolayers were exposed to rabbit anti-rat AQP-1 antiserum (Alpha Diagnostics Intl, San Antonio, TX) diluted in 15% goat serum and 0.2% BSA in PBS. The primary antibody was diluted 1:500. The incubation was done in a humid chamber at room temperature for 60 minutes. The cell layers were subsequently washed three times with PBS. They were then incubated with Alexa-488 conjugated goat anti-rabbit IgG (Invitrogen, Carlsbad, CA) at a dilution of 1:200 (in PBS plus 1% goat serum) for 30 minutes, rinsed with PBS, and then mounted on a microscope slide. The samples were stored in a humid chamber in the dark before imaging with a Leica TCS SP2 AOBS confocal microscope using a 488nm Argon laser.

Confocal Microscopy

Confocal microscopy was done using a Leica TCS SP2 AOBS confocal microscope. Several cautious preliminary steps were taken in order to be able to quantitatively compare confocal images taken from different samples. Firstly, before and during every confocal image acquisition, the confocal microscope's laser intensity was calibrated and the settings strictly maintained in order to make certain that each sample observed received the same level of laser power for the same amount of time. All other external conditions such as room temperature, humidity

and stray lights etc were strictly monitored. The calibration of the microscope was done using a Coherent Ultima LabMaster Power and Energy Dual-Channel Meter attached to a LM-2 silicon HD visible optical detector wand. A sample was placed on the microscope stage and the embedded tissue was brought into focus using the 40x PL APO N.A.1.25 oil immersion objective. The sample was then removed and replaced by the optical detector in the exact position over the objective. The 488nm Argon laser was then initiated and the detector was shifted around in order to find its "sweet spot," that is where the fullest intensity of the laser is felt. Both for different sets of samples obtained after immunohistochemistry on different days and even for different samples from the same sample set, we adjusted the laser settings on the confocal microscope both before and periodically during the measurement procedure to obtain the same calibrated values on the laser meter for confocal scanning.

Quantification of Immunofluorescence after treatment

Ex vivo Rat Aortic ECs

The optical slices (z slices) data from confocal scanning were analyzed using specially-coded custom software that uses active contours or snakes to find the boundaries of objects in an image (Kass, Witkin et al. 1998). This software tightly outlines and encloses the region, corresponding to the endothelium, of intense green staining beyond the IEL in each of the confocal sections/images of the confocal z-stack taken of the aorta. It then integrates the intensity of the Alexa 488 fluorescence enclosed in this region and calculates the perimeter and area of the enclosed region. Simpson's rule is used to integrate these values across a z-stack to obtain the total surface area and the total volume of cell in the z stack and the total integrated green intensity in this same cellular region of the aortic endothelium. We thank Mr. Hadi Fadaifard and Professor George Wolberg, both of Department of Computer Science at the City College of the City University of New York, for working with us on this program.

In vitro SMCs

Slides were imaged on a Leica TCS SP2 AOBS confocal microscope using a 488nm Argon laser. As explained above, all slides were exposed to the same laser duration and intensity. Regions of interests (ROIs) were auto-thresholded using NIH Image-J, which chooses a threshold based on the integrated intensity histogram of a confocal image (z-) stack to obtain cell outlines. Total fluorescence intensity and total area of cell outlines was computed in Image-J by applying outlines to original image. Integration across z-stack gives total (volume) intensity (TI) and total cell volume (TV). Comparing TI/TV for different samples gives relative values of their AQP-1/total cell volume, a measure of cellular AQP-1 concentration.

Results

In Figure 19-Figure 20 below, AQP-1 expression in SMCs is depicted by green fluorescence where greater intensity signifies higher AQP-1 expression. Untreated (0.1% wt DMSO only) SMCs are shown in Figure 19 both in culture and in rat aorta *ex vivo* and display no visually noticeable difference in AQP-1 labeling intensity. In contrast, F treated SMCs clearly express less AQP-1 labeling *ex vivo* (Figure 20, right) compared with F treated SMCs in culture (Figure 20, left). F treated SMCs in culture display similar AQP-1 intensity as untreated SMCs.

Quantification of Immunofluorescence after Treatment

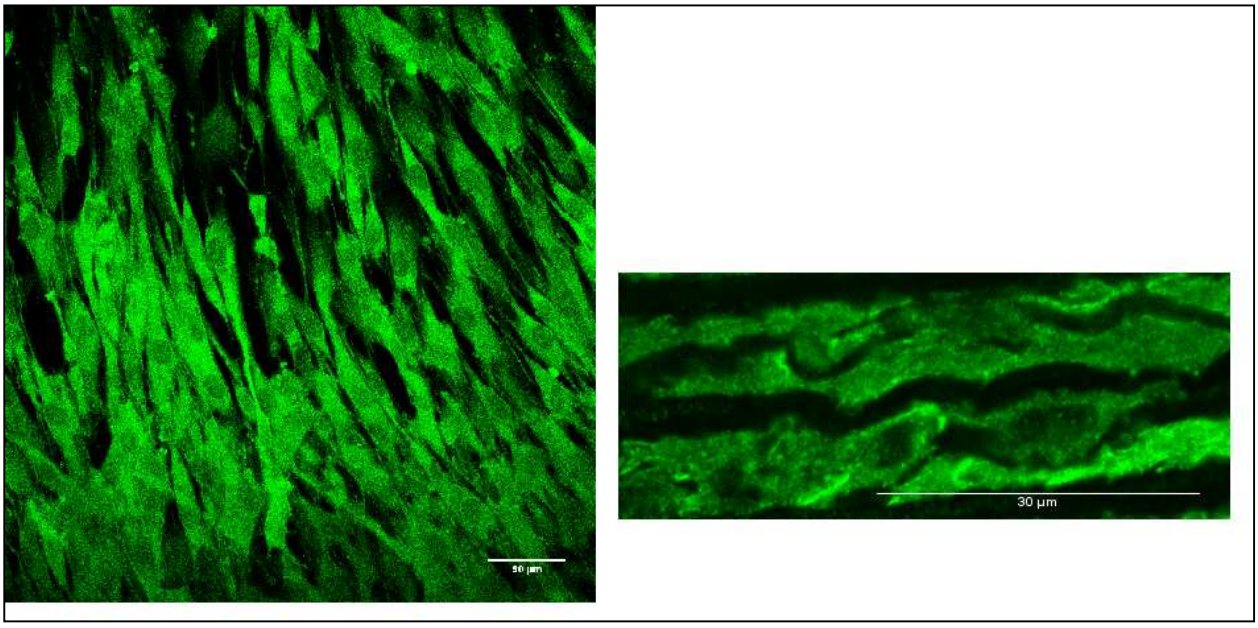

Figure 19: Confocal images (single slice) of untreated SMCs both *in vitro* (left, bar = 50 microns) and *ex vivo* (right, bar = 30 microns). AQP-1 labeling (green) can be seen throughout cells both *in vitro* and *ex vivo*.

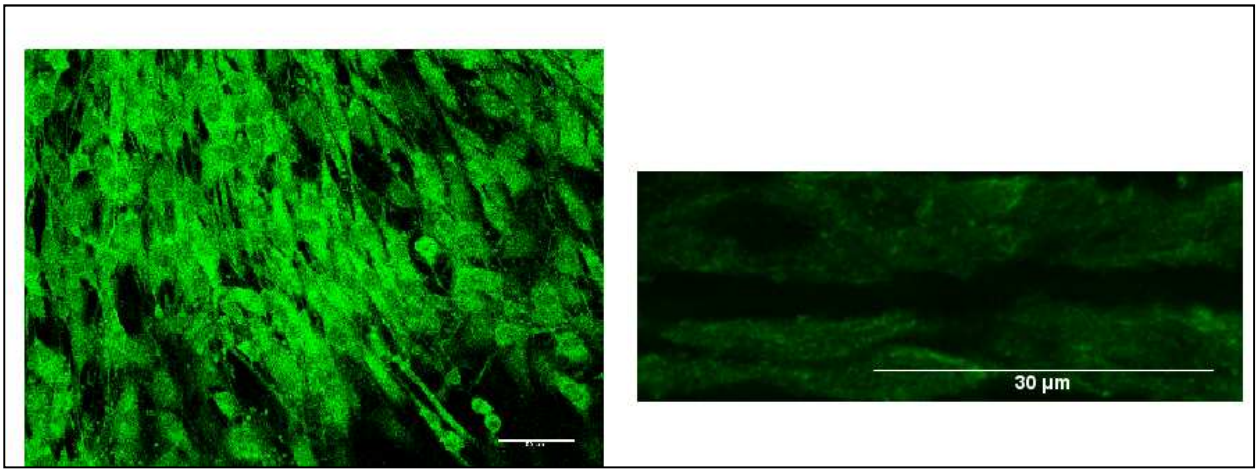

Figure 20: Confocal images (single slice) of F treated SMCs both *in vitro* (left, bar = 50 microns) and *ex vivo* (right, bar = 30 microns). AQP-1 labeling (green) can be seen throughout SMC *in vitro* which is in contrast to F treated SMCs where AQP-1 labeling is far less intense.

Figure 21 and Figure 22 below display untreated and F-treated ECs in culture and in rat aorta *ex vivo*. Untreated ECs in culture express AQP-1 labeling throughout cell *in vitro*, while AQP-1 seems to be preferentially localized to membrane *ex vivo.* F treated ECs display moderate localization of AQP-1 in the membrane in culture, while F treated ECs in rat aorta display

far more intense fluorescence labeling, displaying a strikingly drastic contrast between membrane-bound AQP-1 and intracellular vesicles.

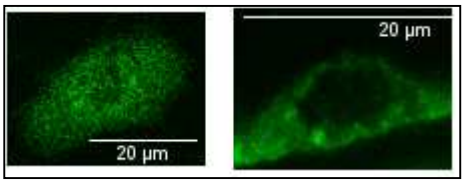

Figure 21: Confocal images (single slice) of untreated ECs *in vitro* (left) and *ex vivo* (right). AQP-1 labeling (green) can be seen throughout cell *in vitro*, while membrane bound AQP-1 labeling is far greater *ex vivo*.

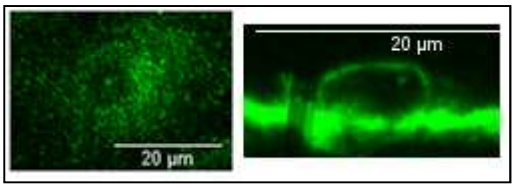

Figure 22: Confocal images (single slice) of F treated ECs *in vitro* (left) and *ex vivo* (right). AQP-1 labeling (green) is localized in the membrane region in both *in vitro* and *ex vivo* F treated ECs, but is far more intense *ex vivo* in F treated vessels.

Figure 23-Figure 24 show representative confocal microscopy images of untreated and F treated rat aortas. We can see the many elastin fibers (red) of the vessel wall and the AQP-1 (green) distribution in both the endothelium and the SMCs. F treated samples displayed preferential AQP-1 labeling in the endothelium relative to the adjacent SMCs. This contrasted directly with untreated samples in which SMCs contained the majority of AQP-1 labeling relative to the endothelium.

Rat Aortic EC

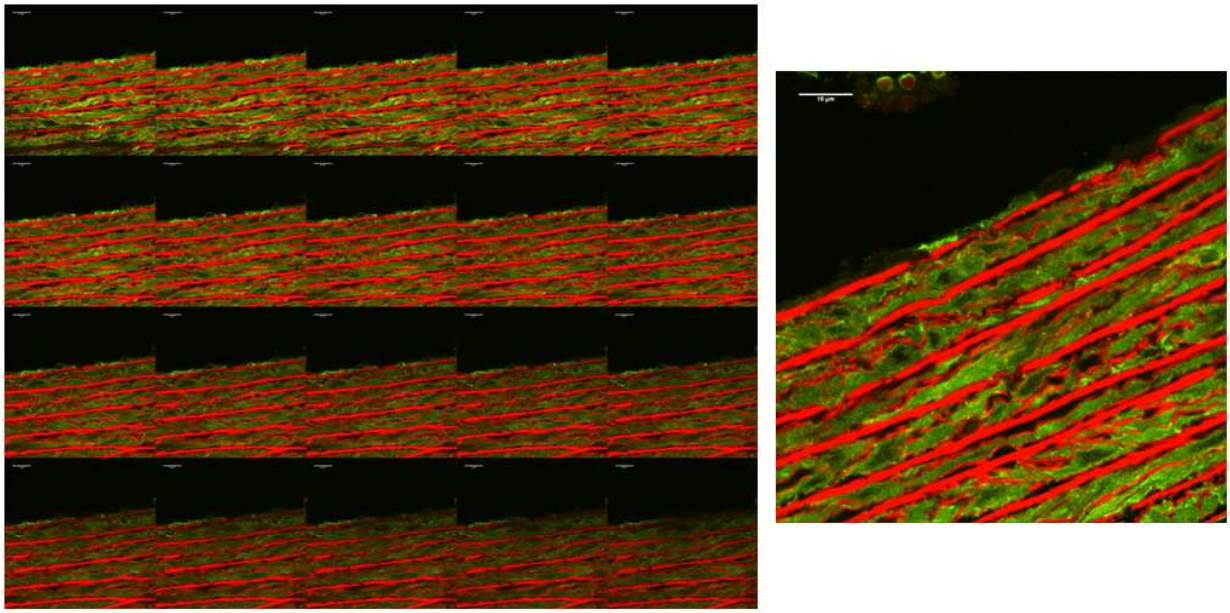

Figure 23: A confocal extended focus image of an untreated rat aorta z-stack gallery (left) and higher magnification cropping (right) that clearly expresses AQP-1 (green fluorescence). AQP-1 expression is clearly visible in the aortic endothelial cells (above the top red line in the figure on the right). Red fluorescence indicates elasitn. Note that AQP-1 is also present at high concentration in the SMCs below the endothelium. There are 20 optical serial sections in this gallery and those that follow (Figure 23-Figure 24) representing a total thickness of ~ 10 μm in the z coordinate center of the sample. Physical thickness of each sample was 10 uM. Untreated monolayers were exposed to blank (0.1%wt DMSO) solution (2 hr.) during treatment. (bar = 15 microns)

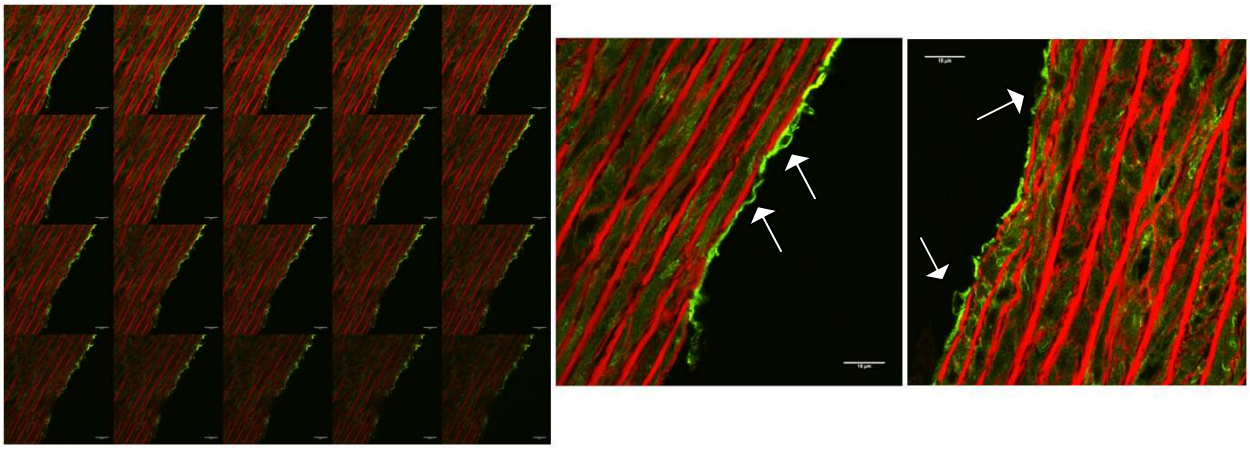

Figure 24: A confocal extended focus image of an F-treated rat aorta z-stack (left), higher magnification crop from left (center) and alternate magnified z stack cropping (right) that clearly expresses AQP-1 (green fluorescence). AQP-1 expression is far greater in the aortic endothelium after F treatment than before (see Figure 23). Unlike Figure 23, endothelial AQP-1 expression seems far higher than in the SMCs after F treatment. Treatment appears to have in-

duced AQP-1 shuttling to EC membrane as seen by bright green rings (white arrows) in the endothelium. (bar = 15 microns)

SMCs

Figure 24 showed bright green rings in the aortic endothelium, indicating that F treatment induced AQP-1 shuttling in RAECs in whole vessels. Interestingly, it also seemed to reduce AQP-1 expression in the media. To determine if F treatment reduces AQP-1 expression in SMCs in the absence of an endothelium we investigated the effect of F treatment on an SMC culture *in vitro*. The following z-stack images depict AQP-1 expression after 0.1% wt DMSO or F treatment. There is no obvious difference between the treated and untreated samples. The SMCs are in a proliferative/migratory state, exhibited by intense AQP-1 labeling throughout the SMCs in culture (Verkman 2005). The cells grow on top of each other as seen in the figures below.

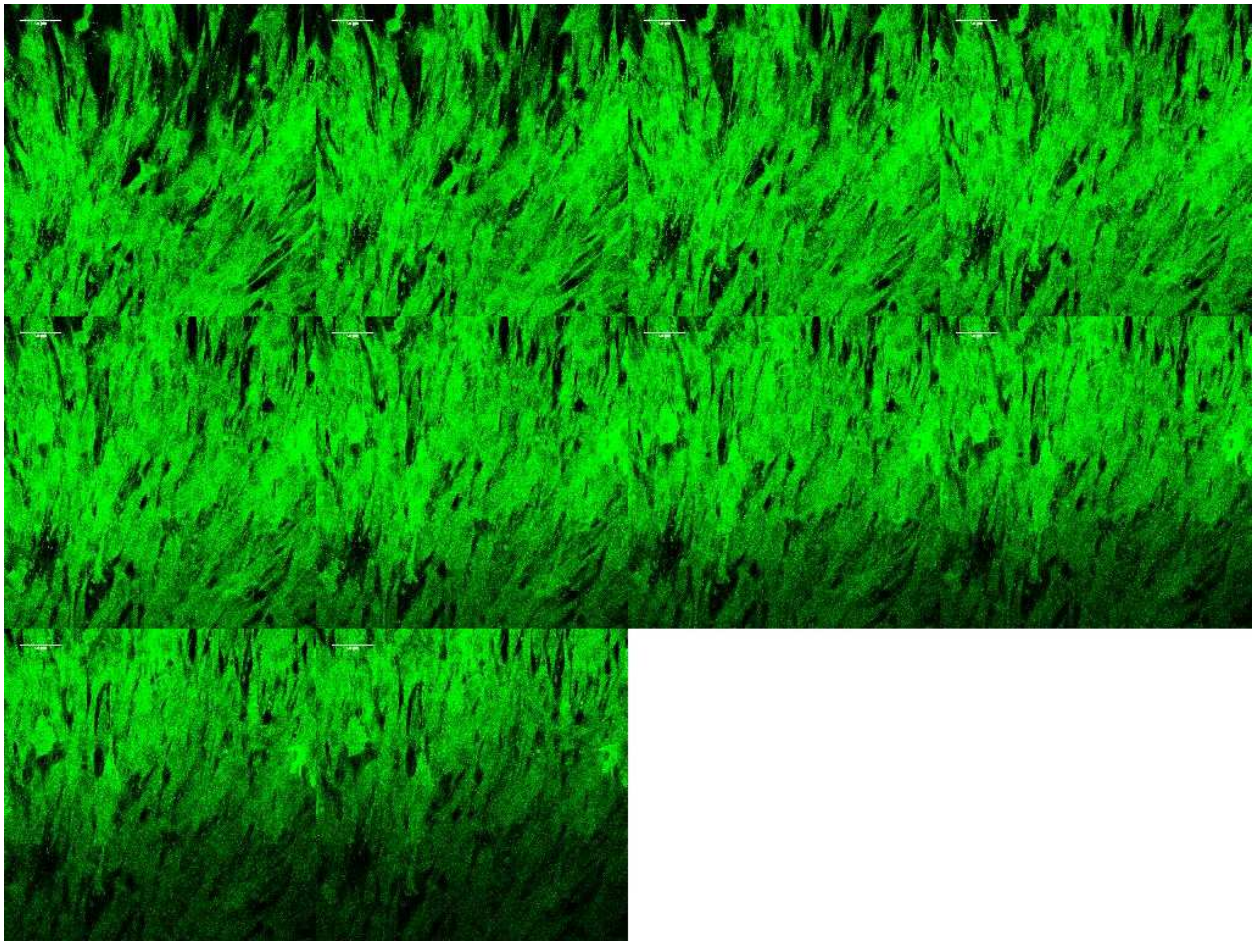

Figure 25: A confocal extended focus image of an untreated bovine aortic SMCs z-stack. There are 10 optical serial sections in theses gallery (fig. 35&36) images representing a total thickness of ~ 5 μm in the z coordinate center of the sample. Untreated monolayers were exposed to blank (0.1%wt DMSO) solution during treatment (2 hr.) Figure 25 shows that SMCs in culture clearly express abundant AQP-1 (green fluorescence). (bar = 50 microns)

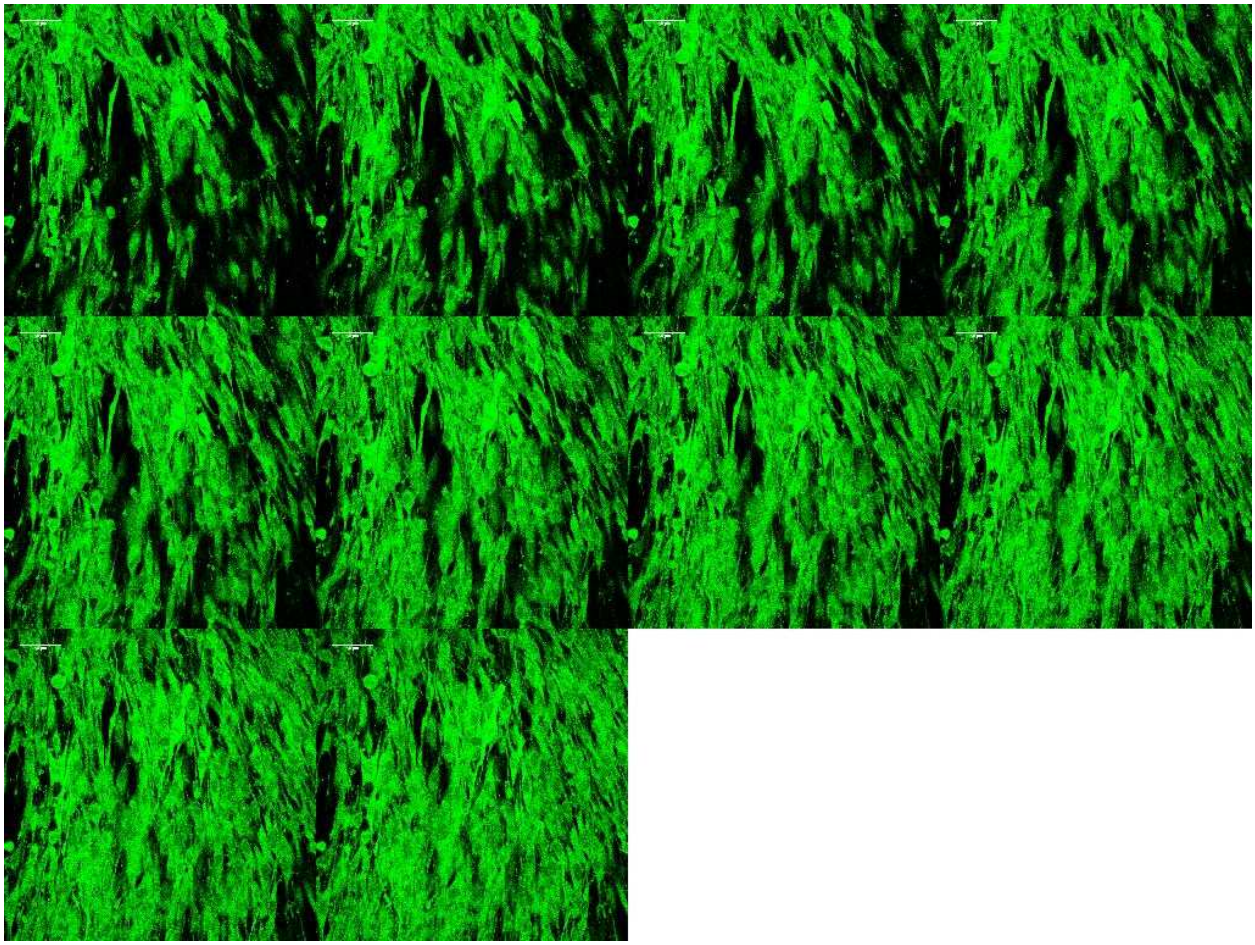

Figure 26: A confocal extended focus image of an F-treated bovine aortic SMCs z-stack which shows SMCs clearly express abundant amounts of AQP-1 (green fluorescence). Unlike in whole rat aorta, F treatment does alter AQP-1 expression in SMCs (compare to Figure 25). These results suggest that the endothelium mediates the effect of F treatment on SMCs. (bar = 50 microns)

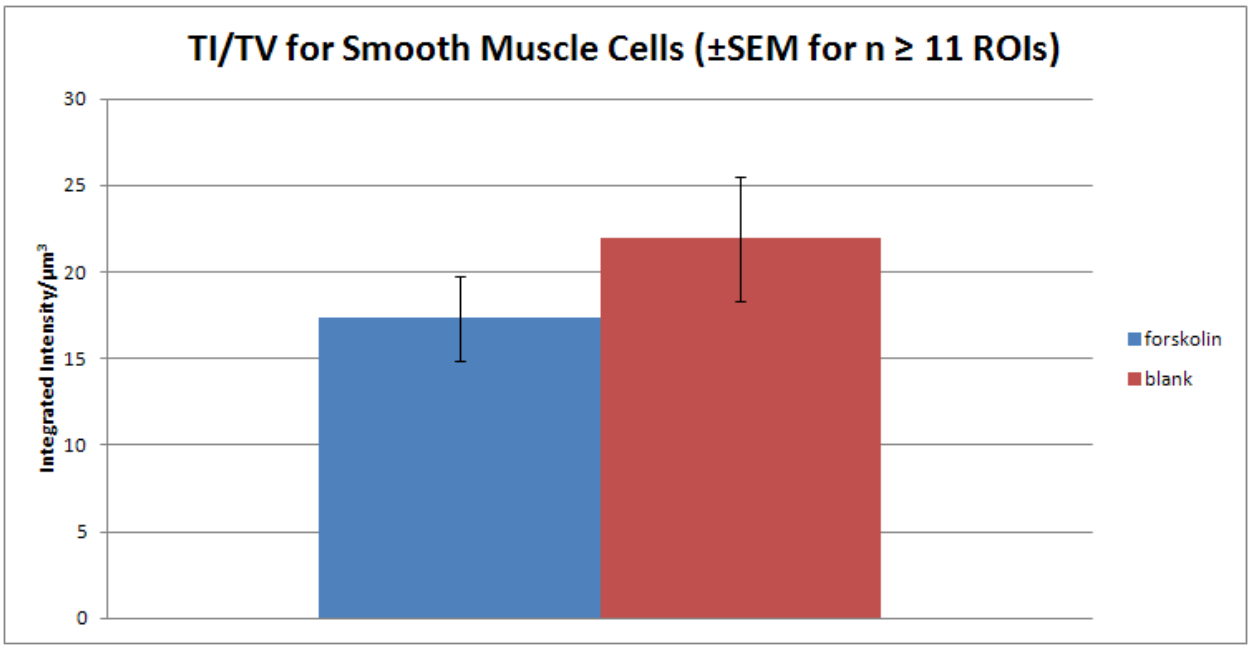

Figure 27: TI/TV for rat aortic SMCs after treatment with F or with a blank solution. F treatment did not change significantly change TI/TV.

Figure 27 quantifies the green fluorescence of the cultured SMCs with and without F treatment. It clearly indicates that F treatment does not significantly alter AQP-1 expression in SMCs in culture. It seems plausible that the F treatment effect observed ex-vivo of a reduction in AQP-1 expression was endothelium dependent.

Lp Measurements on Rat Aorta before and after forskolin treatment at 75 and 120 mmHg

Figure 28 shows the results of our measurements of Lp at 75 and 125 mmHg, first in untreated aortas, then after 2 hr F treatment, then again after $HgCl_2$ treatment and finally again after endothelial denudation, all at the same two pressures and all on the same vessels for n=8. Only 4/8 vessels underwent $HgCl_2$ treatment. Our controls (using a blank (0.1%wt DMSO) solution instead of one containing F) showed no significant difference in Lp before and after blank treatment at either transmural pressure (see table below).

	blank (n=2)	*Forskolin (n=8)*
Condition	**% Δ Lp from 75 to 120 mmHg**	
baseline	-17%	-22%
treated	-18%	-40%
denuded	-2%	-3%
Pressure	**% Δ Lp after 2 hr. of treatment**	
75	-4%	25%
120	-4%	3%

Table 1: Summary of blank (0.1 wt% DMSO only) or Forskolin treatment on Lp for the same vessel (n=4). Blank treatment did not significantly alter vessel Lp after 2 hours at 75. In contrast, F treatment drastically increased Lp at 75 mmHg. Neither blank nor F treatment caused a significant change in Lp at 120 mmHg, which we believe to be because the intima is fully compressed with or without F treatment at this pressure. Neither treatment altered Lp in denuded vessels, which have been found to be relatively pressure invariant (Nguyen 2008). This allows us to elucidate the contribution of the endothelium in mediating the treatment's effects on Lp in the vessel wall.

Baseline Lp values show a 29±5% drop in Lp from 75mmHg to 120mmHg on n=8 fresh aortas, consistent with previous experimenters (Shou 2006; Nguyen 2008). F treatment increased Lp 33±5% at 75 mmHg but did not have a significant effect at 120mmHg. After F treatment increased Lp at 75 mmHg, we administered a flush of $HgCl_2$ to block AQP-1 and remeasured Lp. We found $HgCl_2$ to reduce Lp by 35±5% after F treatment. The final step was to denude the vessel of its endothelium, which increased Lp and made the vessels Lp pressure-invariant in both

untreated and treated vessel. Lp values and trends for baseline, blocking, and after denudation were similar to previous studies (Shou 2006; Nguyen 2008; Xue 2011).

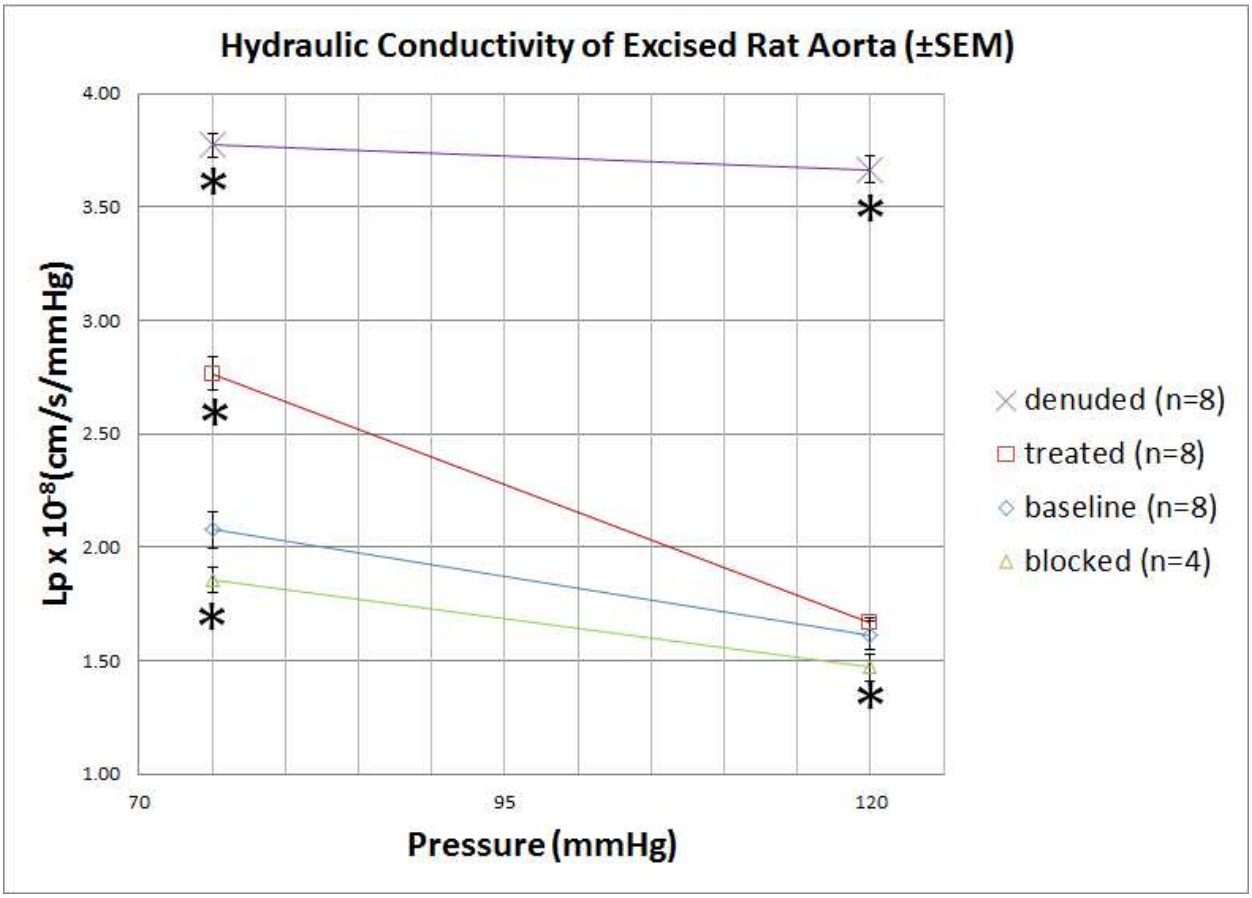

Figure 28: Lp of rat aorta, measured with intact endothelium before and after treatment (either 0.1%wt DMSO or F) and then after the endothelium has been denuded on the same vessel. In 4/8 experiments treatment was followed by a flush with blocker ($HgCl_2$) and Lp measurement before denuding the vessel. Values are means (SEM). Overall Lp drops 29±5% from 75 to 120 mmHg. F treatment increased Lp 33±5% at 75 mmHg, leading to 40% drop in Lp from 75 to 120 mmHg after F treatment. We found $HgCl_2$ reduces Lp by 35±5% after F treatment. Deendothelialization increases Lp by about three-quarters relative to that of the intact vessel and independent of pressure. (*indicate significant statistical difference against untreated sample (paired, $p<0.05$))

P-value (vs. baseline)		
	P = 75 mm Hg	*P = 120 mmHg*
F Treatment (n=8)	4.5E-08	9.8E-02
$HgCl_2$ (n=4)	7.8E-03	4.8E-02
denuded (n=8)	3.6E-08	3.3E-09

Table 2: P-values of *ex vivo* Lp data for various conditions. P-values of less than 0.05 indicate statistical difference. F treatment causes a significant difference at 75 mmHg but not 120 mmHg. Blocking with $HgCl_2$ caused a significant difference at 75 mmHg and a weak statistical difference at 120 mmHg. Denuding the vessel resulted in a strong statistical difference in Lp at both 75 and 120 mmHg.

Discussion

The goal of this paper is to study the effect of F on AQP-1 distribution in aortic ECs in whole vessels *ex vivo* and any simultaneous change in endothelial, and therefore vessel wall, Lp. We know from the results of our *in vitro* study that short term F treatment increases Lpe, and likely causes AQP-1 trafficking from intracellular vesicles to the EC membrane via increasing intracellular cAMP, but does not increase total cellular AQP-1 in EC monolayers. In the present study we first performed immunohistochemistry on treated and untreated (0.1%wt DMSO with or without F) rat aortas to investigate AQP-1 distribution in the endothelium. We found that F treatment caused a redistribution of AQP-1 into the EC membrane to form rings around many of the ECs and, intriguingly, the apparent intensity of fluorescent anti-AQP-1 staining to markedly increase with respect to the untreated case, the latter of which did not occur in EC monolayers in culture.

Our next step was to measure Lp after F treatment to understand the consequence of the observed AQP-1 redistribution. As explained in the introduction, we suspect that an increase in

endothelial AQP-1 will increase endothelial Lpe, which will clearly increase overall wall Lp. More strikingly, however, our theory predicted that the increase in endothelial Lp will have the effect of lowering the fraction of the transmural pressure difference that occurs across the endothelium, and therefore, lower the force/area on the endothelium at a given transmural pressure. In the regime of transmural pressures close to the critical force/area needed to compress the vessel SI, an increase in endothelial AQP-1 would then have the potential to decompress the SI at those pressures. Such decompression would then unblock IEL fenestrae and lead to a significant increase in vessel wall Lp at those pressures. At lower pressures, the SI is decompressed even at normal AQP-1 expression and at higher pressures; this decrease in force/area would be insufficient to decompress the SI. Thus we expect only a narrow dynamic range in which this effect is significant. However, since under normal AQP-1 expression, the critical transmural pressure for SI compression is about 60 mmHg, this dynamic range has the potential to decompress the SI in exactly the region of physiological interest, since the mean physiological pressure in the aorta is ~100 mmHg.

The theoretical predictions derived by Joshi et al. of our group that assume up to a doubling in EC AQP-1 expression predict Lp to increase substantially with greater AQP-1 functionality in the regime of ~70-95 mmHg, but to change only by virtue of a direct increase in Lpe (a likely small, even insignificant change) at 120 mmHg. Our experiments show that F treatment increased whole wall Lp 33±5% at 75mmHg and, according to Joshi et al.'s theory, this increase corresponds to a 50% increase in AQP-1 function/expression, as Figure 40, which overlays our experimental result with the model prediction, shows. Given the error bars on the measurements and the closeness of the curves, this 50% is just an estimate. The main difference between a 50% and a higher increase in AQP-1 expression is not in the magnitude of the increase in Lp at 75

mmHg, since once there are sufficient AQP-1 to decompress the intima, further AQP-1 will only have the very minor effect of increasing Lpe; medial Lp dominates overall wall Lp when the SI is decompressed. The major difference between a 50% and a higher increase in AQP-1 expression is rather in the extent to higher transmural pressures of the dynamic regime, i.e., of how high one can go in transmural pressure and still keep the SI decompressed. As such, the 50% estimate is really a lower bound on the increase in AQP-1 expression needed to decompress the SI. A more complete study of the shift in the dynamic range will require a further Lp study at a larger, more refined number of transmural pressures, which is clearly the next step in our future experimental work.

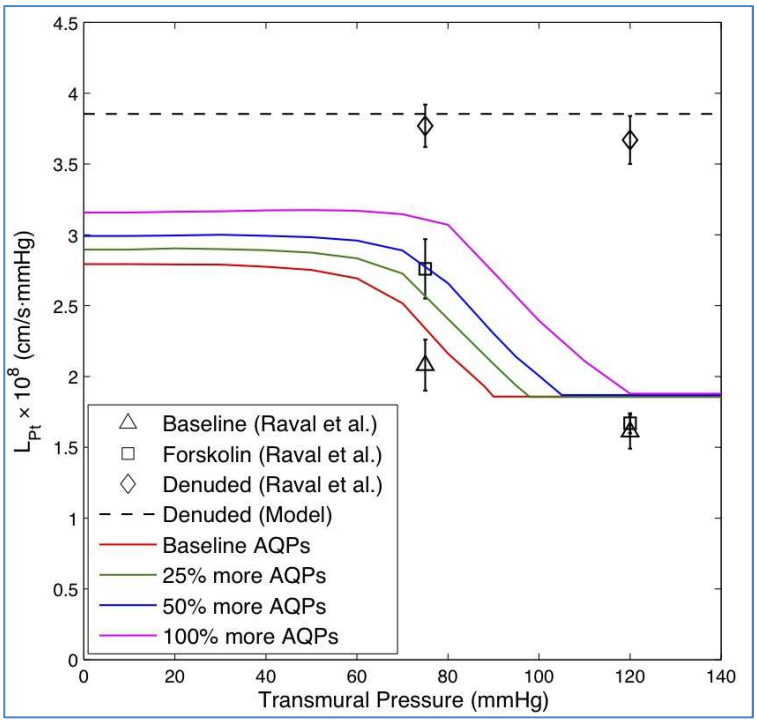

Figure 29: Effect of an increasing AQP-1 contribution on Lp: Theory vs experiment.

Vascular Fluid Transport

Fluid transport across the vascular endothelium is believed to be governed by three distinct pathways: endocytosis, transcytosis, and paracellular transport. (Paracellular) junctions between ECs and certain specific transporter proteins (transcytosis) and receptors (endo/exocytosis) provide avenues for larger solute molecules to traverse the vessel wall.

Physical factors such as shear forces imparted by blood flow or pulsatility created by normal cardiac output provide mechanical queues that initiate varied signaling pathways in the vessel wall. The endocrine system is responsible for hormonal releases into the blood stream and their subsequent action on the endothelium and the vessel wall can drastically alter fluid transport. Vasopressin, which is released from the pituitary gland to conserve water and functions as an antidiuretic, is one such hormone that promotes water reabsorption in the kidney and increases blood volume. Depending on the conditions, EC and SMC phenotypes can vary significantly between activated and quiescent states. The quiescent state in ECs is characterized as a differentiated cell with specific functions including sensing flow and pressure. The cell in this state is resistant to proliferation, inflammation, and coagulation, acting as a Teflon-like surface for tissue protection.

Aberrant shear stress and pressure exposure and the introduction of micro-organisms (e.g. virii and bacteria) and also modified plasma proteins (e.g. glycolicylated proteins and oxidized LDL) triggers the EC activation response. The EC then takes on a velcro-like adherence to leukocytes by virtue of stimulated leukocyte receptors. Platelets adhere and are a part of the coagulation cascade that occurs on the surface of the EC. The geometry and proliferative state of the cell are altered.

It is well known that the endothelium controls the phenotype of the SMC, which can also exist in an activated or quiescent state (Hergenreider, Heydt et al. 2012). The Q SMC is a non-proliferative contractile cell, as opposed to the activated SMC that is a proliferative, reactive, migratory and synthetic cell that is central to both the injury responses of atherosclerosis and NH.

Influence of transport on the subendothelial intima

Fluid transport not only controls (by advection) the residence time of low density lipoprotein (LDL) in the subendothelial intima (SI) where it can be oxidized, but it also controls the availability of other materials (e.g. oxidized LDL, glycocylated proteins, enzymes that degrade both, such as lipases and proteases). In this regard, the SI functions as an interstitial drainage for the vascular wall. Our group has shown that blocking AQP-1 functions to reduce Lpe, which can induce SI compaction at pressures lower than under normal AQP-1 function (Nguyen 2008; Xue 2011). We speculate that AQP-1 serves to increase the efficiency of the vessel wall drainage system by facilitating water transport and promoting advection into and through the SI by partially controlling Lp. In principle, upregulation of AQP-1 might provide a means to delay intima compaction until pressures beyond the physiological regime (data to directly verify this are currently being analyzed by my colleague J. Abrams). By this logic, such upregulation could provide favorable conditions to prevent LDL binding and oxidation in the SI.

cAMP and the Artery Wall

cAMP has been implicated in the regulation of the endothelial barrier (Sayner 2011). cAMP signaling specificity is clearly at work at the tissue level, but may also be important at the cellular level. Several findings suggested that different agonists could generate a cAMP signal yet impart different physiological responses. This fact gave rise to the idea that cAMP signals may be spatially segregated into isolated subcellular compartments within a single cell (Hayes,

Brunton et al. 1979; Jurevicius and Fischmeister 1996; Willoughby and Cooper 2007): Within the endothelium's plasma membrane, cAMP protects the endothelial barrier, whereas cytosolic cAMP disrupts that barrier (Sayner 2011). Thus, cAMP stimulation could cause opposing effects in ECs, and the direction of its effect might depend on the culture system and on its fluidic environment.

Our *in vitro* tracer study results suggest that cAMP stimulation by F treatment improve paracelluar barrier function by reducing paracellular solute permeability, while increasing overall water transport by shuttling AQP-1 to the membrane from the cytosolic compartment. The results of the present study in rat aorta *ex vivo* suggest that F treatment augments AQP-1 shuttling to the membrane of ECs, and, consistently, improving overall transendothelial water transport, as measured by Lp. In order to facilitate this AQP-1 shuttling, F treatment likely induces actin cytoskeleton reorganization to free tethered intracellular vesicles to migrate to the cell membrane. This, in turn, influences cell-cell interactions and decreases intercellular permeability, possibly by tightening the F-actin belt contiguous to the adherens junctions (Thi, Tarbell et al. 2004; Boucher, Laprise et al. 2005).

Noda et al. showed in renal collecting duct cells that when AQP-2 in intracellular vesicles becomes phosphorylated at serine-256, which occurs by the action of cAMP, it binds to tropomyosin 5b which depletes free tropomyosin from the vicinity of the AQP-2 vesicle, thereby fostering local F-actin depolymerization (Noda, Horikawa et al. 2008). This has the effect of cutting a hole in the cortical actin network around the vesicles, liberating AQP-2 vesicles from their F-actin cage to reach the plasma membrane.

While directly affecting the ECs in this way, treatment with F seems to cause a concurrent, EC-dependent SMC suppression of AQP-1 expression relative to untreated rat aortas that is not present in SMC monoclulture. Such AQP-1 down regulation may indicate a change in SMC phenotype into their quiescent, non-proliferative state. In contrast, untreated rat aortic images exhibit strong AQP-1 intensity, suggesting that SMCs are in a proliferative and migratory state (Verkman 2005; Khambata, Panayiotou et al. 2011). These issues of SMC phenotype requires further investigation.

EC - SMC crosstalk?

As noted, short-term F treatment seemed to have the effect of suppressing or reducing AQP-1 expression in SMCs. We have shown that short-term F does not cause this effect in SMC monoculture. A number of potential mechanisms could possibly explain how the EC influences SMC behavior. Paracrine signaling between the EC and SMC has been described in terms of eNOS-produced NO transport from ECs to SMCs, EC natriuretic peptide (NP) release and transport to SMC NP receptors (NPR), and the SMC anti-mitogenic response to microRNA which post-transcriptionally control gene expression mediated by Krüppel-like transcription factor 2 (KLF-2). KLF-2 is a critical regulator of endothelial gene expression patterns triggered by atheroprotective flows.

The recent demonstration of a 15-fold increase in C-type (C) NP transcript in rat thyroid cells in response to dbcAMP (Sellitti, Puggina et al. 2004) invites speculation as to whether cAMP up-regulates endothelial CNP in a similar manner and whether CNP binds to NPR-C on SMCs in a paracrine manner. NPR-C binding by CNP has been reported to inhibit migration and proliferation of rat and human aortic smooth muscle cells (Hutchinson, Trindade et al. 1997; Kohno, Yokokawa et al. 1997; Anand-Srivastava 2005). AQPs facilitate cell migration by a me-

chanism that might involve water transport in lamellipodia of migrating cells (Verkman 2005). Thus antimitogenic cellular responses may lead to reductions in AQP-1 expression in affected cells.

Increases in intracellular cAMP facilitate the insertion of AQP-1 channels, which also transports NO, into the cell membrane. Increased NO transport through upregulated endothelial AQP-1 might be responsible for the reduction in AQP-1 expression in SMCs due to the anti-mitogenic effect of increased endothelial nitric oxide synthase (eNOS) produced NO transport to SMCs. Yamada et al. demonstrated that desmopressin's (DDAVP) relaxation effect on intact rat aorta was blocked by a specific inhibitor of NO synthesis, L-N^G-monomethyl-L-arginine, indicating that the stimulation of vasopressin receptors on the endothelium is at least partially mediated by NO production in the endothelium (Yamada, Nakayama et al. 1993).

cAMP also stimulates a cAMP response element (CRE) region of EC DNA. It is then bound to by a CREB-binding protein (CBP), which coactivates it, allowing it to switch certain genes on or off. This CBP is also a coactivator of Krüppel-like transcription factor 2 (KLF-2) that controls microRNA which regulate SMC function, maintaining its contractile quiescent phenotype (Hergenreider, Heydt et al. 2012). This clearly indicates the endothelium control of SMC function.

Chapter 4. Conclusions

Endothelial and smooth muscle cells: Model systems

ECs line the blood vessels, i.e. arteries, vein, and capillaries in the body as well as the lymphatic channels. Macroarteries, such as the aorta and carotid artery, also have SMCs to provide mechanical response to pulsatile higher pressure blood flow. Arterioles and medium sized arteries control vasomotion and are responsible for pressure in the system as well as the distribution of blood. Microvessels, including capillaries, make up the peripheral vasculature and are exposed to far less transmural pressure. They are the primary determinants of fluid and solute exchange between the circulatory system and the tissue. ECs within the vasculature vary depending on the organ they come from. For example, ECs and SMCs have different functions in vessels from the brain, kidney, and mesentery as a result of the different anatomy and flow conditions and humoral exposure experienced within these organs. Cells originating from different organs have different water transport dynamics, salt and sodium-potassium dependence, and paracellular transport. For instance, ECs derived from the brain allow virtually no paracellular transport, while ECs of renal origin are leaky because they provide significant paracellular transport. The data presented here are representative of large conduit arteries, prone to atherosclerosis; ECs and SMCs from different vessels or different organ systems need not show the same trends.

Even within large conduit vessels there is a heterogeneity in the phenotype of ECs and SMCs, evident in aortic ECs having a different tendency for vascular damage depending on whether they come from the aortic arch, or the descending limb (Wissler and Vesselinovitch 1983). Aortic curvature can be concave, which correlates with reduced development of atherosclerosis, or convex, which correlates with the opposite tendency, with accelerated atherosclerosis

in the vessel wall. The internal carotid artery is very susceptible to atherosclerosis, while the external carotid artery is resistant to plaque development. The great heterogeneity of the vascular tree mandates a clear description of the source and type of tissue under study.

Our culture system consisted of bovine aortic endothelial cell (BAEC) monolayers that were utilized to perform Lp and tracer experiments. The ECs in this *in vitro* culture system form static monolayers that experience no shear induced polarity that would provide their actin fibers configuration queues to organize accordingly. Again, it is important to recognize that culture systems derived from different organs exhibit variability in EC and SMC function, so similar studies may provide different results depending on what was studied, the origin of the culture model, and cell treatment protocols. Since we are interested in studying the variation in normal water transport processes brought on solely by the manipulation of aortic endothelial aquaporin-1 expression and distribution, we have chosen an *ex vivo* model comprised of an excised straight segment of the aorta with no genetic or environmental proclivity to vascular disease. Moreover, these aortas are taken from normotensive rats, which generally exhibit no atherosclerosis development. The resulting system is relatively invulnerable to the atherosclerotic process, that is, it does not have disturbed transport that may correlate with elevated proclivity towards atherosclerosis, in contrast to other segments of the aorta, in contrast to other genetic or dietary induced atherosclerotic and in contrast to more athero-prone species. We know that rats have been shown to develop early plaque with cholesterol feeding (Tarbell, Demaio et al. 1999). Since our studies are short-term (relative to even pre-atherosclerotic event time scales) transport studies, such invulnerability to disease should not be material to their results.

Of course it is possible that the relative disease invulnerability of our model system may or may not indicate different AQP mobilization or Lp when compared with EC monolayers hav-

ing atherosclerotic genes, or abnormal flow or in vessels that have been exposed to atherosclerotic genes or from animals fed atherosclerosis-inducing diets or from athero-prone species The fact that Lp measurements from both athero-susceptible rabbit (Tedgui 1984) and athero-unsusceptible rat (Shou 2006) essentially superimpose argues against that possibility. On the other hand, it has been demonstrated that the effects of cAMP depend on the EC substrate studied (Sayner 2011). Difference exists in macro and micro vessels such as arteries, veins and capillaries where cAMP can improve, or alternatively, disrupt/reduce barrier function.

Cells in quiescent and in activated states

Vessel injury causes ECs and SMCs to behave in their activated forms and plays a key role in the development of atherosclerosis and neointimal hyperplasia (NH). Arterial SMCs and ECs are normally quiescent (Q), but can be activated by mechanical injury and by humeral (hormones, proliferative agents (VEGF etc.), cytokines (TNF-α etc.), and pro-coagulant (thrombin etc.) exposure. Q endothelium is maintained by normal laminar blood flow and functions to resist proliferation, inflammation, and coagulation. The Q endothelium has a defined actin structure to control cell-cell and cell-matrix interactions and thus to maintain a paracellular barrier to transmural solute flow. The Q SMC is a non-proliferative contractile cell, as opposed to the activated SMC that is a proliferative, reactive, migratory and synthetic cell.

Role of cAMP in the artery

The consequence of two-hour short-term EC vasopressin type-2 receptor (V2R) stimulation via arginine vasopressin is the activation of membrane adenylyl cyclase with an increase in cellular cAMP content and in protein kinase A (PKA) activity. Noda et al. showed in renal collecting duct cells that when AQP-2 in intracellular vesicles becomes phosphorylated at serine-256, which occurs by the action of cAMP, it binds to tropomyosin-5b which depletes free tropomyosin from the vicinity of the AQP-2 vesicle, thereby fostering local F-actin depolymerization

(Noda, Horikawa et al. 2008). This has the effect of cutting a hole in the cortical actin network around the vesicles, liberating AQP-2 vesicles from their F-actin cage to reach the plasma membrane. If consistent with the known renal action of V2R stimulation, AVP would trigger an increased rate of insertion of intracellular water channel- (or AQP) containing vesicles (WCVs) from trans-golgi into the EC membrane and a decreased rate of endocytosis of WCVs from the EC membrane. The distribution of WCVs between the cytosolic compartment and the EC membrane compartment would thus shift in favor of the EC membrane component (Nielsen, Kwon et al. 1999) during short term stimulation of V2R or transmembrane (via, e.g. forskolin) cAMP stimulation.

cAMP has also been implicated in potentiating VE-cadherin-mediated endothelial cell-cell junctions via ligand binding to GPCRs, such as AVP binding to V2Rs (Noda, Zhang et al. 2010). It has been recognized for some time that enhanced cAMP in the arterial EC system reduces paracellular permeability by virtue of a mechanism that involves rearranging the actin cytoskeleton network (Noda, Zhang et al. 2010). ECs have demonstrated V2Rs (Kaufmann, Oksche et al. 2000) and AVP binding to V2Rs may entail interruption of the EC's actin web, as noted in the last paragraph. This would suggest that the actin belt adjacent to the adherins junction seem to be enhanced at the same time the actin web is diminished (Thi, Tarbell et al. 2004).

Finally, cAMP plays a role in Q or activated systems. Membrane adenylyl cyclase (AC) suppresses the appearance of the activated state, thereby maintaining a Q phenotype. In contrast, other ACs, in particular AC-8, increases during activation.

Experimental results

Our studies of untreated BAEC monolayers show no preferential AQP-1 distribution in culture while treatments with cAMP agonists seem to stimulate a preferential distribution of the AQP epitope in the cell membrane. In addition to inducing changes in AQP-1 distribution and expression, S, AVP and F simultaneously and consistently cause changes in monolayer Lp. AVP and F treatments increase monolayer Lp, the latter increase being far larger in magnitude while S decreases it. These results are consistent with the interpretation that cell membrane AQP-1 facilitates transcellular water transport (Nguyen 2008). In order to test this interpretation, we performed tracer experiments using 70kD dextran. Since the Peclet number for 70 kDa dextran is order one (DeMaio, Tarbell et al. 2004), both advective and diffusive transport are relevant. We found that F treatment did not change monolayer tracer permeability under diffusive conditions but reduced it slightly under convective conditions. Thus the observed increase in monolayer Lp with F far overcomes the diminished paracellular route that F restricts.

If the monolayer results previously described apply to the whole vessel, it would suggest that forskolin treatment (which, as noted, activates AC) serves to minimize resident times of binding molecules and enzymes in the SI by improving barrier function of larger molecules and enhancing fluid flow through the compartment.

We have no data on the electrolyte channel activity and therefore no ability to predict the resultant osmotic conditions within the SI for various treatments. If water flow is dominant and SI hypotonicity occurs, the oncotic gradient could oppose the hydrostatic pressure-driven flow and the effect on macromolecules and adjoining cells would be of consequence. This effect may be small, since the glycocalyx plays a role as a molecular sieve producing a low oncotic pressure

at the luminal face of the cell membrane and isotonic fluid enters the SI paracellularly. Thus one does not expect a large opposing oncotic gradient across the endothelium.

Our *ex vivo* whole vessel study focuses on the role of AQP-1 in EC water transport in whole rat aorta. In short-term F-treated vessels we saw an increased appearance of rings of AQP-1 around ECs rather than a uniformly distributed AQP-1 in the cytoplasm and in the nuclear regions. Short-term F treatment showed much higher EC AQP-1 intensity than in untreated control aortas, but far lower AQP-1 expression in the adjacent SMCs than in those same untreated control aortas. High EC and low SMC AQP-1 with short-term F is consistent with the Q state and so is consistent with, but does not imply AC increase. Interestingly, this effect of F on the SMCs, contrasts with F-treated SMC monocultures, whose AQP-1 expression appeared unchanged upon F-treatment. The lack of reduction in AQP-1 by F treatment in culture suggests this reduced AQP-1 expression in SMCs in whole vessels is endothelium dependent.

In order to explain why the ECs in the whole vessel seem to contain far more AQP-1 than the cultured EC monolayers upon short-term treatment with F, consider possible differences in EC phenotype between these experiments. We speculate our study in culture may not have been a Q experimental model since the ECs in that study were grown without any transmural pressure or shear stress. Such factors impact EC phenotype dramatically. In contrast, endothelial cells from the native vessel experienced *in vivo* conditions until animal sacrifice and vessel excision; their phenotypes are likely far closer to their respective Q states. The absence of a transmural pressure also results in a dwarfed glycocalyx layer as compared to that in the native state, which may also affect EC phenotype. ECs in the native state experience pressure-driven shear flow, which shrinks and aligns these cells according to cues initiated by shear force. It is conceivable that flow-induced quiescence imparts a higher EC sensitivity to F stimulation similar to studies

in renal epithelial cells (Jang, Cho et al. 2011). On the other hand, transport studies across EC monolayers have proven themselves very relevant for understanding quantitatively the role of the endothelium in artery wall transport (DeMaio, Tarbell et al. 2004; Cancel, Fitting et al. 2007).

Endothelial command of smooth muscle cells

A number of potential mechanisms could possibly explain how the EC influences SMC behavior. EC natriuretic peptide (NP) release and transport to SMC NP receptors (NPR) may play a role in mediating the communication between ECs and SMCs. Recent demonstration of a 15-fold increase in C-type (C) natriuretic peptide (NP) transcript in rat thyroid cells in response to dbcAMP (Sellitti, Puggina et al. 2004) invites speculation as to whether endothelial CNP may be upregulated by cAMP in a similar manner and bind to natriuretic peptide receptor-C (NPR-C) on SMCs in a paracrine manner. NPR-C binding by CNP has been reported to inhibit the migration and proliferation of rat and human aortic smooth muscle cells (Hutchinson, Trindade et al. 1997; Kohno, Yokokawa et al. 1997; Anand-Srivastava 2005). AQPs facilitate cell migration by a mechanism that might involve water transport in lamellipodia of migrating cells (Verkman 2005). Thus CNP-bound NPR-C induced anti-mitogenic cellular responses may lead to - or even occur via - reductions in AQP-1 expression in affected cells. This apparent connection requires further investigation.

Reduction in AQP-1 expression in SMCs could also occur from the anti-mitogenic effect of NO. Increased endothelial nitric oxide synthase (eNOS) synthesizes NO. cAMP-induced membrane insertion of AQP-1 channels, which also transports NO (Herrera and Garvin 2007), can facilitate NO transport, aided by advection through the SI, to the SMCs. Our findings seems to provide a possible explanation for Mechaly et al.'s unresolved experimental finding that low concentrations of AVP in the presence of SR49059, a vasopressin type 1a antagonist, induce re-

laxation in noradrenaline-precontracted vascular preparations of rat aorta. AVP was responsible for inducing a contractile effect on precontracted rat aorta, so their paradoxical observation of relaxation by AVP in the presence of SR49059 led them to suspect a presence of relaxing vasopressinergic non-V1A receptors in their experimental conditions. Our findings would lead us to believe, the action of V2R stimulation promoted eNOS production in ECs concurrently with improved delivery of NO facilitated by AQP-1 into the SI and then on to the SMCs.

cAMP also stimulates a cAMP response element (CRE) region of EC DNA. A CREB-binding protein (CBP) coactivates this DNA, allowing it to switch certain genes on or off. In particular, CBP coactivates the Krüppel-like transcription factor 2 (KLF-2), causing an anti-atherogenic response in SMCs by maintaining the SMC contractile quiescent phenotype (Hergenreider, Heydt et al. 2012) and preventing the SMC transformation to the activated state. This activated state is believed to play an important role in initiating atherosclerosis and NH.

Summary and outlook

Nguyen and Xue showed that decreasing functioning AQP-1s decreases endothelial and whole vessel wall Lp. This thesis has asked the question, does upregulating AQP-1 expression increase Lp (and Lpe)? By chemically increasing endothelial AQP-1 expression, we have increased both of these Lps. Increasing endothelial Lp had the effect, which our theory predicted, of decompressing the SI at higher pressures than with normal AQP-1 expression. That is, the dynamic range of intima compaction, i.e., the pressures over which the SI goes from uncompressed to fully compressed, shifted to higher ΔPs in response to upregulating AQP-1 in whole vessels. Such decompression and resulting Lp increase should increase water flow through SI and therefore lower the tracer (e.g., LDL) concentration in the SI, which may slow its binding to SI ECM and therefore slow the development of atherosclerosis.

To gain insight into the role of AQP-1 in the pathophysiology of atherosclerosis via lesion formation the next step is to consider transgenic animals that are susceptible to plaque formation. AQP-1 knockout animals do not form lesions under normal feeding conditions. Yet even though increasing AQP-1 could potentially slow lesion formation, it does not necessarily follow that decreasing AQP-1 must increase lesion formation, because the basal AQP-1 expression may already be too low to have any positive effect that down-regulation would eliminate.

Recall that EC AQP-1 transports EC-derived NO out of the ECs and allows it to transport to the SMCs (Herrera and Garvin 2007). Thus, in analogy to reduced AQP-1, one could look for hints in the literature by looking at the results of reduced NO. There are three sources of NO synthase (NOS) in the body. Triply NOS knockout mice exhibit hypertension and lesion formation in their coronary arteries and microvessels as well as in their cerebral and renal arteries with no change in serum cholesterol (Tsutsui, Shimokawa et al. 2006). Singly or doubly knockout animals did not exhibit increased lesion formation. We could also speculate from our results that lack of NO causes the media to become stiff, which in turn facilitates compression of the intima and contributes to lesion formation.

The dynamics at play in the cardiovascular system between ECs and SMCs may also occur in other organs and potentially play an important role in the pathophysiology of other organ specific diseases and maladies involving dysfunction in paracrine communication between ECs and SMCs.

Appendix I: Supplemental *in vitro* Images

The figures in Appendix I display z-stacks and single slices of both lower magnification views of BAEC monolayers and higher magnification views of single cells that show our confocal measurements of green fluorescence for each of the treatments: control (0.1%wt DMSO), 20 hr. S, 20 hr. AVP, 2 hr. F, 20 hr. AVP/S and 2 hr. F/20 hr. S. z-stacks assemble in sequence provide a three dimensional picture of the green fluorescence in the cell or monolayer. AVP/S treatment (20 hours) decreased both AQP-1 expression and Lp compared against untreated monolayers. F (2 hours)/S (20 hours) treatment did not significantly change Lp but did decrease AQP-1 expression; apparently the redistribution made up for the overall decrease in number. However, of all of the treatments, the apparent localization of AQP-1 in membrane was starkest in samples treated with F/S. This suggests that while F treatment likely causes a buildup of AQP-1 in the membrane that persists despite S-treatment, that S treatment reduces AQP-1 content in the cell as a whole and, in particular, in the cytosol. The result is an accentuated membrane/cytosol contrast.

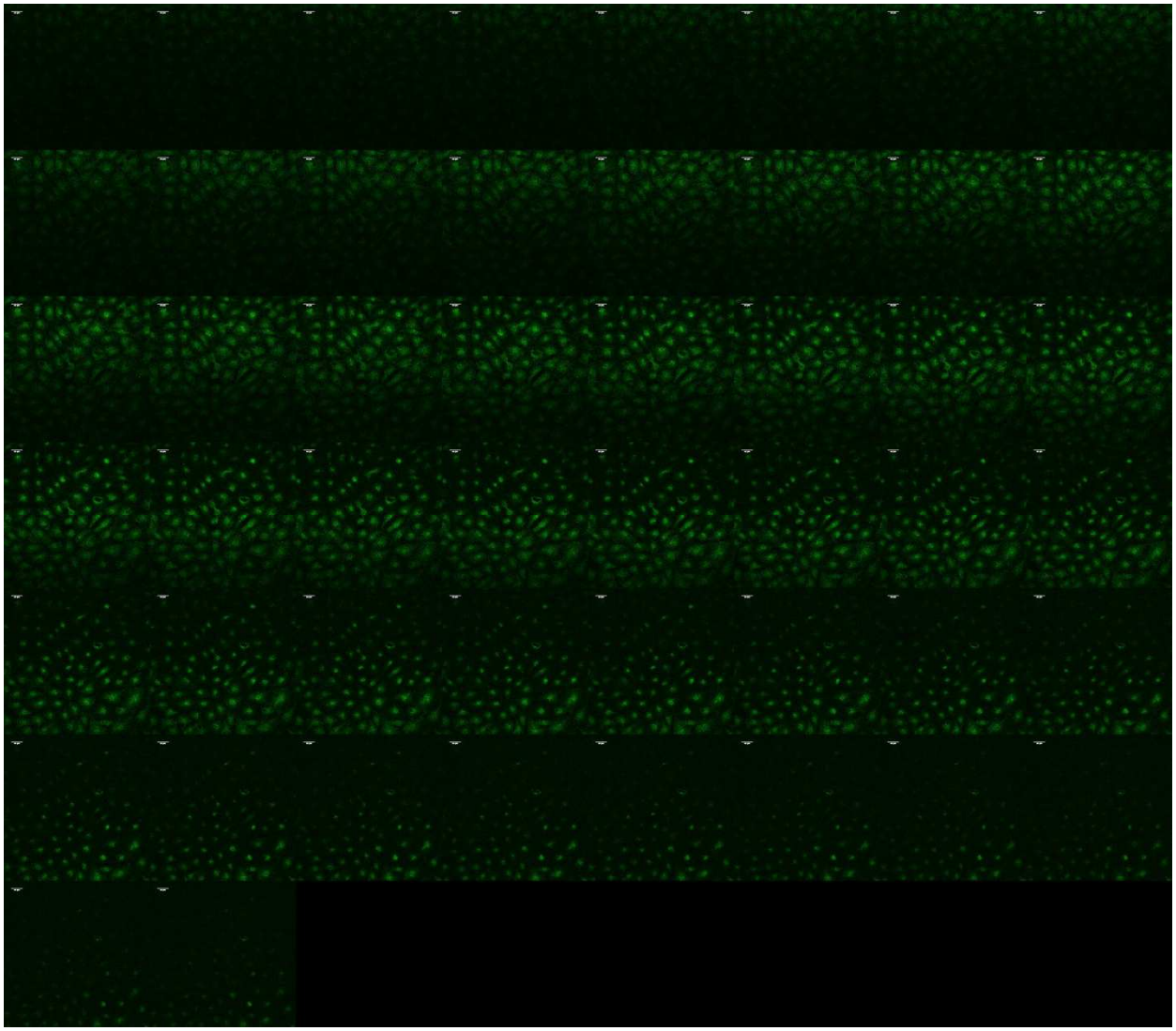

Figure 30: A confocal extended focus image of an untreated BAEC monolayer z-stack that clearly expresses AQP-1 (green fluorescence). There are 50 optical serial sections in this gallery and those that follow (fig. 12-21) representing a total thickness of ~ 4 μm.in the z coordinate center of the monolayer. Physical thickness of each sample (fig. 12-21) varied with range of EC height, which is approximately ~4μm (Liu, Yen et al. 1994). Untreated monolayers were exposed to blank (0.1%wt DMSO) solution during treatment. (bar = 30 microns)

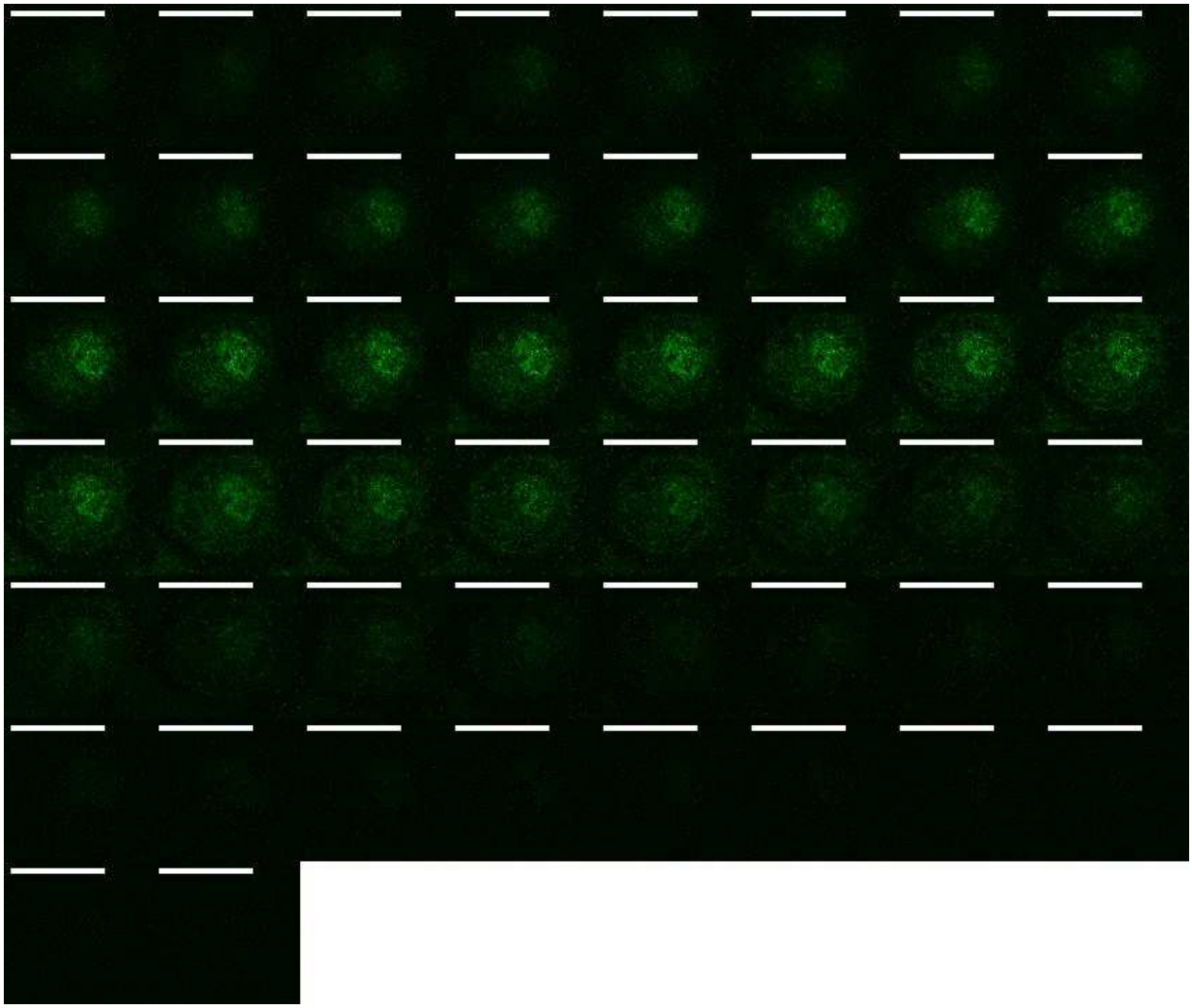

Figure 31: Magnified extended focus image of untreated single BAEC: Cropped from previous figure. The AQP-1 concentration appears higher in the cytoplasmic structures around the nucleus than at the cell border. Untreated monolayers where exposed to blank (0.1%wt DMSO) solution during treatment. (bar = 25 microns)

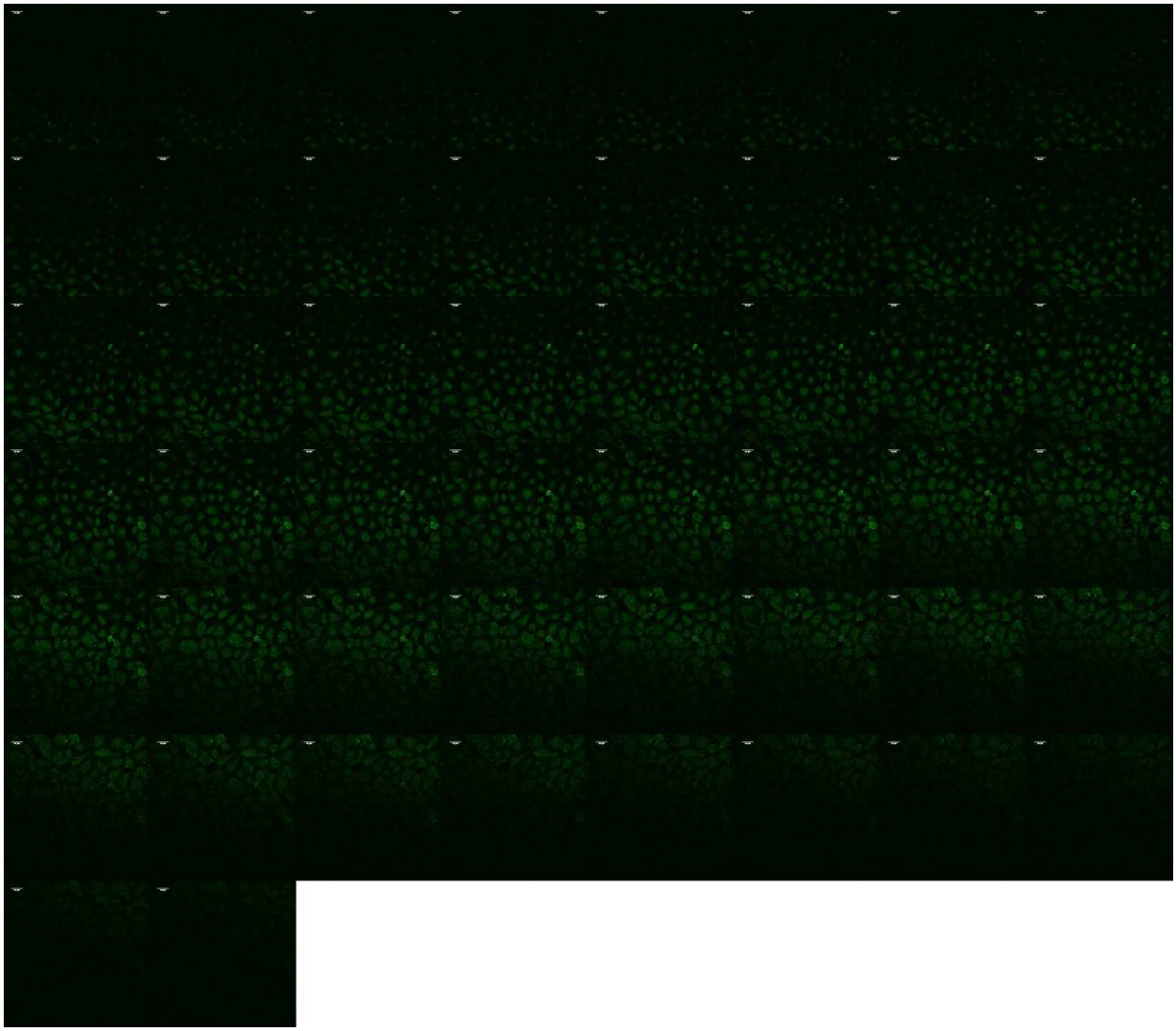

Figure 32: Satavaptan-treated BAECs express AQP-1: A confocal extended focus z-stack of images, that is, views of a large number of cells, of an S-treated (20 hrs.) BAEC mono-layer that clearly expresses AQP-1 (green fluorescence). (bar = 30 microns)

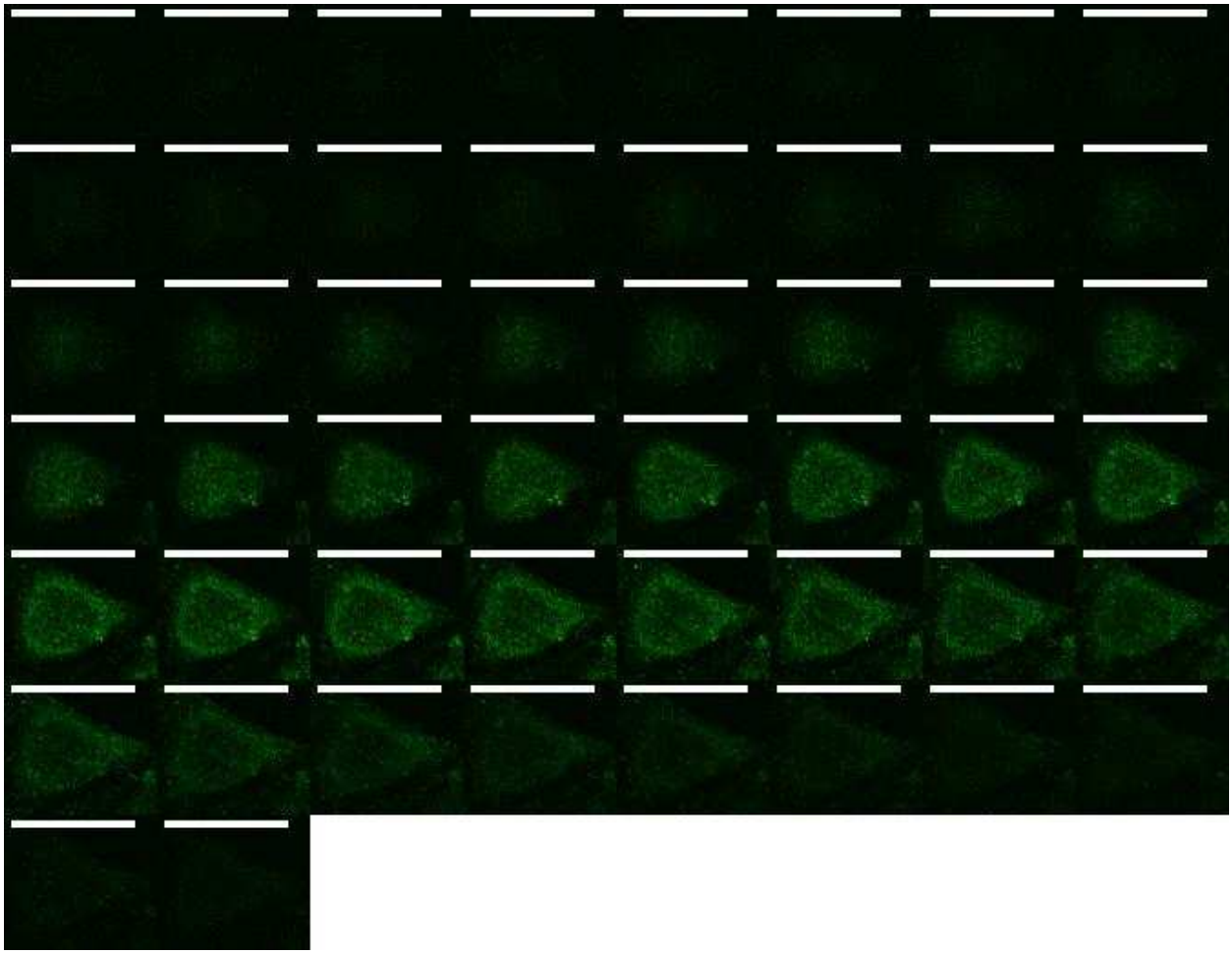

Figure 33: Satavaptan (20 hours) appears to lower intracellular AQP-1: Cropped from previous figure, z-stack of a single BAEC under high magnification after S treatment (20 hours). The AQP-1 concentration appears lower in the cytoplasmic structures around the nucleus than at the cell borders or membrane region. 20 hours is sufficient time to reduce AQP-1 production and thus constitutive expression. Our results, illustrated above, suggest migration of AQP-1 in the cytoplasm to the cell membrane to apparently maintain BAEC membrane AQP-1 concentration after inverse agonist action of S. This could be the product of V2R cytoplasmic shuttling after (inverse) agonist stimulation, as seen 45 minutes after addition of AVP in culture to renal epithelial cells (Bouley, Hawthorn et al. 2006). V2R migration into intracellular vesicular bodies could possibly function as a means to regulate BAEC homeostasis after V2R stimulation. The concentration of AQP-1 in the cytoplasm appears to be less than untreated BAECs. This is depicted qualitatively by the relative contrast of preferential labeling in the membrane versus the cytoplasm in the sample above. (bar = 25 microns)

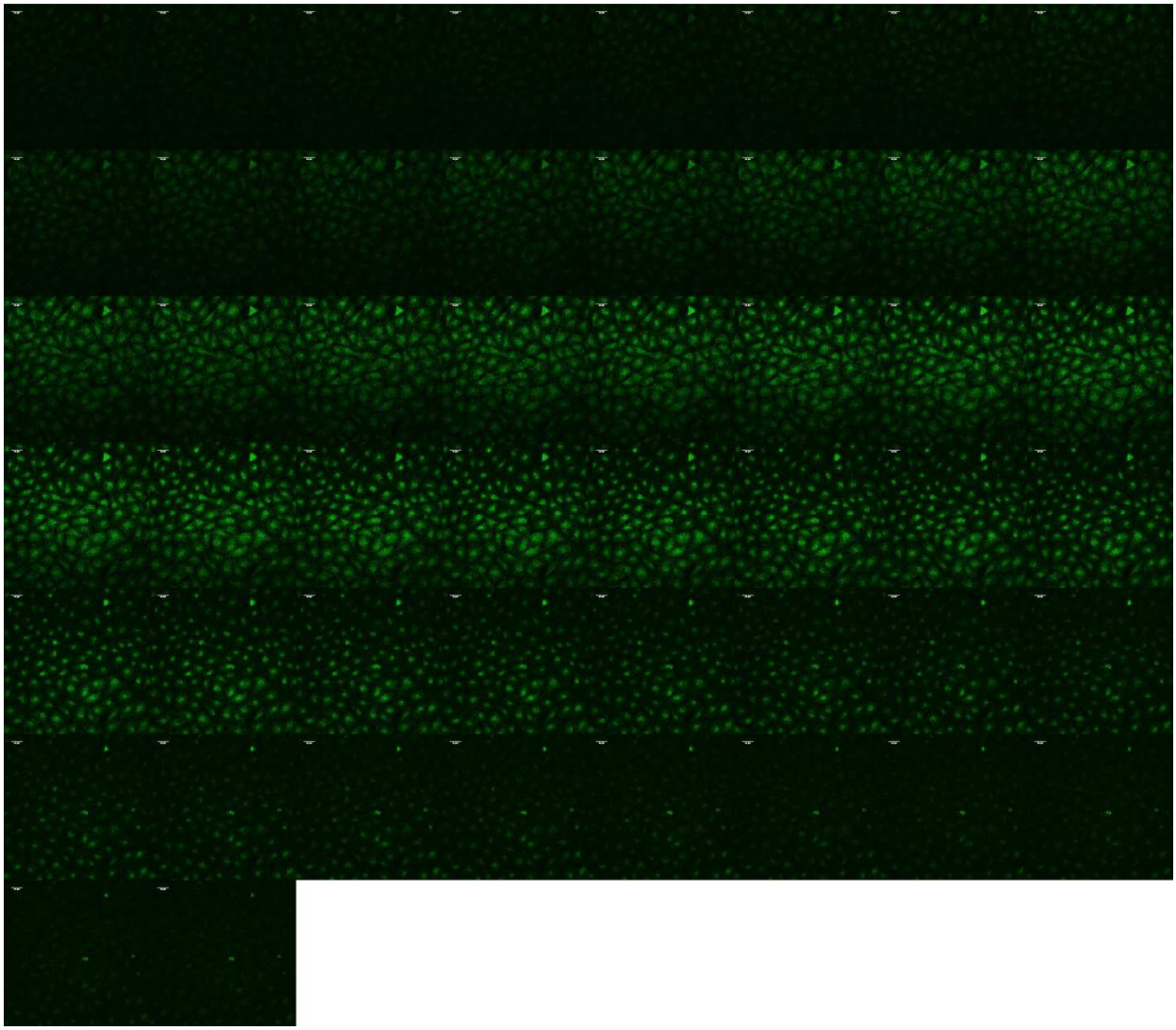

Figure 34: AVP-treated monolayers express high levels of AQP-1. A confocal extended focus image of an AVP treated (20 hours) BAEC z-stack that clearly expresses AQP-1 (green fluorescence). (bar = 30 microns)

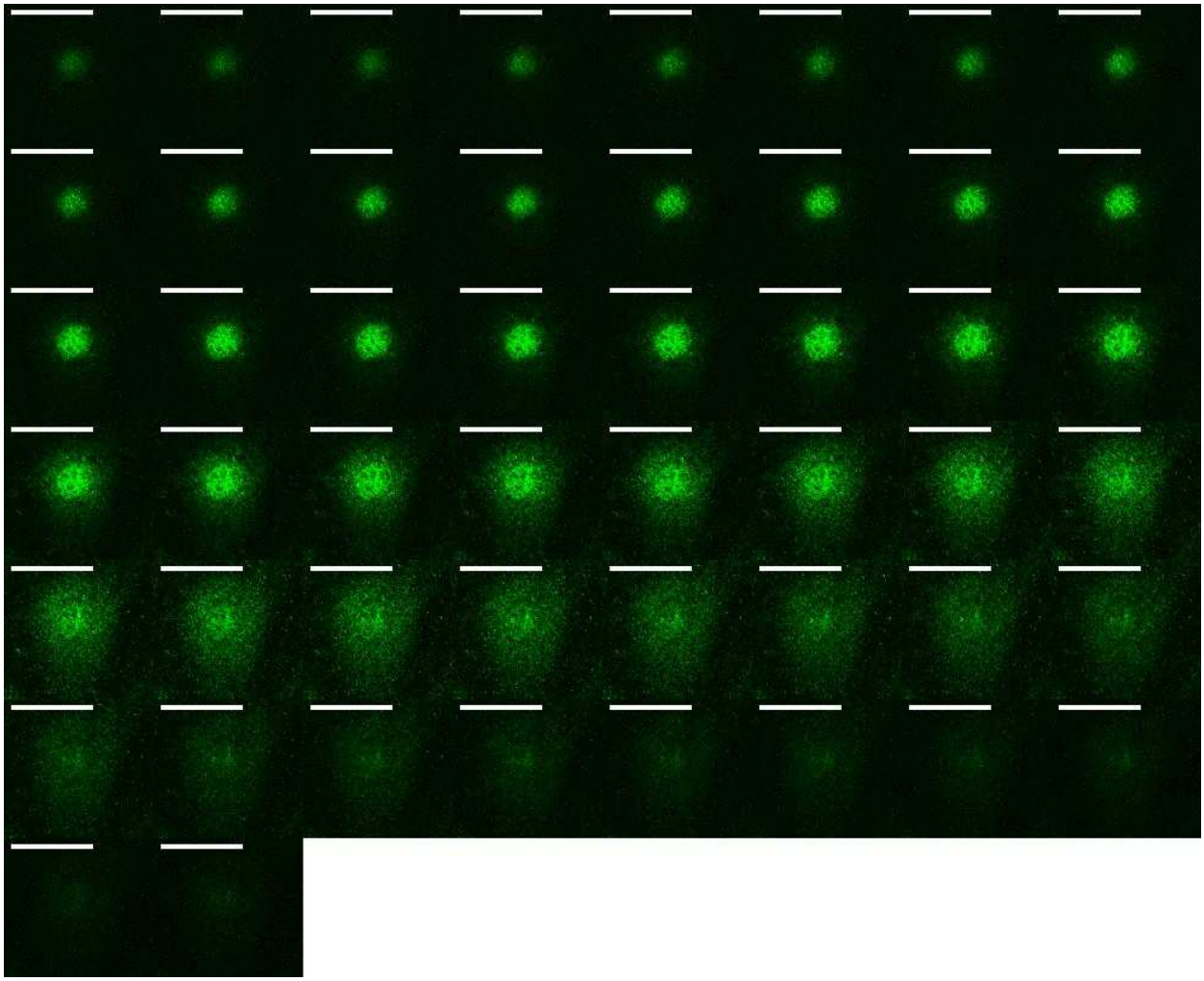

Figure 35: AQP-1 distribution appears greater in cytoplasm and nucleus. Cropped from previous figure. AVP treated single BAEC z-stack. The AQP-1 concentration appears greater in the cytoplasmic structures around the nucleus than at the cell borders or membrane region. After 20 hours, constitutive increases in AQP-1 expression appear to increase the presence of intracellular vesicles containing AQP-1, presumably as a means to store excess protein for later migration to cell membrane in response to cellular demand and/or environmental ques. V2R may also be migrating from the membrane into intracellular vesicles in analogous fashion to epithelial cells after V2R stimulation (Bouley, Hawthorn et al. 2006). Our results, illustrated above, suggest localization of AQP-1 within vesicles in the cytoplasm, apparently to maintain BAEC membrane AQP-1 concentration after agonist action of long term (20 hours) AVP stimulation of V2R. (bar = 25 microns)

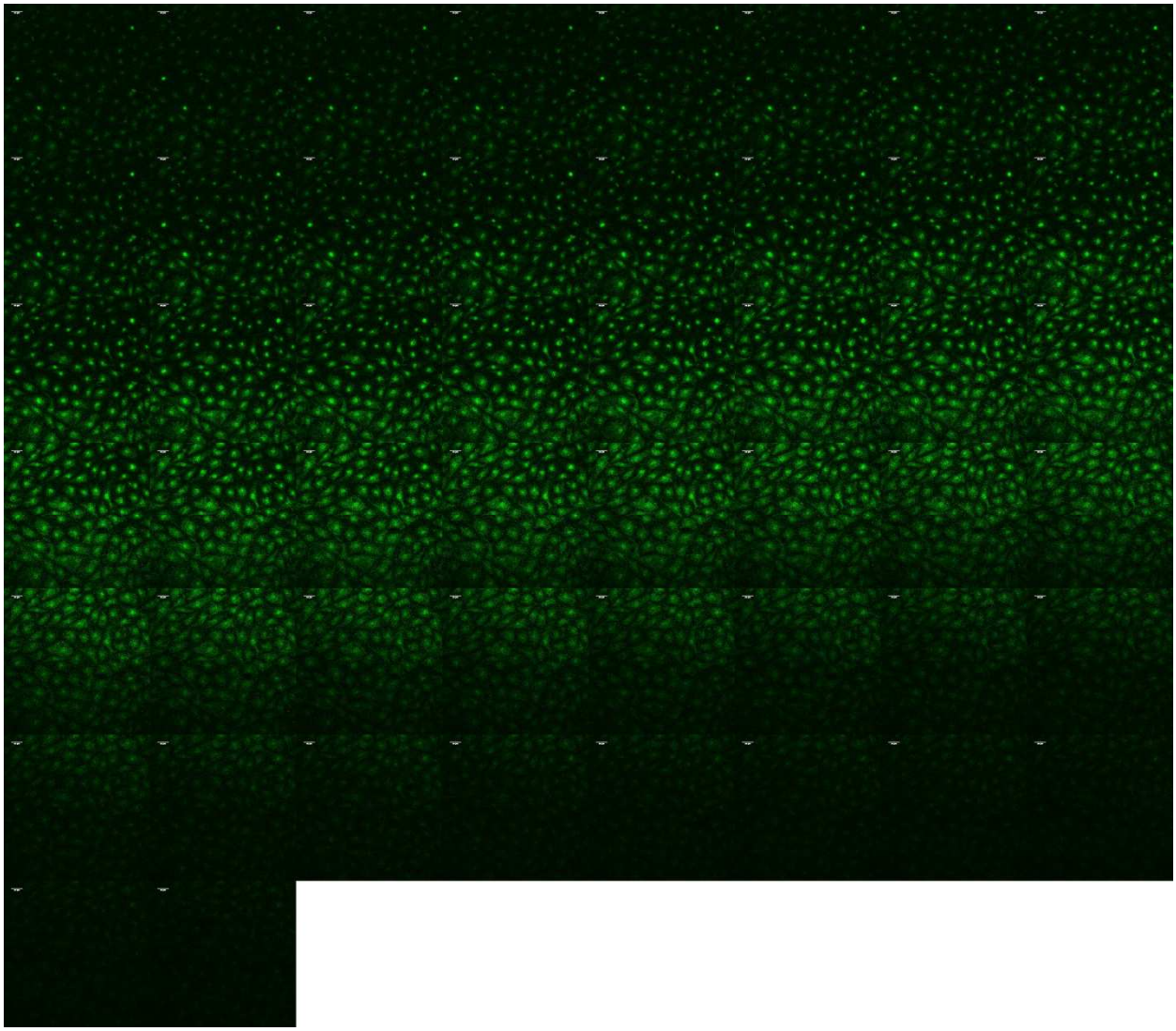

Figure 36: F-treated monolayers express AQP-1. A confocal extended focus image of an F treated (2 hours) BAEC z-stack that clearly expresses AQP-1 (green fluorescence). (bar = 30 microns)

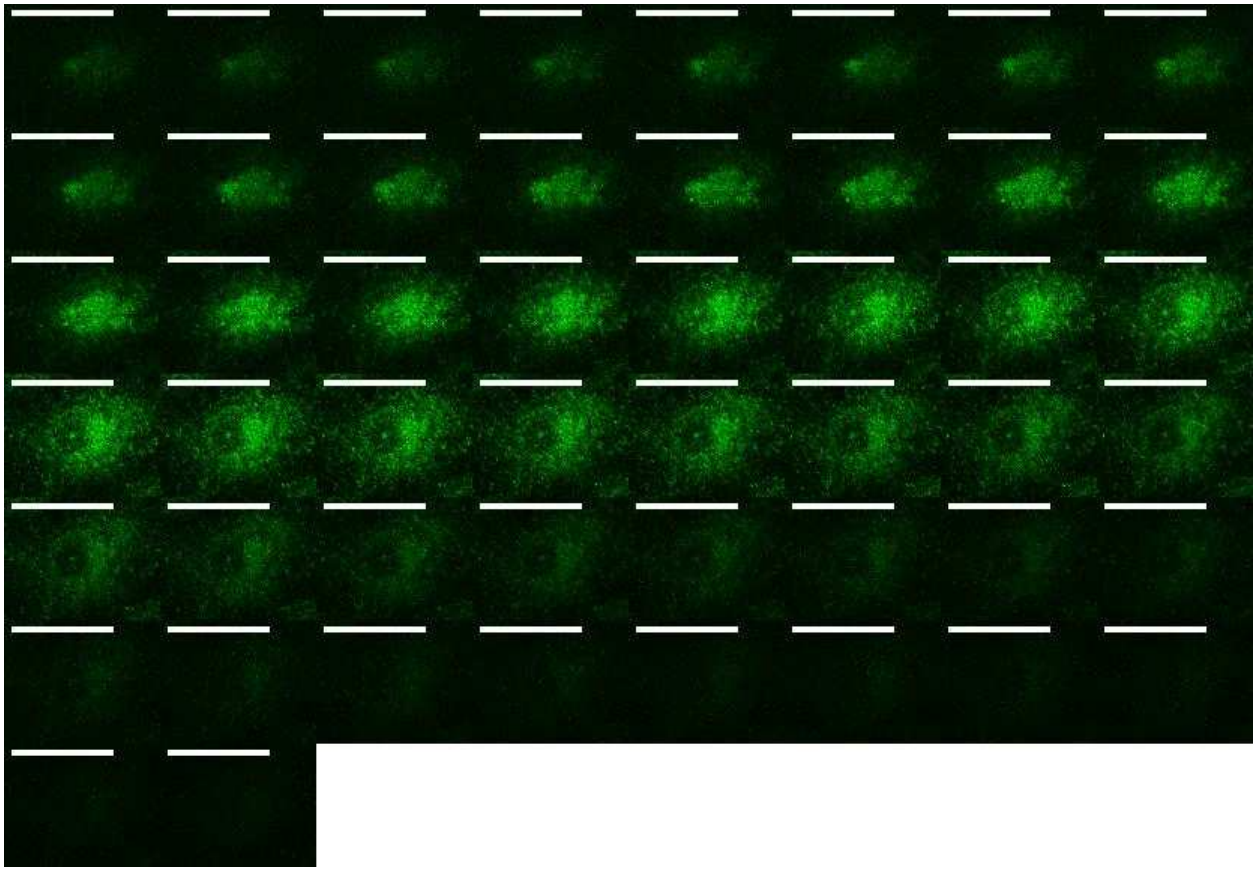

Figure 37: F treated BAEC exhibits contrasting distribution of AQP-1 in cell membrane and cytoplasm. Cropped from previous figure, F treated single BAEC z-stack. The AQP-1 concentration appears lower in the cytoplasmic structures around the nucleus than at the cell borders or membrane region. The dark spot at center particularly shows lack of AQP-1 labeling. Observed AQP-1 localization in membrane is consistent with membrane shuttling of AQP-1 induced by intracellular increases of cAMP via V2R stimulation. Instead of a constitutive upregulation, such as observed with AVP or S, we instead see a redistribution of AQP-1 from intracellular stores to the cell membrane. (bar = 25 microns)

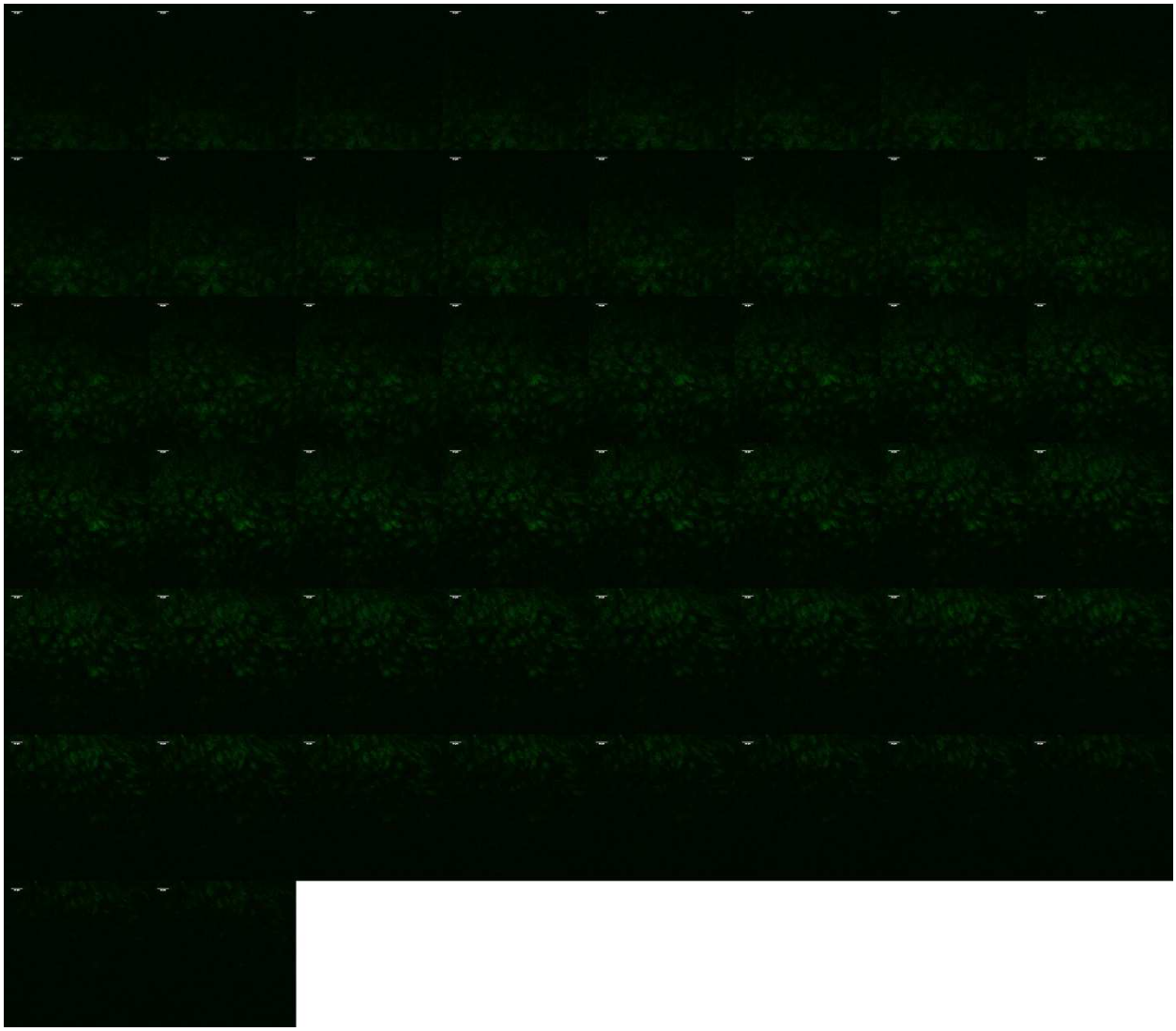

Figure 38: A confocal extended focus image of an F/S treated (2 hours/20 hours) BAEC z-stack that clearly expresses AQP-1 (green fluorescence). After quantification of intensity, F/S treated monolayers exhibited reduced AQP-1 expression compared to untreated monolayers ($P<0.05$). (bar = 30 microns)

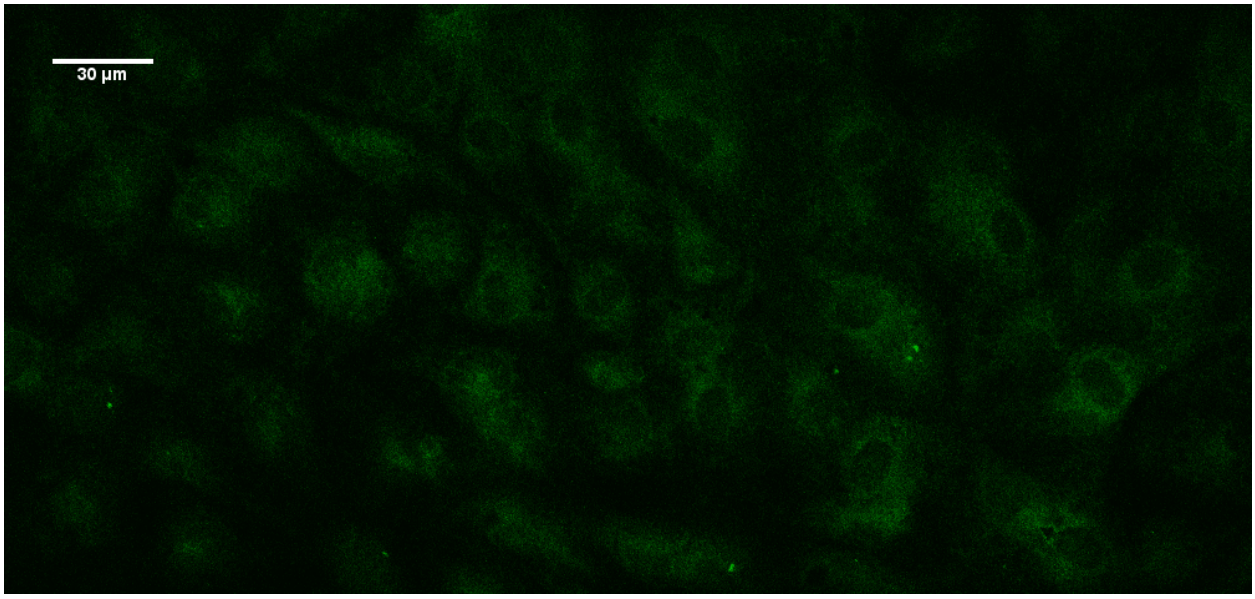

Figure 39: F (2 hours)/S (20 hours) treated single BAEC z-stack express greater AQP-1 labeling in membrane in contrast to cytoplasm where there are many AQP-1 deficient areas (dark egg-like regions). Cropped from previous figure, the AQP-1 concentration appears lower in the cytoplasmic structures around the nucleus than at the cell borders or membrane region. F/S treatment did not cause a significant change in Lp in BAEC monolayers ($P<0.05$). Due to significant redistribution after F/S treatment (bar = 30 microns)

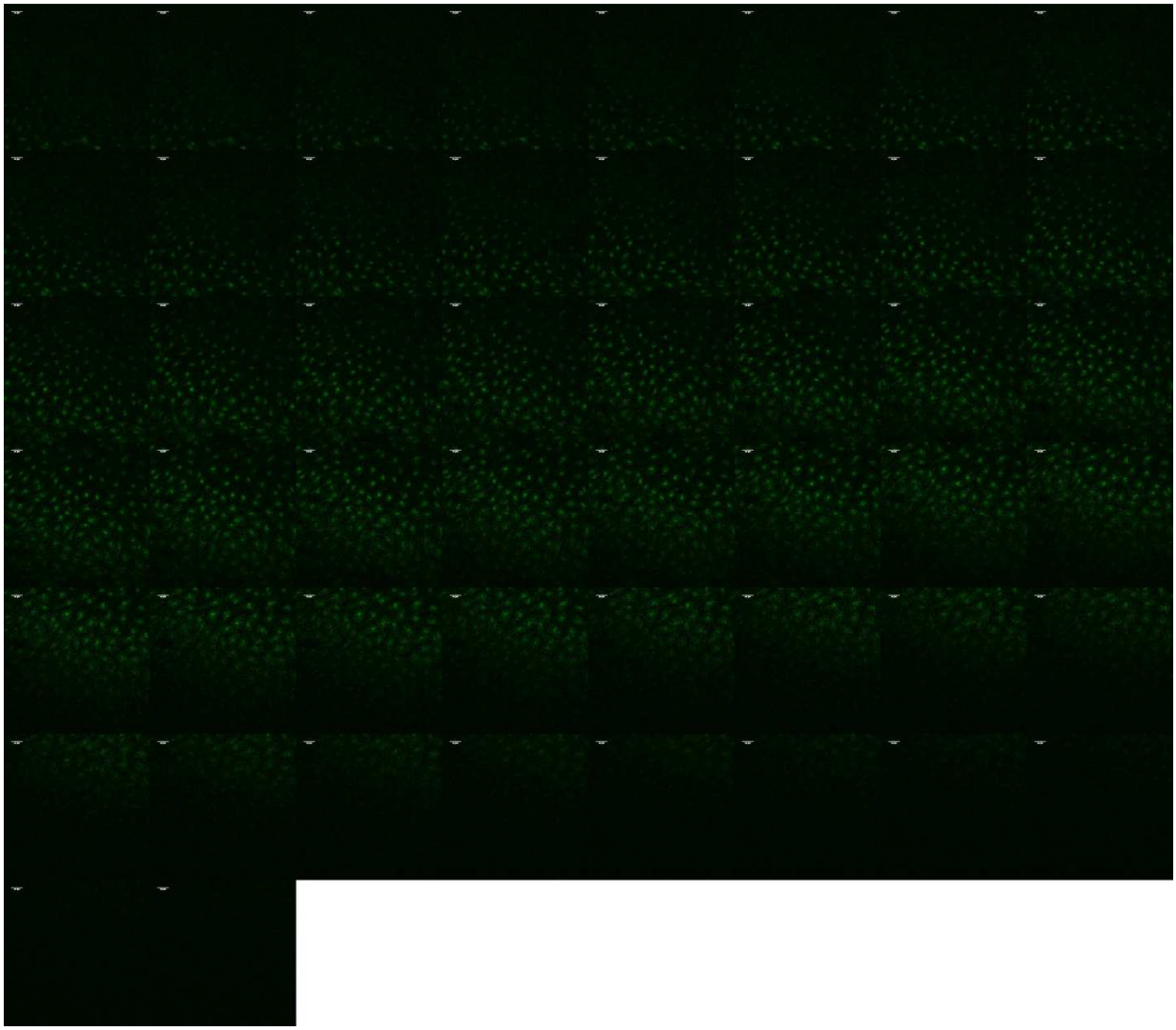

Figure 40: A confocal extended focus image of an A/S treated (20 hours) BAEC z-stack that clearly expresses AQP-1 (green fluorescence). A/S treatment decreased overall AQP-1 expression in BAEC monolayers, as well as Lp, compared to untreated monolayers ($P<0.05$). This would be consistent with S acting as both a blocker and inverse reaction agonist. S both blocks AVP from stimulating V2R as well as potentiating an inverse agonist effect.

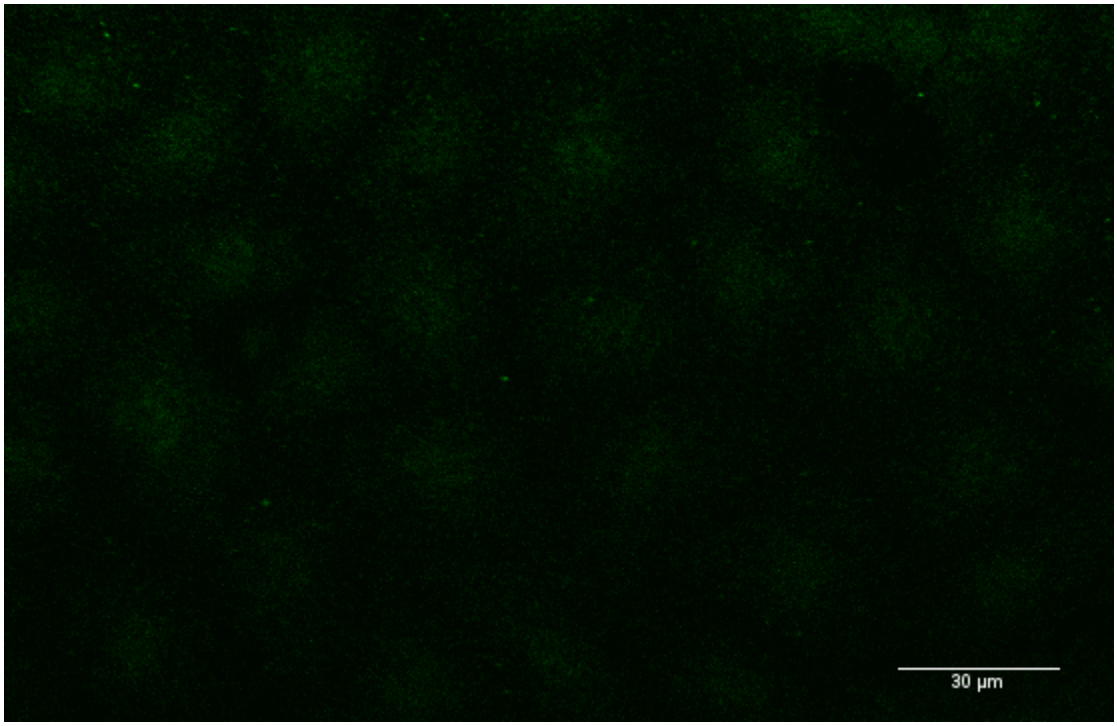

Figure 41: A (20 hours)/S (20 hours) treated single BAEC z-stack express no greater AQP-1 labeling within cytoplasm and nucleus then in cell membrane. (bar = 30 microns)

Appendix II: Literature Review of Historical Experimental Methods

Ex vivo Lp Measurement Methods

The investigation of Lp has progressed through the collaborative and extensive efforts of several key contributors. In order to convey my understanding of the evolution of the theory and the methodology required to obtain reliable measurements of Lp, I will provide a discourse that reviews the studies that have provided the groundwork for our group's experimental protocols and mathematical models.

The Lp of endothelial cell monolayers, both in the microvasculature and *in vitro* have previously been measured by other groups. The first experiments to determine the hydraulic conductivity of the endothelium were those carried out by Landis et al. (Landis 1927) on micro-vessels, and later improved upon by Zweifach et al. (Lee, Smaje et al. 1971) in which the relative movement of red blood cells in occluded vessels was tracked to measure outflow. Developments in cell culture models for the same purpose by various researchers (Baetscher and Brune 1983; Suttorp, Hessz et al. 1988; Tarbell, Lever et al. 1988; Dull, Jo et al. 1991; Turner 1992), introduced a flow marker (air bubble) in a separate impermeable chamber (a calibrated capillary tube) in-stream with the experimental cell preparation, that ensured that marker movement was a result only of volume flow across the monolayer. Further improvements added automated bubble-tracking components and computerized data acquisition as published in Sill et al. (Dull, Jo et al. 1991).

Tedgui and Lever 1984

In 1984 Tedgui and Lever investigated the filtration through damaged and undamaged rabbit thoracic aorta under physiologically representative conditions by maintaining both the geometry and integrity of the vessel endothelium *ex vivo*, as they would be configured *in vivo*.

By carefully maintaining an intact endothelial layer, they examined its contribution to vessel permeability by measuring vessel hydraulic conductivity first with intact, and then with denuded endothelium on the different segments of the same vessel. Because this seminal paper provides the foundation for both the work of our group and other experimental work on these vessels, I will take some time to convey both the methods employed and the results obtained as well as to discuss their implications for the characterization of transport in the arterial wall.

Tedgui and Lever began by anaesthetizing a Male New Zealand White rabbit (2-2.5 kg). The animal was then placed on mechanical ventilation by intubating its trachea. The thorax was exposed at the abdomen nearest to the sternum, and the aorta was revealed between the heart and the diaphragm by displacement of the lungs. Heparin (1000 IU) was administered intravenously, and the arterial branches stemming from the aorta were ligated. A surgical challenge in this procedure is avoiding the compression of the aorta while tying off the branches that are on its underside. Any damage to the cell wall would severely affect (i.e., drastically increase) the hydraulic conductivity measurement, and so a high degree of expertise and precision must be maintained throughout the procedure. The ligation was carried out on all portions of the aorta to be excised, which constituted eight pairs of intercostals arteries, at about 1-2 mm from the aorta.

After the preparation of the vessel, a 16-gauge needle was placed retrograde at the distal end of the rabbit's aorta. This needle was attached to an apparatus that allowed it to deliver solution from an elevated reservoir at an elevated pressure. Along with cardiac pumping, the attached elevated reservoirs continuously maintained the pressure within the vessel so as to avoid even momentary vessel collapse that can cause endothelial damage. The reservoir was secured 80 cm above the animal and contained Tyrode solution with 4% bovine serum albumin (BSA) at pH of 7.4. The needle was secured to the vessel externally, and another ligature was tied around

the proximal aorta just below the arch. This further maintained the pressurization of the vessel by the pressure head of the reservoir. The other end of the vessel was then connected to a needle pointing distally into the midregion of the aorta and secured with string. The two needles were clamped into an adjustable rig that held the lower section of the aorta at its normal *in vivo* length and prevented shortening of the vessel after excision. The Tyrode solution was kept at 40±0.5°C. After excision of the lower section, the upper portion of the aorta was cannulated, excised, and placed into the incubating solution. After removal of the aorta, sectioning showed that a layer of adventitia 20-50 μm in thickness was retained on the vessel's outer surface (Tedgui 1984).

To prevent the vessel from drying and the subsequent loss of cells, they continuously applied a rewetting agent consisting of Tyrode solution containing 2% bovine serum albumin directly on the vessel. The bovine protein was added in order to keep the endothelium intact and to maintain the osmotic pressure gradient across the vessel wall (Tedgui 1984). The aorta was then flushed at *in vivo* conditions with Tyrode solution containing 0.03% Evans blue dye. The dye served a dual purpose in both identifying the presence of leaks as well as in depicting the vitality of the endothelium. In most experiments the luminal surface (>95%) of the vessel was completely white. Intense blue staining over the whole luminal surface was present indicated that there was significant cell death in tissue (Tedgui 1984). Vessels with unligated intercostals caused intense bluing of the adventitia because of perfusion of the vasa vasorum. As noted above, in some experiments the entire endothelium was denuded from the luminal surface, and the Lp and transmural pressures were measured and compared with measurements on the vessel with its endothelium intact. They later used these paired measurements to calculate the contribution of the endothelial layers to the wall's hydraulic conductivity.

Segments of vessels were studied using electron microscopy by performing the aforementioned artery preparation and then dehydrating and mounting arterial segments to aluminum stubs, coated with gold-palladium, and viewed in a Phillip Scanning Electron Microscopy (SEM) 505. The segments were postfixed in osmium tetroxide and, after acetone dehydration, were embedded in epoxy resin. About 20 transverse sections from each arterial segment were post-fixed in osmium tetroxide and after dehydration, were stained with uranyl acetate and lead citrate and viewed in a Phillips EM 400 electron microscope (TEM) (Tedgui 1984). The results of this study provided a very developed characterization of the vessel's structure and its transport properties.

The SEM images provided an assessment of the integrity of the endothelial layer as well as the internal elastic lamella. In de-endothelialized vessels, there was an absence of cellular elements and instead they had a fibrillar structure on the luminal surface. TEM images illustrated that, though the endothelial cells were damaged or absent in those arteries subjected to silicone catheterization, which denudes vessel, the IEL remained intact.

Measurement of filtration or EM preparation was then carried out on the excised portion of the segmented vessel. A 80-cm-nylon tube (0.15-cm diameter) was connected at its upstream end to a manometer pressurized to 80 cm H_2O while the downstream end was connected to the pressurized artery via a three-way connector. The tube was mounted horizontally on a fine-scaled ruler. The connector was then opened to the vessel, and the luminal pressure equilibrated with the pressure of the manometer; this established the distended pressure at 70 or 180 mmHg. At this time, the artery was examined and any leaks were marked by blue dye in the bath solution. Leaks were either re-ligated or, if this did not seal the leak, the artery was discarded (Tedgui 1984).

Tedgui and Lever then injected a small air bubble into the upstream portion of the nylon tube through the three-way connector. The movement of the front meniscus of the bubble in the tube was measured initially every 4 minutes and subsequently every 1-minute. The movement of fluid was observed and recorded for 90 minutes. The pressure during this recording was kept constant to within 1% of its initial value. Since the nylon tube was sealed and of time-invariant dimensions, and since the perfusate was incompressible, the volume flow rate of fluid that entered the vessel at steady state was equal to the volume flow rate of fluid exiting through the vessel walls. By assuming cylindrical vessel geometry, the external surface area of the vessel and the internal volume were estimated with vernier calipers by length and outer diameter measurements at the end of the experiment. The fluid flux was expressed as the inflow per unit external surface area of the artery wall, which was initially a function of time until steady state including vessel mitogenic responses, was achieved. It is important to note that the bubble position, whose change indicated the inflow of liquid into the vessel, typically became linear with time after about 25-30 minutes as the vessel's luminal area adjusted itself to the newly imposed transmural pressure. This was likely due to mechanical creep of the tissue due to the relaxation of the vascular smooth muscle following sectioning of nerves, from tissue consolidation (Kenyon 1979) and from vessel adjustment to the new transmural pressure. The filtration flow of fluid through the artery wall was taken to be a constant times the slope of the linear (steady state) portion of the bubble position vs. time curves.

Both segments of the same aorta were studied either in intact or de-endothelialized form. The pressure applied to the upstream and downstream segments of the vessel were varied in different experiments and no significant variability was observed in the filtration rates. The intact and de- endothelialized vessels' filtration flow rate values were averaged at transmural pressures

of 70 and 180 mmHg (Tedgui 1984). The amount of segments used for Lp calculation of intact and denuded vessels were 32 and 24 aortic segments, respectively.

The hydraulic conductivity of the vessel walls was calculated from the following equation (Kedem and Katchalsky 1958):

$$Jv = Lp (\Delta P - \sigma \Delta \Pi) \qquad (1)$$

where Jv is the filtration flow rate per unit external surface area, Lp is the hydraulic conductivity, ΔP and $\Delta \Pi$ are the hydrostatic and colloid osmotic pressure differences (inside minus outside), and σ is the osmotic reflection coefficient. By experimental design (using the same albumin concentration in the perfusate and in the suffusate) the influence of the osmotic pressure term in Eq. 1 is made small compared with the hydrostatic pressure term (Taylor, Granger et al. 1977). Thus the equation becomes

$$Lp = Jv / \Delta P \qquad (2)$$

The average hydraulic conductivity of the intact vessels was significantly greater ($P < 0.01$) at the transmural pressure of 70 mmHg than at 180 mmHg. The hydraulic conductivity of the de-endothelialized vessels was higher than that of the intact vessels at either pressure ($P < 0.01$) but, interestingly, was not significantly different at these two pressures. Table below summarizes the results reported in this work.

Lp of Vessel Wall cm/(s*mmHg) x 10^{-8}		
Pressure (mmHg)	Intact Endothelium	Damaged Endothelium
70	4.00±1.31	5.36±1.62
180	2.44±0.08	5.27±0.84

Table 3: Hydraulic Conductivity of the total wall. (Tedgui 1984)

Through two-way analysis of variance, it was determined that there was a significant variation due to both transmural pressure and endothelial integrity in the filtration rates of the vessels (Tedgui 1984). The volume change of the vessels after a change in pressurization was considered and such changes were found to have occurred over the range of pressures applied. However, the percent increase in vessel radius did not exceed 3.28%. This volume change during the incubation period appears to have been either the result of a change in smooth muscle tone or simply the effect of the viscoelastic properties of the wall components (Patel, Janicki et al. 1973).

The filtration rate was calculated under the assumption that the fluid passed through the whole thickness of the aortic wall, although some would have passed through the thinner walled ligated stumps of the intercostals arteries. However, due to the relatively small diameter and length of these stumps, such a flow could have only accounted for less than 1% of the total luminal aggregate surface area. It should also be noted that the presence of the blue dye in the intact vessels showed that the wall could be damaged around the intercostal ligatures. These two points would likely have led to an overestimation of the conductivity in the vessel (Tedgui 1984). However, the authors estimate that the surface area of the vessel could not have been damaged beyond 5% due to ligated stumps, and so the calculated Lp could be no more than 5% less than the true Lp.

The Lp calculation did not involve the vessel thickness under the assumption that the resistance to filtration resembles that of a thin membrane. This is assumed in spite of the fact that fluid transport occurs across the endothelial layer and through the matrix comprising the media and adventitia of the wall, which would induce additional resistance (Tedgui 1984).

Tedgui & Lever were able to successfully measure Lp in the aorta segments of rabbits and, although they obtained measurements using different applied pressures, the measurements were not all from the same aorta. The results they obtained suggested that strain in the interstitial matrix may effect the measured Lp values. However, due to possible variation between vessels, they could not draw this conclusion unequivocally. Baldwin & Wilson (Baldwin 1992; Baldwin 1993) extended the work of Tedgui & Lever with the agenda of answering whether Lp was influenced by vascular distension. Their method varied the height of the reservoirs connected to their excised vessel so as to take Lp measurements at different transmural pressures on the same vessel.

Baldwin and Wilson 1992

Baldwin's and Wilson's (Baldwin 1992) initial study measured Lp in whole rabbit aortas at different transmural pressures. The study sought to determine whether Lp depends on aortic wall distension. By dynamically evaluating Lp on the same vessel at various induced pressures, Baldwin and Wilson were able to mitigate complications of vessel variation present in the data of Tedgui and Lever (Tedgui 1984). The technical advance in their procedure was that Baldwin and Wilson carried out their experiments on the same vessel over all pressures, rather than on differing segments. They established different pressures by inflating a pressure cuff around the inlet reservoir and closing off of the vessel from the outlet reservoir. Pressure was then recorded by turning a stopcock that connected the aorta to a pressure transducer.

The results obtained from this study provided a key insight into the effect of pressure–induced distension on convective water flux through the wall of the rabbit aorta. Transverse sections taken from two aortas that underwent the Lp procedure at different pressures were examined to determine their vessel thicknesses. The mean wall thickness of aortas fixed at 55 mm

Hg was 125±12 μm, whereas that of aortas fixed at 100 mm Hg which was 100±14 μm, and this distinction was statistically significant. No further thinning was noted at 150 mm Hg. As in the esarlier work, the flux through the wall needed for the calculation of Lp derived from the plot of the distance traveled by the bubble vs. time during the experiment. The velocity was again determined from the linear portion of the curve, where the bubble reached a constant velocity. Two groups of measurements were plotted. Group 1 data consisted of vessels at pressures of 50, 100, and 150 mm Hg, while group 2 data consisted of Lp values obtained at 75, 100, 125, and 150 mm Hg. The results are illustrated below.

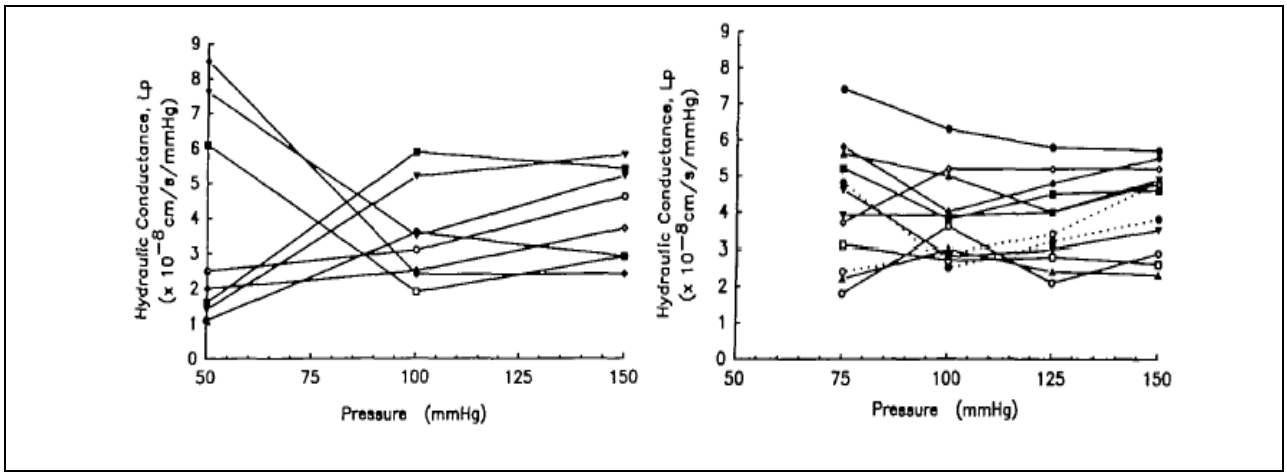

Figure 42: Graphs showing variation of Lp. Each symbol is one experiment (Baldwin 1992)

The overall trend in both data groups is the same, in that there is a much higher degree of variation in Lp at the lowest pressure than at the higher pressures. Paired Student's *t* tests performed on both sets of data indicated no significant change in the mean Lp with pressure(Baldwin 1992). However, there was a poor correlation between Lp values obtain at 50 mm Hg and 100 mm Hg, i.e., Lp values at 50 might be either much higher or much lower than at

100 mm Hg, in contrast to the individual values obtained on the same vessel at 100 and 150 mm Hg being well correlated.

The authors state that the similarity of Lp at pressures of 100, 125, and 150 mm Hg in individual vessels is unlikely to arise from the constancy of the parameters affecting transmural flow within this pressure range; rather, they suggest that the various factors that affect Lp are altered by pressure in different ways such that the combined effect on Lp is negligible within this pressure range. Baldwin and Wilson extended this initial study (Baldwin 1992) to provide further investigation into the observed trends and correlations in their data. Specifically they applied the same experimental techniques to obtain Lp but also included measurement of denuded vessels to quantify the contribution of the endothelium to Lp under changes in transmural pressure.

Baldwin and Wilson 1993

The subsequent study by Baldwin and Wilson continued their work from the previous paper with a focus on the effect of the endothelium on vessel permeability. They cannulated the aortas of eight anaesthetized New Zealand White rabbits *in situ* for the measurement of Lp as a function of transmural pressure (Baldwin 1993). To extend their previous work, they included Lp measurements on de-endothelialized vessels in this study and directly compared these results to Lps of vessels with intact endothelia so as to infer the contribution of the endothelium to whole wall hydraulic conductance. The endothelium was stripped away by removing the distal cannula, inserting a 3-mm or 4-mm Foley catheter, sliding it up to the proximal cannula, and removing it with slow rotation(Baldwin 1993). Visual inspection by eye allowed for verification that all the endothelium was removed. The area where the endothelium was stripped away was

stained with Trypan blue and was observed to stop abruptly in the region of the proximal cannulation. Beyond this point, the vessel looked identical to an intact vessel(Baldwin 1993).

The data obtained provide definitive evidence that the endothelium contributes significantly to vessel Lp beyond 75 mmHg. Results are graphed in below.

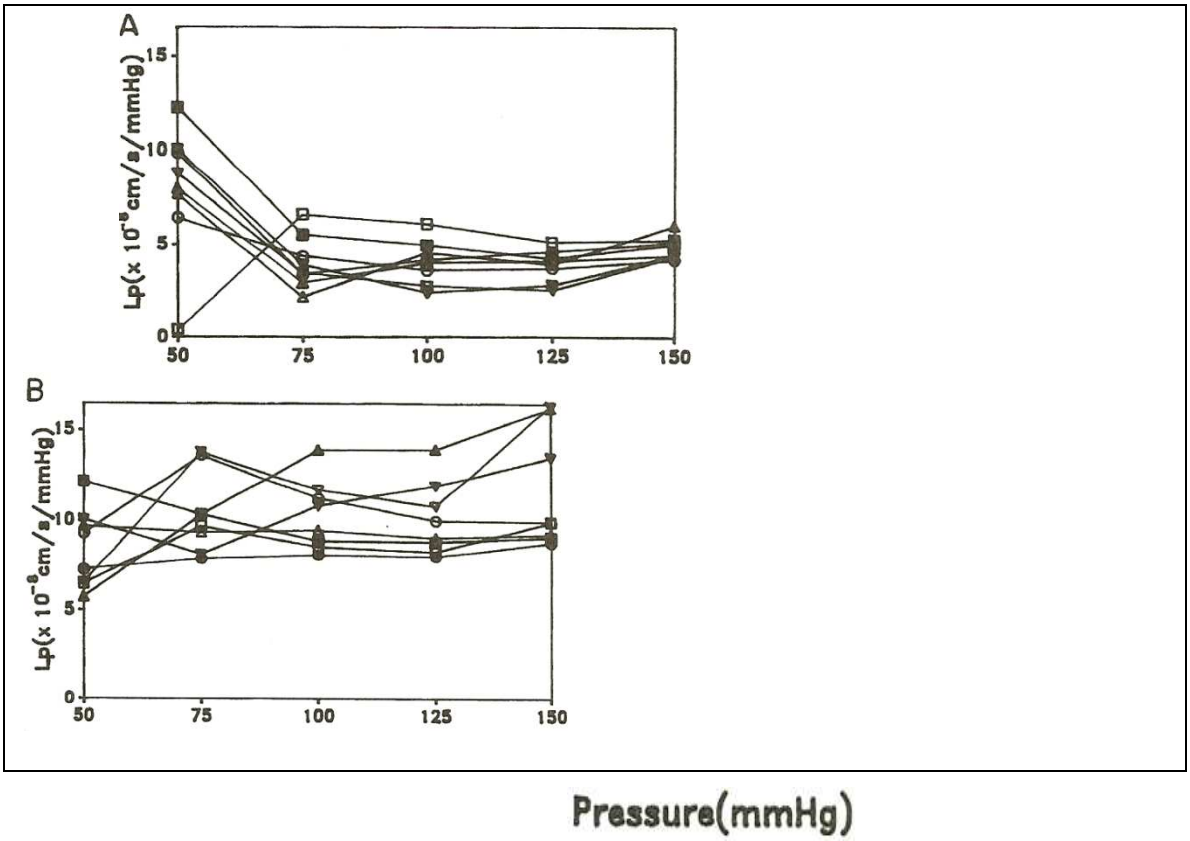

Figure 43: Graphs showing variation of Lp with endothelium intact (A) and removed (B). Each symbol is one experiment (Baldwin 1993)

The figure above shows that for intact vessels most of the figures's Lp curves are significantly higher at 50 mmHg than at higher pressures and, as in the previous study(Baldwin 1993), Lp did not vary greatly from 75 mmHg to 150 mmHg. Endothelium removal, depicted in graph B of figure above, led to a significant increase in Lp at all pressures except 50 mmHg, but with

significant pressure dependence between 50 and 150 mmHg. This study also investigated the effect of endothelium-derived relaxation factor (EDRF) inhibitor to determine EDRF's contribution to Lp; we omit the details here for purposes of brevity and specific relevance to our goals.

The goal of Baldwin's 1993 study was to determine if the endothelium and factors that it produces are responsible for the Lp dependence on pressure in the range from 50 to 125 mmHg observed in the previous study (Baldwin 1992) . Endothelium removal increased Lp, but this increase was only significant for pressures 75-150 mmHg, leaving any possible changes in Lp at 50 mmHg uncharacterizable due to large experimental variation. Since Lp did not appear to increase at 50 mmHg upon denudation, they reasoned that endothelial removal must decrease Lp of the media, and accordingly, the presence of the endothelium must increase Lp of the media at 50 mmHg. By extending the conclusions of their previous study, Baldwin and Wilson suggested a more developed theory of Lp's relation to transmural pressure, specifically the role that the endothelium plays in filtration in the aorta. Huang et al.*'s* theory of intimal compaction discussed at the end of this section and its subsequent experimental confirmation invoked a completely different consistent and quantitative interpretation of these and of Tedgui and Lever's data and thereby shed a different light on the experimental Lp results.

Shou 2006

Shou et al. (Shou 2006) extended the work of Tedgui and Lever and of Baldwin and Wilson to the much smaller rat model, which was a significant accomplishment. Shou et al. modified the procedure followed by Baldwin and Wilson to be applicable to the much smaller-sized vessels of the rat. This study provided Lp measurements at different pressures, both with intact and denuded endothelium, all on the same vessel for the rat aorta as well as for the pulmonary artery (PA) and the inferior vena cava (IVC). These measurements provided transport quantification for

three vessels with very difference susceptibilities to atherosclerosis. Veins are normally very resistant to atherosclerosis. However, veins are often used for coronary artery bypass procedures, and, in such cases, frequently develop atherosclerosis as they remodel under such high-pressure conditions, as observed in autopsies done 6-12 years after the bypass procedure. Shou et al.'s study focuses on the question of how similar are the water filtration processes that drive convective lipid transport in the aorta to those in the PA and the IVC. Figure 44 shows Shou et al's data (Shou 2006). They found that rat aortic Lp, both with and without endothelium, agrees quantitatively with the rabbit aorta data from Tedgui and Lever (Tedgui 1984) and qualitatively with rabbit aorta data from Baldwin and Wilson (Baldwin 1993); thus, there appears to be little species variation in Lp-values in the large arteries between these two species. Shou's data provided evidence of the dominant role of convection in the macromolecular transport within the arteries and veins examined. The Lps of all three vessels were quantitatively different from each other. However, Shou et al's curves for intact and denuded vessels showed qualitative similarities in the Lp dependences on pressure and on denudation among the two arteries, which also shared many structural similarities, but somewhat less so with the vein, whose structure differed markedly from those of the arteries. This suggested that intimal compression under pressure loading, a theory that Huang et al. developed to explain the experimental aortic Lp data, may also play a role in Lp as a function of pressure in the PA.

Compared with the Lp experiments on rabbit vessels, the bubble in the catheter moves far more slowly in experiments involving the smaller rat vessels. Frictional losses caused by the resistance of bubble motion in the catheter are negligible as long as the wetting layer between the bubble and the tube wall remains intact (Shou 2006). Due to its short length the PA has the smallest surface area of the three rat vessels in this experiment and special care was applied to

search for leaks while performing the measurement of Lp. Half of the Lp measurements were taken from the low pressure to high-pressure regions while the other half were taken in the opposite manner, which allows for evaluation of preconditioning effects. On average there was a slightly higher Lp on vessels where Lp was measured from low to high pressures, but this difference was not statistically significant and, moreover, the trends of how Lp varied with pressure were independent of pressure order; thus the data were not segregated(Shou 2006).

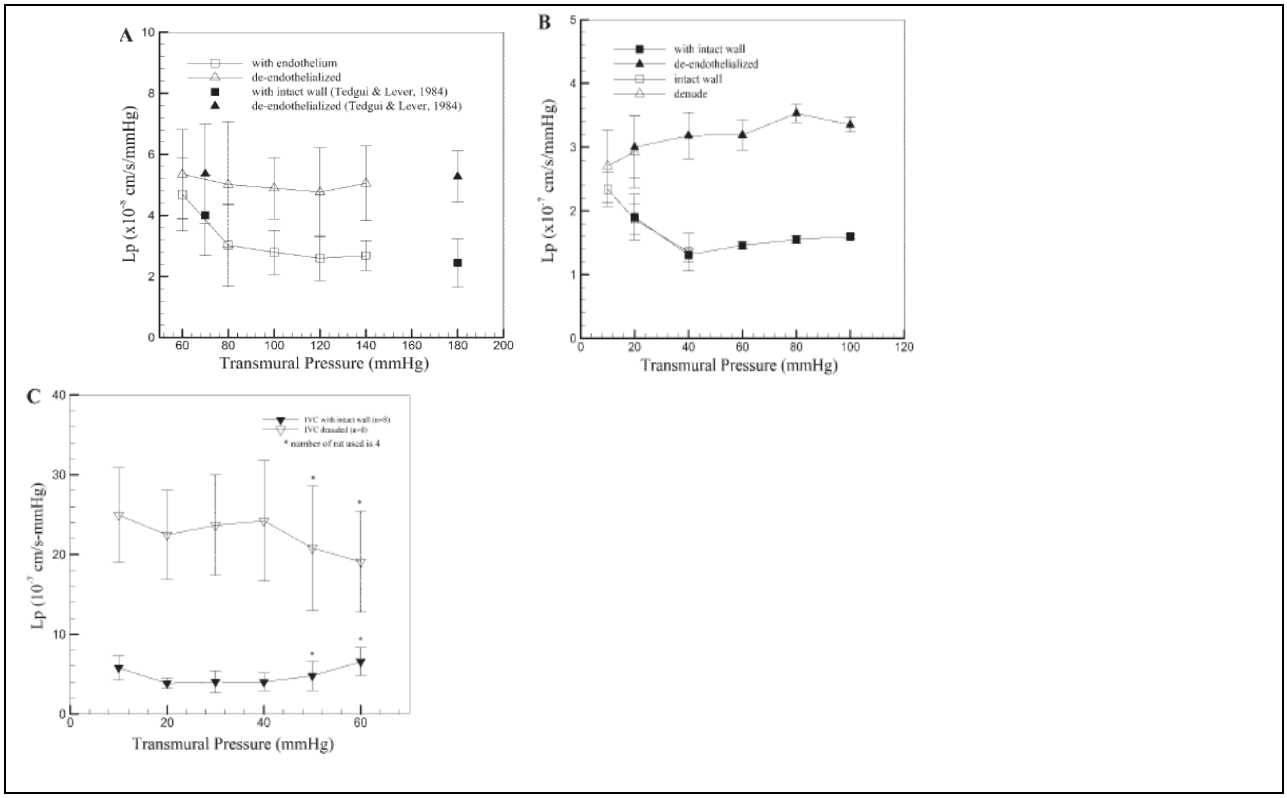

Figure 44: Lp of rat aorta (A), PA (B), and IVC (C), measured with and without endothelium. (Shou 2006)

Nguyen's 2008 thesis

Nguyen et al., also of our group, carried out further studies on the Lp of rat aortas, and the work is being prepared now for publication. The technique utilized is similar to, but improved from, the aforementioned studies. Rather than manually tracking bubble movement by periodically reading its position from an attached ruler form at specific times that read from a

stopwatch, she has modified the experimental setup to include a spectrophotometer tracking system that automatically tracks bubble movement and digitally stores and displays its position vs. time curve.

Figure 45 depicts a schematic of Nguyen's experimental setup. Two pressure setups; each connected to two solution reservoirs and each using a mercury sphygmomanometer to maintain reservoir pressure, set (including the appropriate hydrostatic correction) the desired transmural pressure. A three-way connector attaches tubing emanating from the excised vessel and the injection syringe to a borosilicate glass tube (0.50 ±0.01 mm ID x 5.5±0.5mm OD x 550mm) (Wilmad Labglass, NJ) mounted on a spectrophotometer tracking system. A syringe injects an air bubble into the capillary tube and the bubble is driven into the tracking system and postioned under the spectrophotometer tracker. One clamps off the proximal end of the excised vessel, attached to reservoirs A and B. The valve connected to reservoir 2 is opened and reservoir 2 is pumped to the desired pressure. As fluid permeates through the vessel wall, the spectrophotometer continuously tracks the position of the bubble's leading meniscus and records it to a computer. This motion is allowed to continue until it has been steady for at least 30 minutes. The vessel length and outer diameter are the measured at three different points with mechanical calipers (accurate to ±0.1 mm (Shou 2006)) 3-4 times after the vessel has reached steady state. Our group has previously shown that this method accurately estimates the external *en face* aortic surface area, which is critical in calculating precise Lp-values (Shou 2006). We repeat the entire protocol at each desired ΔP on the same vessel. The solution used to perfuse the vessel contains 4% (w/v) bovine serum albumin (BSA), phosphate buffered saline (PBS), 10^{-3}M NaNO3, and 0.03% trypan blue dye. The dye is used to identify leaks and nonviable cells (Tedgui 1984;

Baldwin 1992). Vessels with blue dye seen seeping out were quickly retied; those that could not be fixed were discarded.

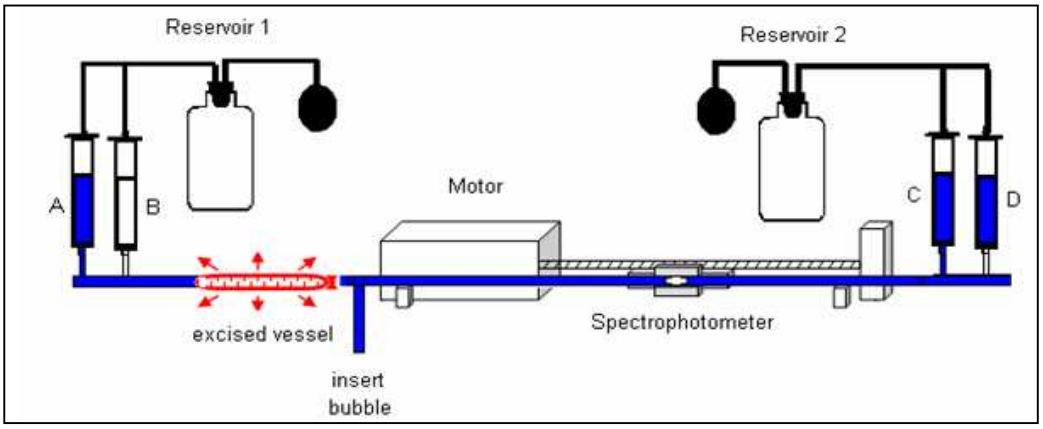

Figure 45: Schematic of Lp measurement set up with bubble tracker. (Nguyen 2008)

In all of the above studies of Lp, water crossed the endothelium and entered the subendothelial space, driven by a transmural pressure gradient. It was natural to assume initially that water transport across the endothelium occurred almost completely via the paracellular pathway across the intercellular junctions. Shou's pilot experiments and Nguyen et al.'s subsequent refined study proposed to investigate the possible contribution of the transcellular route through the endothelial cells via one or more members of the well-known water channel membrane protein aquaporin (AQP) family. These studies aimed to establish the existence of a transcellular route and, if successful, to clarify the nature of the water flow in the vessel by separating the contribution of water flux through normal and leaky tight junctions from that through the transcellular route via aquaporin channels.

Nguyen began by carrying out *in vitro* studies showing that chemically blocking AQP with mercuric chloride (25 μM, a concentration titrated to not cause cell toxicity, as monitored by Propidium Iodide that stained only the permeable cell membranes of dying cells) decreases Lp of cultured bovine aortic endothelial cell (BAEC) monolayers. Nguyen then turned to the measurement of the transmural water flux through the aortic wall of a rat using Nguyen's modification of the well-established *ex vivo* model (Tedgui 1984; Baldwin 1993; Shou 2006). She began by measuring Lp of the intact vessel at three different transmural pressures. The vessel then was exposed to this same AQP blocking agent (titrated to 5 μM in vessels to eliminate artifacts) and Lp was remeasured on the same vessel at the same pressures. The vessel was then mechanically denuded to remove its endothelium and intima layers and Lp was again measured on the same vessel at the same pressures.

Lp values after AQP blocking were lower than their baseline measurements in all vessels, at all pressures. This decrease averaged 32±4%, 11±3%, and 5±3% at 60, 100, and 140 mmHg, respectively. These drops represent the fraction of Lp contribution by the endothelium plus the SI (Lp_{e+i}) that is attributed to AQP-1. Using a back of the envelope argument, Nguyen et al. proposed that the drop in Lp upon blocking is not simply due to a change in endothelium Lp (Lpe), but rather is the result of a combination of effects. They propose that blocking AQPs at constant transmural pressure increases the force per unit area on the endothelium. This is because the blocking of the AQP channels decreases the pores available for water transport, thus decreasing Lpe. This shifts a larger fraction of the overall transmural pressure (or force per unit area) from the media to the endothelium. Intima compaction theory would predict this shift can therefore compress an initially uncompressed intima, e.g., the intima at 60 mmHg, without raising ΔP, and enhance fenestral blocking, thereby further lowering Lp. At higher pressures, where partial/full

fenestral blocking has already taken place, this $HgCl_2$-induced shift would provoke no further compression, but rather would simply reflect a change in Lpe. Thus the observed change in total Lp would be smaller at these higher pressures than at 60 mmHg, as observed. Figure below displays Nguyen's experimental results.

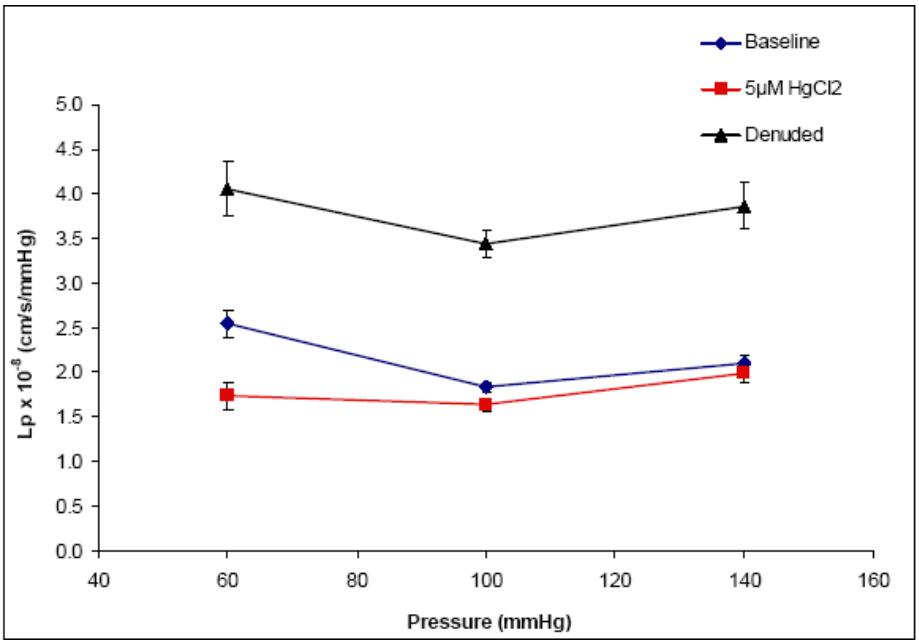

Figure 46: Lp(ΔP) of an excised rat aorta before (blue) and after (red) administration of 5μM $HgCl_2$ and post denuding. Values are means ± SEM (n=6) (Nguyen 2008).

In vitro Lp and Solute Flux Measurement Methods

The basis for the experimental methods and set up for our *in vitro* Lp system come from the work of Dr. John Tarbell's group. We perform our Lp measurements in his biomedical engineering laboratory. In this set up our group uses, endothelial monolayers are cultured to confluence on porous polycarbonate Transwell filters, and placed in a fluid-filled chamber with an upper and lower compartment. The lower compartment is connected to a glass capillary tube with an air bubble in it. When pressure is applied to the fluid in the upper compartment, fluid flows through the monolayer, into the lower compartment, pushing the bubble along the tube. The en-

tire apparatus is maintained in at 37 C, 5% CO_2. After inducing a 10 cm H_20 pressure gradient across the monolayer, one allows the bubble to travel for 20-30 minutes as the monolayer undergoes a pressure-induced partial junctional sealing, and then one records data is for 60 minutes.

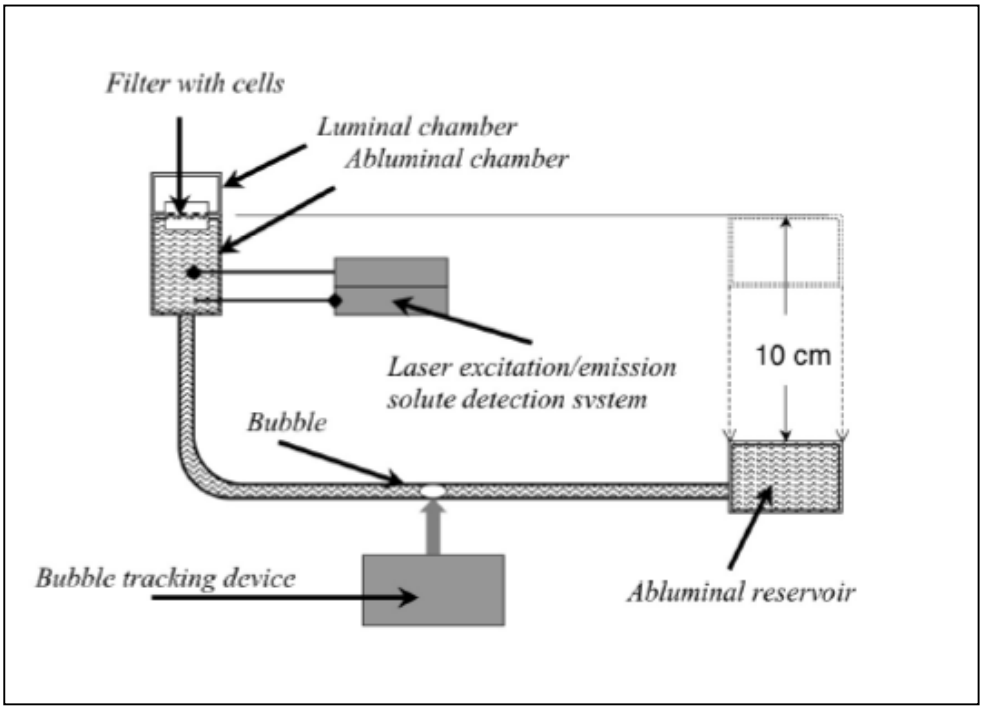

Figure 47: Schematic diagram of the pressure-flow apparatus. (Russell 2009)

Slight changes in ambient temperature, environmental vibrations, noise in the trans-endothelial flow, rupture of the lubricating liquid film surrounding the bubble leading to a three-phase contact line on the tube wall and subsequent rewetting, etc. can all have a small effect on the progress of the bubble, resulting in noisy data. Also as the flow attenuates, the movement of the bubble slows, causing the signal to noise ratio to decrease. The numerical approximation of the volume flow rate from noisy marker position data is the largest source of error. A typical curve for bubble position vs. time *in vitro* is graphed in figure below. S. Russell of our group has formulated a protein diffusion model of this sealing effect. In response to an application of hy-

drostatic pressure and subsequent increase in water flow through breaks in the tight junctions, junctional proteins, which are initially evenly distributed on the inside of the endothelial cells, diffuse towards the tight junctions located at the cell-cell borders. These additional junctional proteins help to close the breaks in the junction.

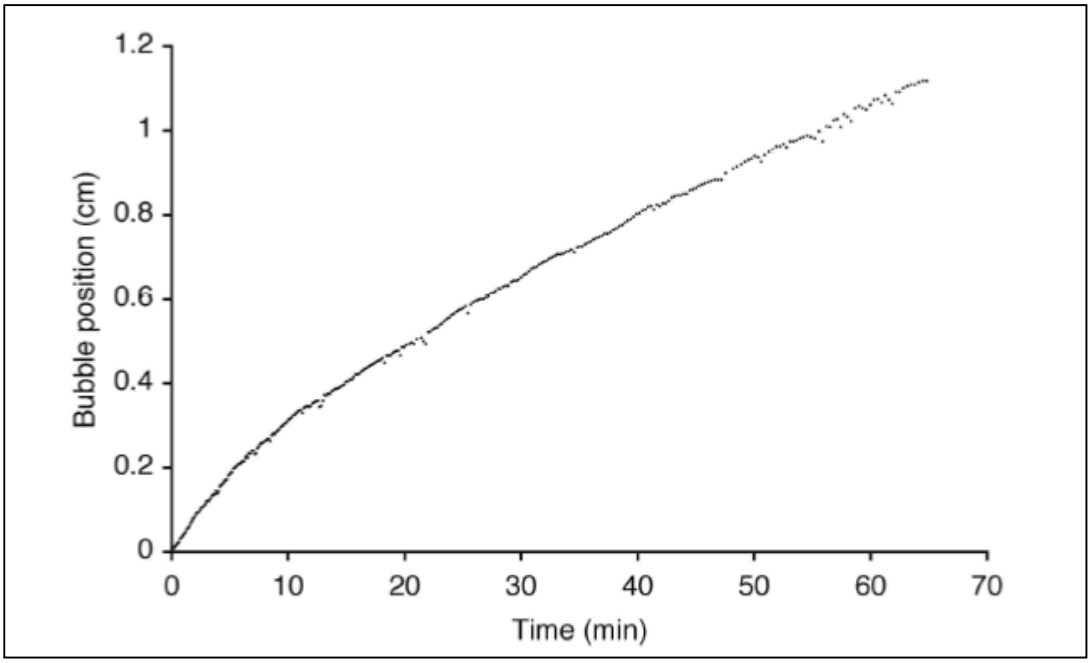

Figure 48: Raw data showing bubble position vs. time. Typical raw data for BAEC monolayers. (Russell 2009)

Cancel 2007

One of the recent publications from Dr. Tarbell's group that motivated our study and methods was Limary Cancel's 2007 paper *In vitro* study of LDL transport under pressurized (convective) conditions. Transport pathways that carry LDL into the artery wall were critically examined. Water, albumin, and LDL fluxes across BAEC monolayers were measured and a 3-pore model was developed to mathematically separate out the contributions of vesicles, paracellular transport via breaks in the tight junctions, and paracellular transport through leaky junctions in transporting LDL across endothelial monolayers (Cancel, Fitting et al. 2007). Along with the

aforementioned *in vitro* Lp setup, solute flux was also measured in this study. The solute drag experiment uses a fluorescent detection system that was incorporated into the experimental apparatus allowing for the simultaneous measurement of water flux and fluorescent conjugate macromolecule permeability (Cancel, Fitting et al. 2007). The schematic below includes the laser excitation source that was used to measure the concentration of fluorescently labeled tracer molecules that have crossed into the abluminal volume after having been introduced into the luminal chamber, along with optical fibers, a photomultiplier, and a data acquisition program (not pictured). A helium-argon laser produced excitation light and the emission signal was sent to the photomultiplier where a software program and model PC-DAQ control card were used for data acquisition and control of the photomultiplier(Cancel, Fitting et al. 2007). Solute permeability was obtained from the following equation, which is based on the rate of change in the abluminal solute concentration with respect to time, $\Delta C_a/\Delta t$:

$$P_e = [(\Delta C_a / \Delta t) \times V_a] / (C_p \times A) \qquad (3)$$

Here Va is the fluid volume of the abluminal chamber, and Cp is the luminal concentration of the solute. Changes in both Va and Cp were negligible during an experiment, and Ca << Cp (Cancel, Fitting et al. 2007). To block transcytosis in vesicles, cells were fixed with 1% paraformaldehyde in phosphate buffered saline. The protocol described above was then followed to determine solute permeability. To test the role that LDL receptors play in transport across the endothelium an excess of untagged native LDL was utilized. This was accomplished by saturating LDL receptors with untagged native LDL and then performing the solute drag experiment (Cancel, Fitting et al. 2007) to ascertain the contribution LDL receptors play in transport across the endothelium.

Cancel reported results that show that leaky junctions are the dominant pathway for LDL (>90%) under convective conditions and that albumin also has a significant component of transport through leaky junctions (44%). Transcellular transport of LDL by other, e.g., receptor-mediated, processes makes a minor contribution (<10%) to overall transport. Thus, LDL infiltration into the vessel wall is primarily driven by transendothelial water flow. Control of transmural water transport may provide means to increase water flow through the aortic endothelium and allow for LDL dilution or washout out of the SI. This could to beneficial preventative strategy to the earliest stages of atherosclerosis. Solute tracer studies allow us to determine the contribution of paracellular versus transcellular transport in EC monolayers, and thus the route chemical treatment influences.

Appendix III: Signal Processing of blood pressure measurement from ADInstruments ML125 NIBP (Non-Invasive Blood Pressure) system.

The ADInstruments ML125 NIBP (Non-Invasive Blood Pressure) Controller performs non-invasive blood pressure measurement on rats and mice using specialized tail cuffs. Below is a sample output of the system for one measurement cycle.

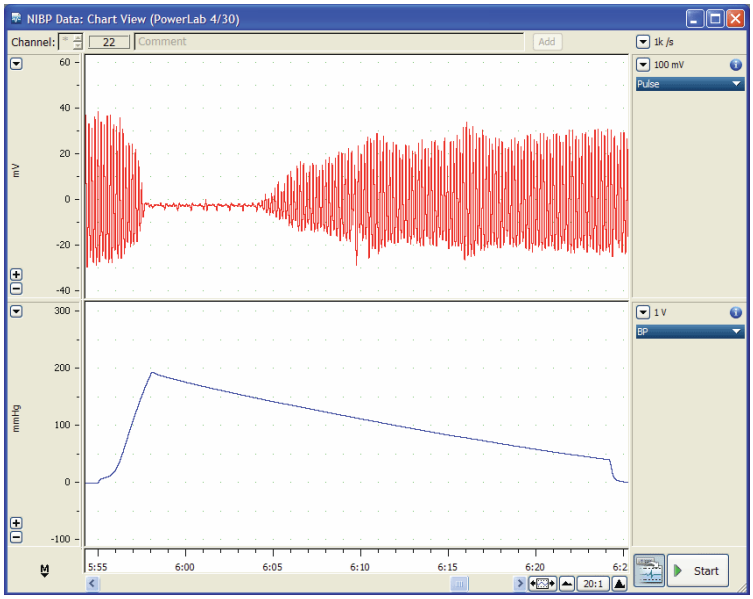

Figure 49: Typical recording using LabChart showing the pulse and pressure signals.

This technique has been used routinely for the non-invasive measurement of blood pressure in rats, and more recently in mice. The technique provides a good estimate of actual systolic pressure. Although non-invasive, the protocol details related to the technique (warming, handling, restraint and so on) will inevitably have some effect on the actual blood pressure. The technique is useful as a comparative measurement, particularly when carried out on a well habituated animal.

Most animals require some training, habituation to the protocol, and careful handling to produce repeatable results; rats are more readily trained than mice. Two to three training sessions

may be necessary to acclimatize the animals. Even when the animal has been trained it may take a few minutes before a distinct pulse is measurable on the tail. Sudden motion and sounds should be restricted as much as possible, since they cause animal movement. It sometimes helps to cover the restraint cage with a cloth to reduce the impact of external stimuli. Warming rats and mice improves blood circulation in the tail and the signal to noise ratio in the recording. Typically animals should be preheated to 28–30 ˚C and maintained at that temperature during the test. The tail cuff is used to occlude blood flow in the tail and thereby interrupt the pulse that is measurable in the caudal artery. The tail cuff is positioned at the proximal end of the tail.

The basic signals recorded by the ML125 NIBP system are the cuff pressure and the caudal artery pulse. Cuff pressure is an accurate high level signal with noise of less than +/– 0.1 mmHg and absolute error of less than +/– 2 mmHg (after calibration). This data is used in association with the reappearance of the caudal artery pulse to determine the systolic pressure. The caudal artery pulse is a low level pulse requiring significant amplification. The signal is therefore mixed with noise, and subject to movement and respiratory artifacts. The signal amplitude may alter significantly as the animal moves and repositions the transducer in relation to the caudal artery. A significant feature of the caudal artery pulse is its frequency. For a conscious rat this is typically in the range 200–500 BPM. For a given set of circumstances this frequency is relatively constant. A sampling rate of 1000 samples per second was used for pulse measurements. Movement and respiratory artifacts in tail pulse measurements are particularly disruptive because they often occur at times coincident with actual measurements. However, it should be noted that the technique is dependent not on the amplitude of the pulse, but rather its onset. As such the algorithm developed involves discerning intensity of the pulse immediately after pulse signal returns after occlusion.

Systolic measurement can normally be made with relative ease. Systolic blood pressure (SBP) occurs when the cuff pressure corresponds to the restoration of the first caudal artery pulse. The presence of noise will inevitably introduce some uncertainty in this estimate, but typical SBP measurements will be within 5% of direct blood pressure measurements. Measurements are repeated five to six times to ensure reproducible results are being obtained.

The spectral density captures the frequency content of a stochastic process and helps identify periodicities. Power spectrum with strong spectral component can be estimate on short sequences, and hence, followed as it develops over time. Spectral analysis on a range of measurements yielded frequency characteristics of the pulse signal specifically during and after occlusion for 300-400g rats. The collection of pulse signals had a frequency range of 5-10 Hz. A band pass filter was developed in MATLAB Signal Processing Toolbox to pass frequencies within our specific range and attenuate frequencies outside that range. This allows us to increase the contrast between noise obtained during pressure cuff occlusion and pulse signal obtained during deflation of pressure cuff to determine SBP level. Spectrogram of data files is below.

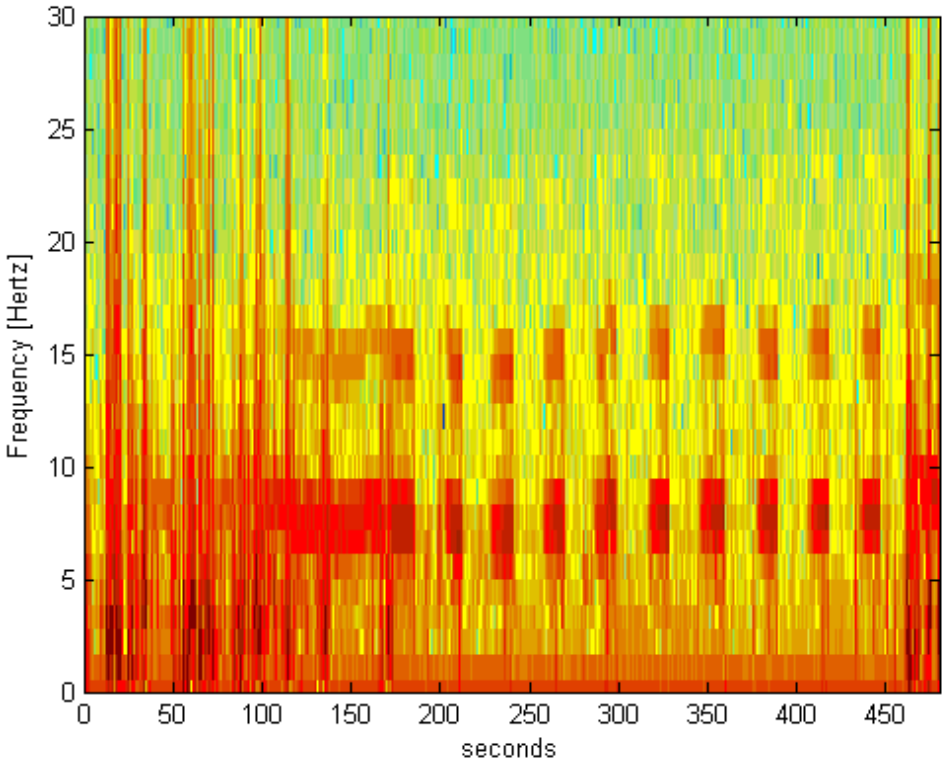

Figure 50: Spectrogram of NIBP recordings.

An automatic process such as one which utilizes a filter, does not allow for variations that may occur within a data recording. The algorithm is subject to the integrity of the data. Training animals to remain in a relatively docile state is required to obtain reliable data. This training ensures occlusion signal is undisturbed by critter movement. Keep in mind that the filter parameters may need to be adjusted if pulse signal for an animal is outside of band pass thresholds.

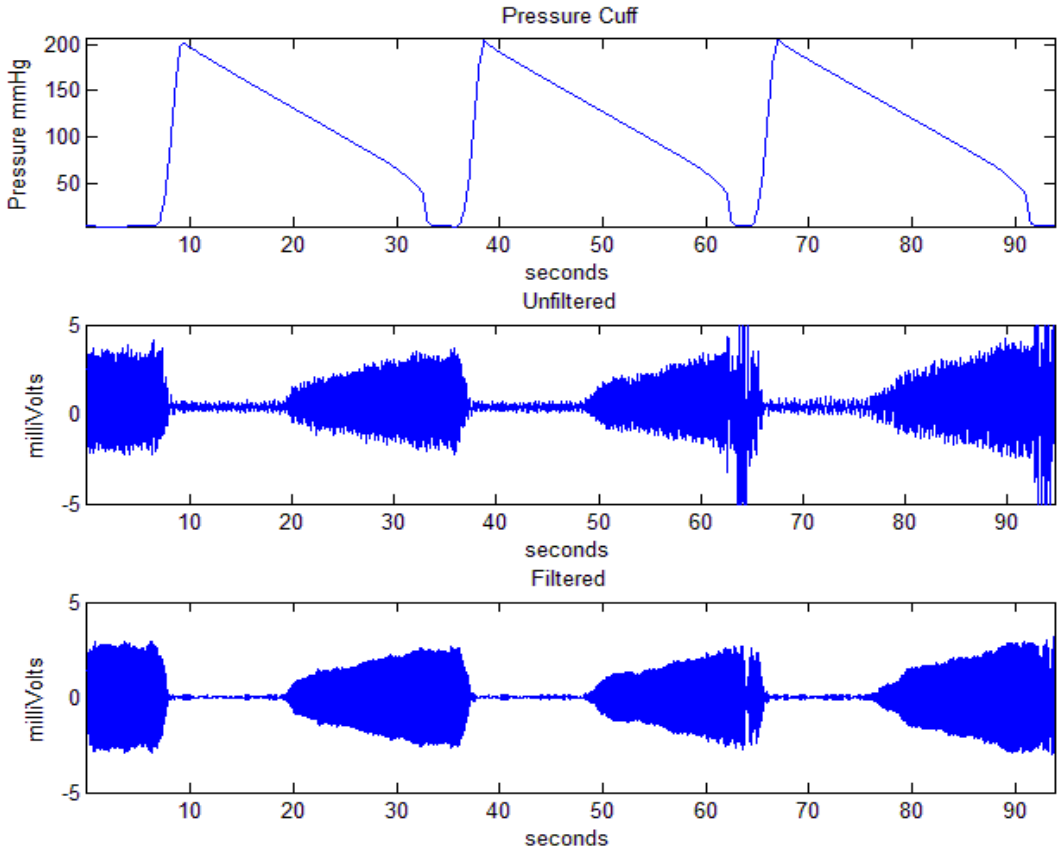

Figure 51: Filtered and Unfiltered pulse data with pressure cuff signal.

As can be seen from figure above, our filtered signal not only removed much of the noise from critter movement, but also eliminated the offset in our signal alignment which centered our filtered signal at zero on pulse axis.

After filtering our signal we need to perform a transformation of our data to obtain intensity of the cycles. In signal processing, the Hilbert Transform, E(t) is useful for analyzing non stationary signals by expressing frequency as a rate of change in phase, so that the frequency can vary with time.

$$y(t) = \frac{1}{\pi} \int_{-\infty}^{\infty} \frac{x(\tau)}{\tau - t} d\tau \tag{A1}$$

Where the principle value of the integral is used. Given x(t) and y(t), a complex analytic signal z(t) can be defined as, (Cohen 1995):

$$z(t) = x(t) + jy(t) \tag{A2}$$

which can be expressed as,

$$z(t) = x(t) + jy(t) = E(t)e^{j\psi(t)} \tag{A3}$$

where $E(t)$ is the envelope of $z(t)$ given as

$$E(t) = \left| x(t) + jy(t) \right| \tag{A4}$$

and $\psi(t)$ is the phase of $z(t)$ given as

$$\psi(t) = \tan^{-1} \frac{y(t)}{x(t)} \tag{A5}$$

Squaring the absolute value of our Hilbert transform allows us to obtain a time-dependent expression for the instantaneous power. Thus, the Hilbert transform analysis provides a method for determining the instantaneous frequency and power of our signal. Our pulse signal is now transformed into power spectrum density, the magnitude of which reflects the strength of our

pulse signal. By conditioning our instantaneous power signal with an algorithm we can obtain the time when blood flow returns after occlusion based on the intensity of the instantaneous power. Figure below contrasts the instantaneous power of the signal with the filtered pulse signal. The power is greatest corresponding to the time the pressure cuff is at a minimum, which allows for maximum blood flow through tail, and at a minimum during occlusion by the tail cuff.

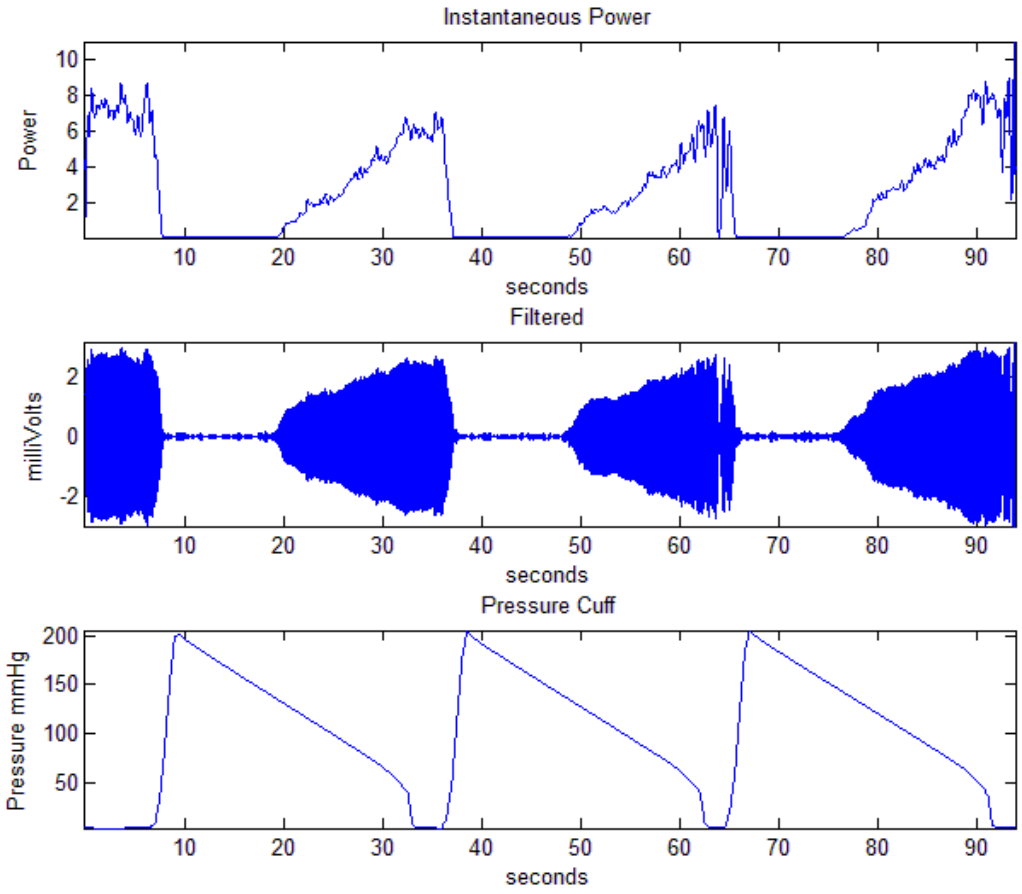

Figure 52: Instantaneous power and filtered pulse data with pressure cuff signal.

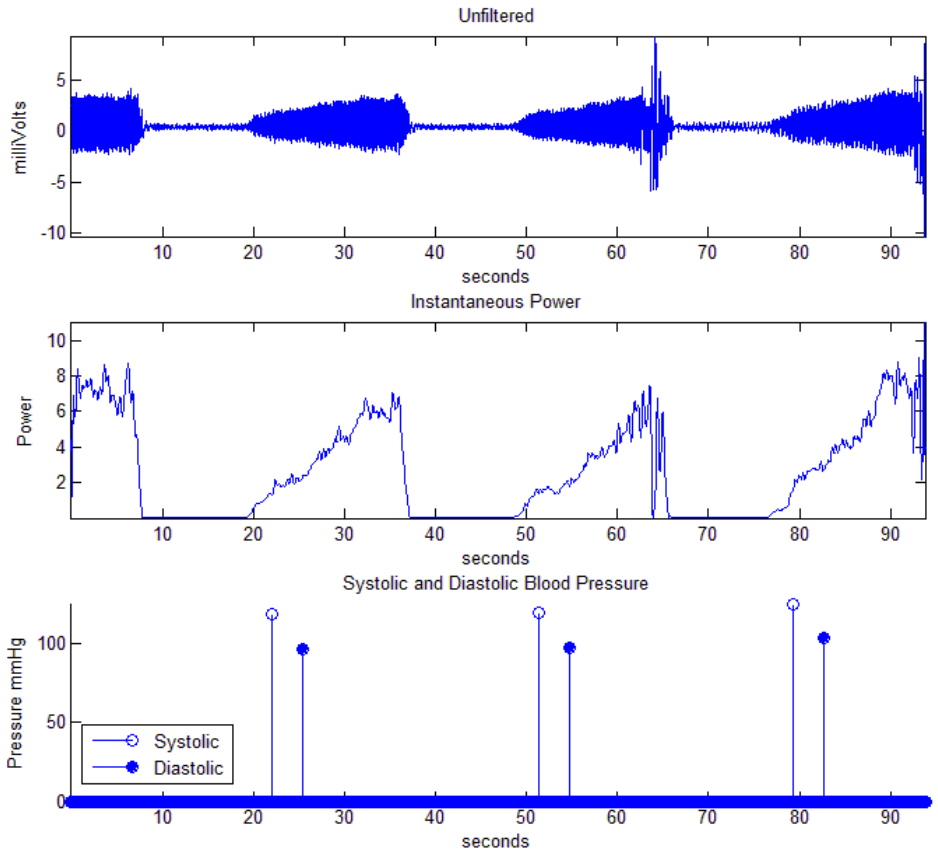

Figure 53: Instantaneous power and unfiltered pulse data with calculated SBP and DBP levels 350g rat.

The figure above provides SBP and DBP levels for the data files after implementation of our developed algorithm. The program also computes mean and standard deviations for the data file as returned output for the recording.

The algorithm works by creating an intensity threshold for white noise in terms of instantaneous power during occlusion. Coupled with pressure channel data, the moment of occulusion was determined and then the instantaneous power of the pulse was compared to white noise until a sustained pulse signal returned. This physically corresponded with the end of occlusion, and thus the systolic blood pressure. Diastolic blood pressure was conditioned after this point and

required the instantaneous power to meet a higher threshold in terms of signal strength. Outputs of our algorithm for rats of differing sizes are provided in figures below.

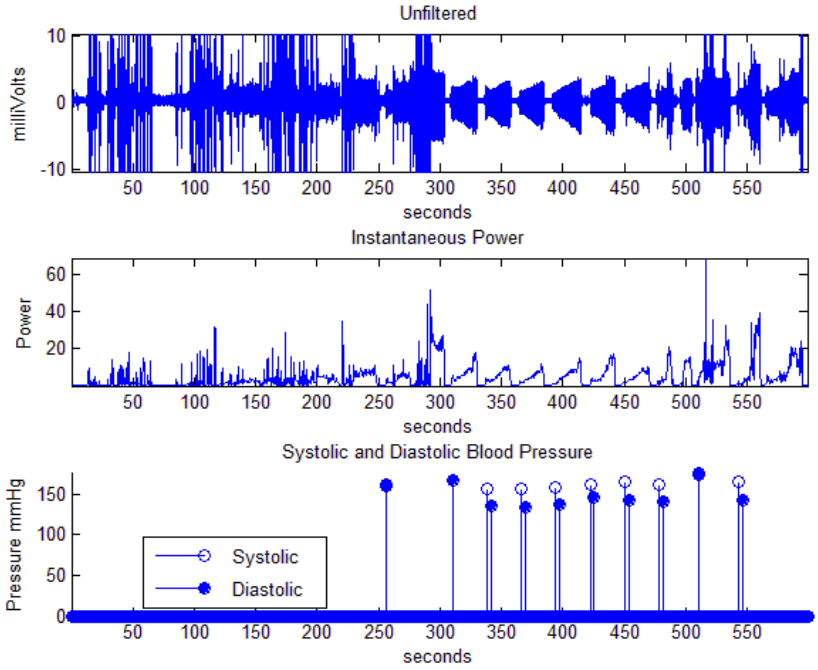

Figure 54: Instantaneous power and unfiltered pulse data with SBP and DBP levels for 400g rat.

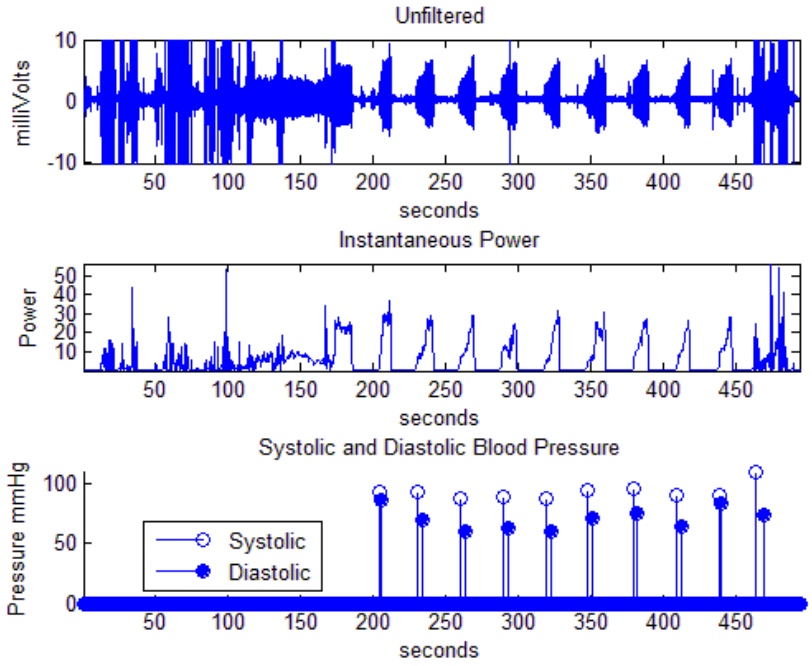

Figure 55: Instantaneous power and unfiltered pulse data with SBP and DBP levels for 350 g rat.

Code for obtaining SBP level on NIBP data

```
close all
clear all
load data2  %CHOOSE DATA SET
load filtercoeffb
x = C1B1;
p = C2B1;
delay = round((length(b)-1)/2);
xfilt = filter(b,1,x);
xtrun = xfilt(delay:length(x));
Fs = 1000;
t = (1:length(x))/Fs;
tp = (1:length(xtrun))/Fs;
ptrun = length(tp);
hil = hilbert(xtrun);
```

```
ipower = abs(hil).^2;
bp = zeros(ptrun,1);
bpp = zeros(ptrun,1);
bpd = zeros(ptrun,1);
bppd = zeros(ptrun,1);
bpres = 0;
bpresd =0;
j=0;
jd=0;

MinBP = 50;

IPmax = 0.08;
IPmin = 0.07;

IPdiff = 1.1961;
IPdiffd = 1.4;

diff = 2610;
diffd = 6000;


for i=1:ptrun
   if  ((ipower(i)) < IPmax && (p(i)) > MinBP)
      if (ipower(i)) > IPmin && (ipower(i + diff)-ipower(i)) > IPdiff
        bp(i + diff) = p(i+diff);
      end
   end
end

for i = 1:ptrun
   if (bp(i))>MinBP
      if (bp(i-1)) == 0
         for k = 1:25000
         bp(i+k) = 0;
         end
         j = j+1;
         bpres(j) = bp(i);
         bpp(i) = bp(i);
      end
    end
end

for i=1:ptrun
   if  ((ipower(i)) < IPmax && (p(i)) > MinBP)
      if (ipower(i)) > IPmin && (ipower(i + diffd)-ipower(i)) > IPdiffd
```

```
            bpd(i + diffd) = p(i+diffd);
          end
        end
    end


    for i = 1:ptrun
      if (bpd(i))>MinBP
        if (bpd(i-1)) == 0
          for k = 1:25000
          bpd(i+k) = 0;
          end
          jd = jd+1;
          bpresd(jd) = bpd(i);
          bppd(i) = bpd(i);
        end
       end
    end
    figure(1);
    subplot(3,1,1);
    plot(tp,p(1:ptrun));title('Pressure Cuff');xlabel('seconds');ylabel('Pressure mmHg');axis
tight;
    subplot(3,1,2);
    plot(t,x);title('Unfiltered');xlabel('seconds');ylabel('milliVolts');axis tight;
    subplot(3,1,3);
    plot(tp,xtrun);title('Filtered');xlabel('seconds');ylabel('milliVolts');axis tight;
    figure(4);
    subplot(3,1,1);
    plot(tp,ipower);title('Instantaneous Power');xlabel('seconds');ylabel('Power');axis tight;
    subplot(3,1,2);
    plot(tp,xtrun);title('Filtered');xlabel('seconds');ylabel('milliVolts');axis tight;
    subplot(3,1,3);
    plot(tp,p(1:ptrun));title('Pressure Cuff');xlabel('seconds');ylabel('Pressure mmHg');axis
tight;
    figure(5);
    subplot(3,1,1);
    plot(tp,x(1:ptrun));title('Unfiltered');xlabel('seconds');ylabel('milliVolts');axis tight;
    subplot(3,1,2);
    plot(tp,ipower);title('Instantaneous Power');xlabel('seconds');ylabel('Power');axis tight;
    subplot(3,1,3);
    stem(tp',bpp);title('Systolic and Diastolic Blood Pres-
sure');xlabel('seconds');ylabel('Pressure mmHg');axis tight;
    hold on
    stem(tp,bppd,'filled');legend('Systolic','Diastolic');axis tight;
    MeanSystolicBP = mean(bpres)
    STD= std(bpres)
```

MeanDiastolicBP = mean(bpresd)
STD = std(bpresd)

References

Adamson, R. H., B. Liu, et al. (1998). "Microvascular permeability and number of tight junctions are modulated by cAMP." Am J Physiol **274**(6 Pt 2): H1885-1894.

Agre, P., L. S. King, et al. (2002). "Aquaporin water channels--from atomic structure to clinical medicine." J Physiol **542**(Pt 1): 3-16.

Ali, M. H. and P. T. Schumacker (2002). "Endothelial responses to mechanical stress: where is the mechanosensor?" Critical Care Medicine **30**(5 Suppl): S198-206.

Anand-Srivastava, M. B. (2005). "Natriuretic peptide receptor-C signaling and regulation." Peptides **26**(6): 1044-1059.

Anand-Srivastava, M. B., A. K. Srivastava, et al. (1987). "Pertussis toxin attenuates atrial natriuretic factor-mediated inhibition of adenylate cyclase. Involvement of inhibitory guanine nucleotide regulatory protein." Journal of Biological Chemistry **262**(11): 4931-4934.

Baetscher, M. and K. Brune (1983). "An Invitro System for Measuring Endothelial Permeability under Hydrostatic-Pressure." Exp Cell Res **148**(2): 541-547.

Baldwin, A. L., and Wilson, L. M. (1993). "Endothelium increases medial hydraulic conductance of aorta, possibly by release of EDRF." Am. J. Physiology **264**: H26-H32.

Baldwin, A. L., Wilson, L.M., and Simon, B.R. (1992). "Effect of pressure on hydraulic conductance." Arteriosclerosis and Thrombosis **12**: 163-171.

Barakat, A. I., E. V. Leaver, et al. (1999). "A flow-activated chloride-selective membrane current in vascular endothelial cells." Circulation Research **85**(9): 820-828.

Barakat, A. I., D. K. Lieu, et al. (2006). "Secrets of the code: Do vascular endothelial cells use ion channels to decipher complex flow signals?" Biomaterials **27**(5): 671-678.

Bazzoni, G. and E. Dejana (2004). "Endothelial cell-to-cell junctions: molecular organization and role in vascular homeostasis." Physiol Rev **84**(3): 869-901.

Belkacemi, L., M. H. Beall, et al. (2008). "AQP1 gene expression is upregulated by arginine vasopressin and cyclic AMP agonists in trophoblast cells." Life Sciences **82**(25-26): 1272-1280.

Belkacemi, Y., H. Marsiglia, et al. (2008). "Accelerated partial breast irradiation: a true therapeutic option for breast cancer patients who have good prognoses." Oncologie **10**(1): 16-21.

Bell, F. P., I. L. Adamson, et al. (1974). "Aortic endothelial permeability to albumin: focal and regional patterns of uptake and transmural distribution of 131I-albumin in the young pig." Exp Mol Pathol **20**(1): 57-68.

Birukov, K. G., C. Csortos, et al. (2001). "Differential regulation of alternatively spliced endothelial cell myosin light chain kinase isoforms by p60(Src)." Journal of Biological Chemistry **276**(11): 8567-8573.

Boucher, M. J., P. Laprise, et al. (2005). "Cyclic AMP-dependent protein kinase A negatively modulates adherens junction integrity and differentiation of intestinal epithelial cells." J Cell Physiol **202**(1): 178-190.

Bouley, R., G. Hawthorn, et al. (2006). "Aquaporin 2 (AQP2) and vasopressin type 2 receptor (V2R) endocytosis in kidney epithelial cells: AQP2 is located in 'endocytosis-resistant' membrane domains after vasopressin treatment." Biology of the Cell **98**(4): 215-232.

Brown, M. S. and J. L. Goldstein (1984). "How Ldl Receptors Influence Cholesterol and Atherosclerosis." Scientific American **251**(5): 58-&.

Bruecke, E. (1843). "Beitraege zur Lehre von der Difffusion tropftbare Flussigkeiten durch poroese Scheidewaende." Am. Phys. Chem. **58**: 77-94.

Cahill, P. A. and A. Hassid (1991). "Clearance receptor-binding atrial natriuretic peptides inhibit mitogenesis and proliferation of rat aortic smooth muscle cells." Biochem Biophys Res Commun **179**(3): 1606-1613.

Callies, C., J. Fels, et al. (2011). "Membrane potential depolarization decreases the stiffness of vascular endothelial cells." J Cell Sci **124**(Pt 11): 1936-1942.

Cancel, L. M., A. Fitting, et al. (2007). "In vitro study of LDL transport under pressurized (convective) conditions." American Journal of Physiology-Heart and Circulatory Physiology **293**(1): H126-H132.

Chien, S., Lin, S., Weinbaum, S., Lee, M. M. L., and Jan, K., (1988). "The role of Arterial Endothelial Cell Mitosis in Macromolecular Permeablity." Advances in Experimental Medicine and Biology **242**: 59-73.

Chuang, P., Cheng, J., Lin, S., Jan, K., Wang, D., and Chien, S. (1990). "Macromolecular transport across arterial and venous endothelium in rats: studies with evans blue-albumin and horseradish peroxidase." Arteriosclerosis **Arteriosclerosis**: 188-197.

Chuang, P. T., H. J. Cheng, et al. (1990). "Macromolecular transport across arterial and venous endothelium in rats: Studies with Evans blue-albumen and horseradish peroxidase." Arteriosclerosis **10**: 188-197.

Clayman, C. B. (1989). The American Medical Association encyclopedia of medicine. New York, NY, Random House.

Connolly, D. L., C. M. Shanahan, et al. (1998). "The aquaporins. A family of water channel proteins." Int J Biochem Cell Biol **30**(2): 169-172.

Curry, F. E., C. C. Michel, et al. (1976). "Osmotic reflextion coefficients of capillary walls to low molecular weight hydrophilic solutes measured in single perfused capillaries of the frog mesentery." J Physiol **261**(2): 319-336.

De Matteis, M. A. and J. S. Morrow (2000). "Spectrin tethers and mesh in the biosynthetic pathway." Journal of Cell Science **113 (Pt 13)**: 2331-2343.

DeMaio, L., J. M. Tarbell, et al. (2004). "A transmural pressure gradient induces mechanical and biological adaptive responses in endothelial cells." Am J Physiol Heart Circ Physiol **286**(2): H731-741.

Denker, B. M., B. L. Smith, et al. (1988). "Identification, purification, and partial characterization of a novel Mr 28,000 integral membrane protein from erythrocytes and renal tubules." Journal of Biological Chemistry **263**(30): 15634-15642.

Dull, R. O., H. Jo, et al. (1991). "The Effect of Varying Albumin Concentration and Hydrostatic-Pressure on Hydraulic Conductivity and Albumin Permeability of Cultured Endothelial Monolayers." Microvasc Res **41**(3): 390-407.

Fels, J., C. Callies, et al. (2010). "Nitric oxide release follows endothelial nanomechanics and not vice versa." Pflugers Arch **460**(5): 915-923.

Frank, J. S. and A. M. Fogelman (1989). "Ultrastructure of the intima in WHHL and cholesterol-fed rabbit aortas prepared by ultra-rapid freezing and freeze-etching." J. Lipid Research **30**: 967-978.

Fushimi, K., S. Uchida, et al. (1993). "Cloning and Expression of Apical Membrane Water Channel of Rat-Kidney Collecting Tubule." Nature **361**(6412): 549-552.

Gloerich, M., B. Ponsioen, et al. (2010). "Spatial regulation of cyclic AMP-Epac1 signaling in cell adhesion by ERM proteins." Molecular and Cellular Biology **30**(22): 5421-5431.

Hayes, J. S., L. L. Brunton, et al. (1979). "Hormonally specific expression of cardiac protein kinase activity." Proc Natl Acad Sci U S A **76**(4): 1570-1574.

Hergenreider, E., S. Heydt, et al. (2012). "Atheroprotective communication between endothelial cells and smooth muscle cells through miRNAs." Nat Cell Biol **14**(3): 249-256.

Herrera, M. and J. L. Garvin (2007). "Novel role of AQP-1 in NO-dependent vasorelaxation." American Journal of Physiology-Renal Physiology **292**(5): F1443-F1451.

Huang, Y., Jan, K.-M., Rumschitzki, D. , Weinbaum, S. (1998). "Structural changes in rat aortic intima due to transmural pressure." ASME Journal of Biomechanical Engineering **120**: 476-483.

Huang, Y., D. Rumschitzki, et al. (1997). "A fiber matrix model for the filtration through fenestral pores in a compressible arterial intima." American Journal of Physiology **272**(4 Pt 2): H2023-2039.

Huang, Y., Rumschitzki, D., Chien, S., Weinbaum, S. (1994). "A fiber matrix model for the growth of macromolecular leakage spots in the arterial intima." ASME Journal of Biomechanical Engineering **116**: 430-445.

Hutchinson, H. G., P. T. Trindade, et al. (1997). "Mechanisms of natriuretic-peptide-induced growth inhibition of vascular smooth muscle cells." Cardiovasc Res **35**(1): 158-167.

Jang, K. J., H. S. Cho, et al. (2011). "Fluid-shear-stress-induced translocation of aquaporin-2 and reorganization of actin cytoskeleton in renal tubular epithelial cells." Integr Biol (Camb) **3**(2): 134-141.

Javot, H. and C. Maurel (2002). "The role of aquaporins in root water uptake." Ann Bot (Lond) **90**(3): 301-313.

Jung, J. S., R. V. Bhat, et al. (1994). "Molecular characterization of an aquaporin cDNA from brain: candidate osmoreceptor and regulator of water balance." Proc Natl Acad Sci U S A **91**(26): 13052-13056.

Jurevicius, J. and R. Fischmeister (1996). "cAMP compartmentation is responsible for a local activation of cardiac Ca2+ channels by beta-adrenergic agonists." Proc Natl Acad Sci U S A **93**(1): 295-299.

Katsura, T., J. M. Verbavatz, et al. (1995). "Constitutive and regulated membrane expression of aquaporin 1 and aquaporin 2 water channels in stably transfected LLC-PK1 epithelial cells." Proc Natl Acad Sci U S A **92**(16): 7212-7216.

Kaufmann, J. E., A. Oksche, et al. (2000). "Vasopressin-induced von Willebrand factor secretion from endothelial cells involves V2 receptors and cAMP." Journal of Clinical Investigation **106**(1): 107-116.

Kedem, O. and A. Katchalsky (1958). "Thermodynamic Analysis of the Permeability of Biological Membranes to Non-Electrolytes." Biochim Biophys Acta **27**(2): 229-246.

Kenyon, D. E. (1979). "Mathematical-Model of Water Flux through Aortic Tissue." Bulletin of Mathematical Biology **41**(1): 79-90.

Khambata, R. S., C. M. Panayiotou, et al. (2011). "Natriuretic peptide receptor-3 underpins the disparate regulation of endothelial and vascular smooth muscle cell proliferation by C-type natriuretic peptide." Br J Pharmacol **164**(2b): 584-597.

King, L. S. and M. Yasui (2002). "Aquaporins and disease: lessons from mice to humans." Trends Endocrinol Metab **13**(8): 355-360.

Kishimoto, I., T. Yoshimasa, et al. (1994). "Natriuretic peptide clearance receptor is transcriptionally down-regulated by beta 2-adrenergic stimulation in vascular smooth muscle cells." Journal of Biological Chemistry **269**(45): 28300-28308.

Kohno, M., K. Yokokawa, et al. (1997). "Effect of natriuretic peptide family on the oxidized LDL-induced migration of human coronary artery smooth muscle cells." Circulation Research **81**(4): 585-590.

Koyama, Y., T. Yamamoto, et al. (1999). "Expression and localization of aquaporins in rat gastrointestinal tract." American Journal of Physiology **276**(3 Pt 1): C621-627.

Kozono, D., M. Yasui, et al. (2002). "Aquaporin water channels: atomic structure molecular dynamics meet clinical medicine." Journal of Clinical Investigation **109**(11): 1395-1399.

Landis, E. M. (1927). "Micro-injection studies of capillary permeability II. The relation between capillary pressure and the rate at which fluid passes through the walls of single capillaries." American Journal of Physiology **82**(2): 217-238.

Lee, J. S. and A. I. Gotlieb (2003). "Understanding the role of the cytoskeleton in the complex regulation of the endothelial repair." Histol Histopathol **18**(3): 879-887.

Lee, J. S., L. H. Smaje, et al. (1971). "Fluid Movement in Occluded Single Capillaries of Rabbit Omentum." Circ Res **28**(3): 358-&.

Lee, T. Y. and A. I. Gotlieb (2003). "Microfilaments and microtubules maintain endothelial integrity." Microsc Res Tech **60**(1): 115-127.

Levin, E. R., D. G. Gardner, et al. (1998). "Natriuretic peptides." N Engl J Med **339**(5): 321-328.

Lin, S. J., K. M. Jan, et al. (1988). "Enhanced macromolecular permeability of aortic endothelial cells in association with mitosis." Atherosclerosis **73**(2-3): 223-232.

Lin, S. J., K. M. Jan, et al. (1989). "Transendothelial transport of low density lipoprotein in association with cell mitosis in rat aorta." Arteriosclerosis **9**(2): 230-236.

Lin, S. J., K.M. Jan and S. Chien (1990). "The role of dying endothelial cells in transendothelial macromolecular tranport." Arteriosclerosis **10**: 188-197.

Liu, S. Q., M. Yen, et al. (1994). "On measuring the third dimension of cultured endothelial cells in shear flow." Proc Natl Acad Sci U S A **91**(19): 8782-8786.

Majno, G., J. M. Underwood, et al. (1985). "The significance of endothelial stomata and stigmata in the rat aorta. An electron microscopic study." Virchows Arch A Pathol Anat Histopathol **408**(1): 75-91.

Malek, A. M. and S. Izumo (1996). "Mechanism of endothelial cell shape change and cytoskeletal remodeling in response to fluid shear stress." Journal of Cell Science **109 (Pt 4)**: 713-726.

Marchenko, S. M. and S. O. Sage (1994). "Smooth muscle cells affect endothelial membrane potential in rat aorta." American Journal of Physiology **267**(2 Pt 2): H804-811.

Marinelli, R. A., P. S. Tietz, et al. (1999). "Secretin induces the apical insertion of aquaporin-1 water channels in rat cholangiocytes." American Journal of Physiology-Gastrointestinal and Liver Physiology **276**(1): G280-G286.

Mechaly, I., F. Laurent, et al. (1999). "Vasopressin V2 (SR121463A) and V1a (SR49059) receptor antagonists both inhibit desmopressin vasorelaxing activity." Eur J Pharmacol **383**(3): 287-290.

Millard, T. H., S. J. Sharp, et al. (2004). "Signalling to actin assembly via the WASP (Wiskott-Aldrich syndrome protein)-family proteins and the Arp2/3 complex." Biochem J **380**(Pt 1): 1-17.

Moon, C., L. S. King, et al. (1997). "Aqp1 expression in erythroleukemia cells: genetic regulation of glucocorticoid and chemical induction." American Journal of Physiology-Cell Physiology **42**(5): C1562-C1570.

Mora, R., Lupu, F., and Simionescu, N. (1987). "Prelesional events in atherogenesis. Colocalization of apoprotein B unesterified cholesterol nd extracellular phospholipid liposomes in the aorta of hyperlipidemic rabbits." Atherosclerosis **67**: 143-154.

Murata, K., K. Mitsuoka, et al. (2000). "Structural determinants of water permeation through aquaporin-1." Nature **407**(6804): 599-605.

Murthy, K. S., B. Teng, et al. (1998). "G protein-dependent activation of smooth muscle eNOS via natriuretic peptide clearance receptor." American Journal of Physiology **275**(6 Pt 1): C1409-1416.

Nguyen, T. (2008). Aquaporin-1's Contribution to Rat Aortic Endothelial Hydraulic Conductivity and How Chronic Transmural Pressure Affects It. Doctorate of Philosophy Ph.D Thesis, City University of New York.

Nielsen, S., C. L. Chou, et al. (1995). "Vasopressin Increases Water Permeability of Kidney Collecting Duct by Inducing Translocation of Aquaporin-Cd Water Channels to Plasma-Membrane." Proc Natl Acad Sci U S A **92**(4): 1013-1017.

Nielsen, S., T. H. Kwon, et al. (1999). "Physiology and pathophysiology of renal aquaporins." Journal of the American Society of Nephrology **10**(3): 647-663.

Nielsen, S., B. L. Smith, et al. (1993). "Distribution of the aquaporin CHIP in secretory and resorptive epithelia and capillary endothelia." Proc Natl Acad Sci U S A **90**(15): 7275-7279.

Noda, K., J. Zhang, et al. (2010). "Vascular endothelial-cadherin stabilizes at cell-cell junctions by anchoring to circumferential actin bundles through alpha- and beta-catenins in cyclic AMP-Epac-Rap1 signal-activated endothelial cells." Molecular Biology of the Cell **21**(4): 584-596.

Noda, Y., S. Horikawa, et al. (2008). "Reciprocal interaction with G-actin and tropomyosin is essential for aquaporin-2 trafficking." J Cell Biol **182**(3): 587-601.

Pannekoek, W. J., J. J. van Dijk, et al. (2011). "Epac1 and PDZ-GEF cooperate in Rap1 mediated endothelial junction control." Cell Signal **23**(12): 2056-2064.

Patel, D. J., J. S. Janicki, et al. (1973). "Dynamic Anisotropic Viscoelastic Properties of Aorta in Living Dogs." Circ Res **32**(1): 93-107.

Patil, R. V., Z. Q. Han, et al. (1997). "Regulation of water channel activity of aquaporin 1 by arginine vasopressin and atrial natriuretic peptide." Biochem Biophys Res Commun **238**(2): 392-396.

Patterson, C. E. and H. Lum (2001). "Update on pulmonary edema: the role and regulation of endothelial barrier function." Endothelium **8**(2): 75-105.

Prasain, N. and T. Stevens (2009). "The actin cytoskeleton in endothelial cell phenotypes." Microvasc Res **77**(1): 53-63.

Preston, G. M. and P. Agre (1991). "Isolation of the cDNA for erythrocyte integral membrane protein of 28 kilodaltons: member of an ancient channel family." Proc Natl Acad Sci U S A **88**(24): 11110-11114.

Preston, G. M., T. P. Carroll, et al. (1992). "Appearance of water channels in Xenopus oocytes expressing red cell CHIP28 protein." Science **256**(5055): 385-387.

Qiu, W. P., Q. H. Hu, et al. (2003). "Differential effects of pulsatile versus steady flow on coronary endothelial membrane potential." American Journal of Physiology-Heart and Circulatory Physiology **285**(1): H341-H346.

Reitsma, S., D. W. Slaaf, et al. (2007). "The endothelial glycocalyx: composition, functions, and visualization." Pflugers Arch **454**(3): 345-359.

Riethmuller, C., H. Oberleithner, et al. (2008). "Translocation of aquaporin-containing vesicles to the plasma membrane is facilitated by actomyosin relaxation." Biophysical Journal **94**(2): 671-678.

Rosengren, B. I., O. Carlsson, et al. (2004). "Transvascular passage of macromolecules into the peritoneal cavity of normo- and hypothermic rats in vivo: Active or passive transport?" Journal of Vascular Research **41**(2): 123-130.

Ross, R. (1986). "The pathogenesis of arherosclerosis - an update." N. Eng. J. Med. **314**: 488-500.

Ross, R. (1993). "The pathogenesis of atherosclerosis: a perspective for the 1990s." Nature **362**(6423): 801-809.

Russell, S. (2009). Energy Depletion Causes Endothelial Hyperpermeability in hyperglycemia. Doctorate of Philosphy, The Graduate Center at the City University of New York.

Sayner, S. L. (2011). "Emerging themes of cAMP regulation of the pulmonary endothelial barrier." Am J Physiol Lung Cell Mol Physiol **300**(5): L667-678.

Schrier, R. W. and M. A. Cadnapaphornchai (2003). "Renal aquaporin water channels: from molecules to human disease." Prog Biophys Mol Biol **81**(2): 117-131.

Schwenke, D. C., and T. E. Carew (1988). "Initiation of aterosclerotic lesions in cholesterol-fed rabbits. I. Focal increases in arterial LDL concentration precede development of fatty streak lesions." Arterioscleosis **9**: 895-907.

Schwenke, D. C., and T.E. Carew (1989). "Initiation of atherosclerotic lesions in cholesterol-fed rabbits. II. Selective retention of LDL vs. selective increases in LDL permeability in susceptible sites of arteries." Arteriosclerosis **9**: 908-918.

Sellitti, D. F. and S. Q. Doi (1999). "Regulation of natriuretic peptide receptors by thyrotropin in FRTL-5 rat thyroid cells: evidence for nonguanylate cyclase atrial natriuretic factor-binding sites in cells lacking the natriuretic peptide receptor C." Endocrinology **140**(3): 1365-1374.

Sellitti, D. F., E. Puggina, et al. (2004). "cAMP inhibits natriuretic peptide receptor-B activity and increases C-type natriuretic peptide in FRTL-5 rat thyroid cells." Journal of Endocrinology **180**(1): 23-34.

Serradeil-Le Gal, C., C. Lacour, et al. (1996). "Characterization of SR 121463A, a highly potent and selective, orally active vasopressin V2 receptor antagonist." Journal of Clinical Investigation **98**(12): 2729-2738.

Shou, Y. (2005). "Water and Macromolecular Transport into the Walls of Vessels with Differing Atherogenic Susceptibilities."

Shou, Y., Jan, Kung-ming., and Rumschitzki,David. (2006). "Transport in rat vessel walls. I. Hydraulic conductivities of the aorta,pulmonary artery, and inferior vena cava with intact and denuded endothelia." American Journal of Physiology **291**: H2758–H2771.

Sidel, V. W. and A. K. Solomon (1957). "Entrance of water into human red cells under an osmotic pressure gradient." J Gen Physiol **41**(2): 243-257.

Simionescu, N., Vasile, E., Lupu, F., Popescu, G., and Simionescu, M. (1986). "Prelesional events in atherogenesis. Accumulation of extracellular cholesterol-rich liposomes in the

arterial intima and cardiac valves of the hyperlipidemic rabbit." Amer. J. Pathol. **123**: 109-125.

Smith, B. L. and P. Agre (1991). "Erythrocyte Mr 28,000 transmembrane protein exists as a multisubunit oligomer similar to channel proteins." Journal of Biological Chemistry **266**(10): 6407-6415.

Srinivasan, S. R., M. G. Frontini, et al. (2003). "Longitudinal changes in risk variables of insulin resistance syndrome from childhood to young adulthood in offspring of parents with type 2 diabetes: The Bogalusa heart study." Metabolism-Clinical and Experimental **52**(4): 443-450.

Steinberg, D. (1983). "Lipoproteins and atherosclerosis: A look back and a look ahead." Arteriosclerosis **3**: 283-301.

Stemerman, M. B., Morrel, E.M., Burke, K.R., Colton, C.K., Smith, K.A. and Lees, R.S. (1986). "Local variation in arterial wall permeability to low density lipoprotein in normal rabbit aorta." Arteriosclerosis **6**: 64-69.

Strong, J. P., M. L. Richards, et al. (1969). "On Association of Cigarette Smoking with Coronary and Aortic Atherosclerosis." Journal of Atherosclerosis Research **10**(3): 303-&.

Suttorp, N., T. Hessz, et al. (1988). "Bacterial Exotoxins and Endothelial Permeability for Water and Albumin Invitro." American Journal of Physiology **255**(3): C368-C376.

Tarbell, J. M., L. Demaio, et al. (1999). "Effect of pressure on hydraulic conductivity of endothelial monolayers: role of endothelial cleft shear stress." J Appl Physiol **87**(1): 261-268.

Tarbell, J. M., M. J. Lever, et al. (1988). "The Effect of Varying Albumin Concentration of the Hydraulic Conductivity of the Rabbit Common Carotid-Artery." Microvasc Res **35**(2): 204-220.

Taylor, A. E., D. N. Granger, et al. (1977). "Estimation of Reflection Coefficient and Permeability Surface of Plasma-Protein in Capillaries of Intestine, Subcutaneous Tissue, and Lung." Biophysical Journal **17**(2): A186-A186.

Tedgui, A., and Lever, M.J. (1984). "Filtration through damaged and undamaged rabbit thoracic aorta." Am .J. Physiol. **247**(16): H784-H791.

Tedgui, A., and Lever, M.J. (1987). "Effect of presure and intimal damage on ^{131}I-albumen and [^{14}C] sucrose spaces in the aorta." American Journal of Physiology **253**: H1530-H1539.

Tedgui, A., R. Merval, et al. (1992). "Albumin transport characteristics of rat aorta in early phase of hypertension." Circulation Research **71**(4): 932-942.

Thi, M. M., J. M. Tarbell, et al. (2004). "The role of the glycocalyx in reorganization of the actin cytoskeleton under fluid shear stress: a "bumper-car" model." Proc Natl Acad Sci U S A **101**(47): 16483-16488.

Toussaint, J. (2009). Aquaporin-1 and pressure driven water transport across aortic endothelia. Aquaporin-1 expression, distribution and regulation. Doctorate of Philosophy Ph.D, The City University of New York.

Tsutsui, M., H. Shimokawa, et al. (2006). "Development of genetically engineered mice lacking all three nitric oxide synthases." Journal of Pharmacological Sciences **102**(2): 147-154.

Turner, M. R. (1992). "Effects of Proteins on the Permeability of Monolayers of Cultured Bovine Arterial Endothelium." Journal of Physiology-London **449**: 21-35.

Vander, A., J. Sherman, and D. Luciano (2001). Human Physiology: the Mechanisms of Body Function. New York, McGraw Hill Companies, Inc.

Vargas, C. B., Vargas, F.F., Pribyl, J.G. and Blackshear, P.L. (1979). "Hydrodraulic conductivity of the endothelial and outer layers of the rabbit aorta." American Journal of Physiology **236**: H53-H60.

Verkman, A. S. (2005). "More than just water channels: unexpected cellular roles of aquaporins." Journal of Cell Science **118**(Pt 15): 3225-3232.

Weinbaum, S., G. Tzeghai, P. Ganatos, R. Pfeffer and S. Chien (1985). "Effect of cell turnover and leaky junctions on arterial macromolecular transport." Am. J. Physiol. **248**: H945-H960.

Willoughby, D. and D. M. Cooper (2007). "Organization and Ca2+ regulation of adenylyl cyclases in cAMP microdomains." Physiol Rev **87**(3): 965-1010.

Wilson, J. D., et al, editors (1991). Harrison's Principles of Internal Medicine. New York, McGraw-Hill.

Wissler, R. W. and D. Vesselinovitch (1983). "Atherosclerosis--relationship to coronary blood flow." American Journal of Cardiology **52**(2): 2A-7A.

Wu, C. H., J. C. Chi, et al. (1990). "Transendothelial macromolecular transport in the aorta of spontaneously hypertensive rats." Hypertension **16**(2): 154-161.

Xue, Y. (2011). THE TRANSCELLULAR PATHWAY IS A SIGNIFICANT CONTRIBUTOR TO WATER FLOW THROUGH VASCULAR ENDOTHELIA, The City College of New York.

Yamada, K., M. Nakayama, et al. (1993). "Endothelium-dependent vasorelaxation evoked by desmopressin and involvement of nitric oxide in rat aorta." American Journal of Physiology **264**(2 Pt 1): E203-207.

Yamartino, E., Jr.,R. Bratzler, C. Colton, K. Smith and R. Lees (1974). "Hydraulic permeability of arterial tissue." Circulation 49-50, Suppl **3**: 273.

Yool, A. J., W. D. Stamer, et al. (1996). "Forskolin stimulation of water and cation permeability in aquaporin 1 water channels." Science **273**(5279): 1216-1218.

Yuan, F., S.Chien and S. Weinbaum (1991). "A new view of convective-diffusive transport processes in the arterial intima." J. Biomechanical Engineering **114**: 314-329.

Zeng, Z., K. M. Jan, et al. (2011). "A theory for water and macromolecular transport in the pulmo-nary artery with a detailed compariuson to the aorta." Am J Physiol Heart Circ Physiol.

Zhang, W., E. Zitron, et al. (2007). "Aquaporin-1 channel function is positively regulated by protein kinase C." Journal of Biological Chemistry **282**(29): 20933-20940.